

國立臺灣大學醫學院生理學研究所



博士論文

Graduate Institute of Physiology

College of Medicine

National Taiwan University

Doctor of Philosophy

使用命運追蹤方式研究間皮細胞, 間皮下纖維母細胞,

及纖維球細胞在腹膜纖維化過程的變化

Lineage tracing the fates of mesothelial cells,

submesothelial fibroblasts, and fibrocytes in peritoneal

fibrosis

陳怡婷

Yi-Ting Chen

指導教授：林水龍 博士

Advisor: Shuei-Liong Lin, M.D., Ph.D.

中華民國 105 年 6 月

June 2016



中文摘要

關鍵詞：腹膜透析；腹膜纖維化；間皮細胞；間皮下纖維母細胞；肌纖維母細胞；骨髓纖維細胞；單核球/巨噬細胞

慢性腎臟病病患近年來在台灣逐年增加，而多數慢性腎臟病患者最後會進展至末期腎病，須藉由進行透析將體內產生的毒素及多餘的水分排出。目前的透析模式有腹膜透析和血液透析兩種。利用腹膜透析的患者約占台灣末期腎病病患中約10-15%。腹膜透析患者因長期使用高葡萄糖透析液，使得腹膜長期浸泡在高濃度葡萄糖溶液中，促使氧化因子GDPs (Glucose degradation products) 和 AGEs (Advanced glycated end-products) 產生，使得腹膜通透性發生改變，若加上反覆的腹膜炎，都會促使腹膜纖維化的發生。雖然高葡萄糖透析液與反覆腹膜炎是最可能的致病因素，然而包囊性腹膜硬化症(encapsulating peritoneal sclerosis)的確實病因並不十分清楚。正常腹膜是由單一層細胞的間皮細胞(mesothelial cells)，基底膜(basement membrane)，和間皮下組織(submesothelial layer)等組成。間皮細胞是由中胚層發育而來具有上皮及間質細胞的特性。間皮下組織內含間皮下纖維母細胞(submesothelial fibroblasts)，微血管，淋巴球及結締組織。腹膜發生纖維化過程為喪失間皮細胞，間皮下組織增生纖維化，血管新生以致血管通透性增加。臨床上患者會出現腹膜超過濾率降低 (ultrafiltration failure)，腸阻塞，營養不良，嚴重者腹腔內器官整個被包裹沾黏在一起。造成腹膜纖維化的主要細胞是肌纖維母細胞，肌纖維母細胞的來源一直有爭議。目前最廣為接受的理論是間皮細胞受到葡萄糖透析液或感染等的刺激，使得間皮細胞轉分化為肌纖維母細胞，即所謂的上皮-間質細胞轉分化(epithelial-mesenchymal transition, EMT)。且間皮細胞進入間皮下組織轉變為肌纖維母細胞的過程為轉分化transdifferentiation。但有關這部分的動物實驗都是間接性證據，沒有直接動物實驗的結果。

我們利用基因改造小鼠與譜系追蹤技術發現小鼠的腹膜在損傷後會引發腹膜間皮細胞與腹膜間皮下纖維母細胞產生截然不同的命運。在餵食 $Col1a2-CreERT^Tg; Rosa26^{fstdTomato/+}$ 小鼠tamoxifen以誘導其腹膜間皮下纖維母細胞表現出紅色螢光蛋白(RFP)以作為譜系標誌之後，不論是利用次氯酸鈉、高糖腹膜透析液、或腺病毒表現乙型轉分化生長因子來傷害腹膜，我們都證實腹膜間皮下纖維母細胞是腹膜肌肉纖維母細胞的主要來源。而在 $WT1^{CreERT2/+}; Rosa26^{fstdTomato}$ 小鼠利用相同的譜系追蹤技術研究則發現 $WT1-RFP^+$ 腹膜間皮細胞則主要負責修補受傷害的間皮層。但我們同時發現一小部份的 $WT1-RFP^+$ 細胞位於腹膜基底膜之下，也會表現第一型膠原蛋白，但並不表現cytokeratin；而且受傷增厚的間皮下層結疤

組織中則有少數的肌肉纖維母細胞源自WT1-RFP⁺細胞。因此WT1促進子活化的CreERT2重組酶並無法專一性地活化間皮細胞的標記螢光蛋白或修改間皮細胞的表現基因。因此腹膜間皮下纖維母細胞雖是腹膜肌肉纖維母細胞的主要來源。我們也觀察到當腹膜受傷時是由存活下來的間皮細胞進行修補。

亦有其他研究指出來自骨髓的纖維細胞會在腹膜纖維化中轉變為肌纖維母細胞，為更瞭解肌纖維母細胞的來源，我利用parabiosis及骨髓移植技術將collagen I(α 1)-GFP基因轉植小鼠的骨髓細胞移植到野生型小鼠，誘發腹膜纖維化後發現，受傷的腹膜上僅有少許綠色螢光(GFP)細胞且同時表現骨髓標記因子CD45，表示這些綠色螢光細胞是由骨髓來的纖維細胞，但藉由螢光染色發現這些來自骨髓的纖維細胞在腹膜纖維化過程中並沒有表現肌纖維母細胞特定因子(α -smooth muscle actin; α SMA)。此同時我也發現有許多巨噬細胞在受傷的腹膜上，我再利用基因譜系追蹤研究，並且將巨噬細胞去除以瞭解它在腹膜纖維化過程的角色，發現將巨噬細胞去除時，原本因纖維化而增厚的腹膜厚度不僅減少，連肌纖維母細胞的數量也減少了。此表示巨噬細胞對於間皮下纖維母細胞轉變為肌纖維母細胞的過程有特定的作用，這些仍是我需要再進一步研究瞭解的。

經由這些腹膜纖維化研究發現，間皮下纖維母細胞是肌纖維母細胞的主要來源，非來自骨髓的纖維細胞或間皮細胞。而巨噬細胞在間皮下纖維母細胞轉變為肌纖維母細胞過程中扮有一定角色，可能透過釋放細胞激素或因子作用在間皮下纖維母細胞。然而當腹膜受傷時，是透過存活的間皮細胞所修復的。



Abstract

Key word: peritoneal dialysis; peritoneal fibrosis, mesothelial cells; submesothelial fibroblasts; myofibroblasts; circulation fibrocytes; monocytes/macrophages

Peritoneal dialysis (PD) is one modality of renal replacement therapy for end-stage renal disease. Preservation of peritoneal membrane function is important for peritoneal dialysis. However, there are many challenges for peritoneal dialysis, such as peritonitis and peritoneal fibrosis. Peritoneal fibrosis means adhesion, calcification and fibrosis between peritoneal contents, leads to ultrafiltration failure and loss peritoneal function, then finally cocooning intra-abdominal organs. The severe type of peritoneal fibrosis is encapsulating peritoneal sclerosis (EPS). There is high mortality for EPS due to ileus, malnutrition, and intestinal obstruction. The risk factors to predisposing peritoneal fibrosis are peritonitis, high glucose PD solution, and glucose degradation products (GDPs), etc.

Normal peritoneum is composed of single layer of mesothelial cells, basement membrane, and submesothelial layer. There are submesothelial fibroblasts, capillaries, lymphocytes, vessels and connective tissue in submesothelial layer. Peritoneal fibrosis is characterized by peritoneal thickening, and progressive fibrosis, which can be seen as with thickening of basal lamina and accumulation of α -smooth muscle actin (α SMA)⁺ myofibroblasts. There are three origins of myofibroblasts in peritoneal fibrosis, like mesothelial cells, submesothelial fibroblasts, and circulating fibrocytes.

The major theory is epithelial-mesenchymal transition (EMT). Mesothelial cells are mesodermal origin and have both epithelial and mesenchymal characteristics. EMT means that mesothelial cells transform to myofibroblasts and/then migrate into submesothelial layer after injury. But there are most in vitro studies to support EMT and in vivo study is lacking.

We used tamoxifen-inducible Cre/Lox techniques to genetically label and fate map mesothelial cells and submesothelial fibroblasts. We used sodium hypochlorite, TGF- β 1, 4.25% PD solution plus methylglyoxal (MGO) to induce mice models of peritoneal fibrosis. After pulse labeling induced by tamoxifen, the cell number of Col1 α 2-tdTomato⁺ submesothelial fibroblasts increased markedly in fibrotic peritoneum. And more than 60% of Col1 α 2-tdTomato⁺ submesothelial fibroblasts are α SMA

positive. However, WT1-tdTomato⁺ mesothelial cells are cytokeratin positive, Ki67 positive but α SMA negative in injured peritoneum. We also found surviving Ki67⁺ mesothelial cells repair injured peritoneum.

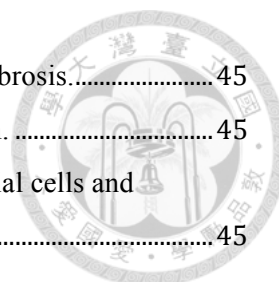
For studying roles of circulating fibrocytes during peritoneal fibrosis, we used bone marrow transplantation and parabiosis to create chimeric mice. The bone marrow cells of Collagen I (α 1)-GFP transgenic mice were transferred to wild type C57BL/6 mice. We induced peritoneal fibrosis models by sodium hypochlorite. In immunofluorescence stain, only few Coll1a1-GFP⁺ fibrocytes expressing CD45, not α SMA, were seen in fibrotic peritoneum, however, many Coll1a1-GFP⁻;CD11b⁺ cells were seen. Thereafter we also used tamoxifen-inducible Cre/Lox techniques to genetically label and fate map monocytes/macrophages. After pulse labeling induced by tamoxifen, the cell number of Csf1r-tdTomato⁺ macrophages increased markedly in fibrotic peritoneum. Ablation of macrophages in vivo in Csf1r-Cre/Esr1;tdTomato;iDTR mice were performed by diphtheria toxin during peritoneal fibrosis. The thickness of injured peritoneum and the number of myofibroblasts were decreased markedly under macrophage depletion.

Thereafter, we conclude that submesothelial fibroblasts are major origin of α SMA⁺ myofibroblasts during peritoneal injury. Few circulating fibrocytes are recruited into injured peritoneum but do not transform into myofibroblasts directly. The significance of recruited fibrocytes in peritoneal fibrosis needs further study. Macrophages may cross talk with submesothelial fibroblasts that will transit to myofibroblasts during injury. And injured peritoneum is repaired by surviving mesothelial cells.



Table of contents 目錄

中文摘要.....	i
Abstract	iii
Table of contents 目錄.....	v
Table of figures	viii
Abbreviations	ix
Chapter 1. Introduction	1
1.1. Chronic kidney disease and end-stage renal disease in Taiwan.....	1
1.2. Peritoneal dialysis (PD).....	3
1.3. Physiology of peritoneum	4
1.3.1. Mesothelial cells (MC).....	6
1.4. Peritoneal fibrosis.....	10
1.4.1. Risk factors	12
1.4.2. The mechanism of peritoneal fibrosis	14
1.4.3. Cytokines and growth factors involved in peritoneal fibrosis	29
1.5. Animal models of peritoneal fibrosis.....	35
1.5.1. Supernatant of <i>Staphylococcus epidermidis</i> (SES).....	36
1.5.2. Overexpression of TGF β 1.....	36
1.5.3. Chlorhexidine gluconate (CG).....	37
1.5.4. Sodium hypochlorite (NaOCl, bleach)	38
1.5.5. Low-pH solution	38
1.6. Prevention and treatment of peritoneal fibrosis.....	40
1.6.1. Corticosteroid.....	41
1.6.2. Tamoxifen	42
1.6.3. ACEi (inhibitors of angiotensin-converting enzyme) and ARB (Angiotensin II receptor blockers).....	43
1.6.4. Other antifibrotic medications	43
1.6.5. Surgery (Enterolysis).....	44
1.7. Mesothelial repair	44
1.8. The aim of my study.....	45



1.8.1. Identify the cell source of myofibroblasts during peritoneal fibrosis..... 45

1.8.2. Identify the cell source of mesothelial repair and regeneration. 45

1.8.3. Clarify the cross talk between mesothelial cells, submesothelial cells and macrophages in injured peritoneum..... 45

Chapter 2. Material and Method 46

2.1. Materials..... 46

2.1.1. Animals 46

2.1.2. Tamoxifen administration 48

2.1.3. Imatinib administration..... 49

2.1.4. Diphtheria toxin (DT)..... 49

2.1.5. Chemicals 49

2.1.6. Buffer 56

2.1.7. Antibodies 60

2.1.8. Instruments..... 64

2.2. Methods 66

2.2.1. Peritoneal fibrosis model..... 66

2.2.2. Chimeric mice model..... 68

2.2.3. Sample preparation..... 69

2.2.4. Fluorescence-activated cell sorting (FACS) system 70

2.2.5. Immunofluorescence stain 70

2.2.6. Masson’s trichrome stain..... 71

2.2.7. Isolation of bone marrow cells and measurement of engraftment efficiency 71

2.2.8. Statistical analysis..... 72

Chapter 3. Result 73

3.1. Expanded population of myofibroblasts in models of peritoneal fibrosis..... 73

3.2. The Fate Marker Activated in WT1^{CreERT2/+} Mice Identified MCs and a Small Population of SM Fibroblasts 75

3.3. Injured peritoneum was remesothelialized by WT1-RFP+ MCs 76

3.4. TGF-β1 upregulated αSMA in WT1-RFP+ MCs in vitro but not in vivo..... 79

3.5. SM fibroblasts were the major precursors of peritoneal myofibroblasts 80

3.6. Imatinib reduced peritoneal myofibroblasts and fibrosis 84

3.7. Chimeric mice are created by bone marrow transplantation and parabiosis..... 84

3.8. Circulating fibrocytes do not transform to myofibroblasts in peritoneal fibrosis..... 86

3.9. Macrophages accumulated in injured peritoneum but do not produce collagen. 87

3.10. Animal model of conditional ablation of macrophages.....	88
3.11. Ablation of macrophages could attenuate peritoneal fibrosis.....	89
Chapter 4. Discussion	91
Chapter 5. Conclusion and future prospects.....	98
Chapter 6. References.....	150





Table of figures

Figure 1	100
Figure 2	103
Figure 3	104
Figure 4	106
Figure 5	109
Figure 6	110
Figure 7	112
Figure 8	114
Figure 9	115
Figure 10	116
Figure 11	118
Figure 12	120
Figure 13	121
Figure 14	122
Figure 15	124
Figure 16	126
Figure 17	127
Figure 18	129
Figure 19	131
Figure 20	132
Figure 21	134
Figure 22	136
Figure 24	140
Figure 25	143
Figure 26	145
Figure 27	146
Figure 28	147
Figure 29	149



Abbreviations

ACEi	Inhibitors of angiotensin-converting enzyme
AdTGF β 1	Adenovirus expressing TGF β 1
AGEs	advanced glycation end-products
ANOVA	Analysis of variance
ARB	Angiotensin II receptor blockers
α SMA	Alpha smooth muscle actin
BM	Bone marrow
CAPD	Continuous ambulatory peritoneal dialysis
CCL	Chemokine (C-C motif) ligand
CG	Chlohexidine gluconate
CKD	Chronic kidney disease
COX-2	Cyclooxygenase-2
CRP	C-reactive protein
Csflr	Colony stimulating factor 1 receptor
CT	Computer tomography
CTGF	Connective tissue growth factor
DAPI	4', 6-diamidino-2-phenylindole
DMEM	Dullbecco's modified eagle medium
DT	Diphtheria toxin
DTR	Diphtheria toxin receptor
ECM	Extracellular matrix
EDTA	Ethelenediaminetetraacetic acid
EGF	Epidermal growth factor
EMT	Epithelial-mesenchymal transition
EPS	Encapsulating peritoneal sclerosis
ESRD	End-stage renal disease
FACS	Fluorescence-activated cell sorting
FBS	Fetal bovine serum
FGF	Fibroblast growth factor
FoxP	Forkhead box P
FSP	Fibroblast specific protein



GDPs	Glucose degradation products
GFP	Green fluorescent protein
GFR	Glomerular filtration rate
GPCRs	G-protein-coupled receptors
GRO- α	Growth-related oncogene- α
HBEGFR	Heparin-binding epithelial growth factor receptor
HD	Hemodialysis
HGF	Hepatocyte growth factor
HRQoL	Health-related quality of life
HSP	Heat shock protein
ICAM-1	Intercellular cell adhesion molecule-1
IFN- γ	Interferon- γ
IGF-1	insulin-like growth factor 1
IL	Interleukin
IP	Inducible protein
KDOQI	Kidney Disease Outcomes Quality Initiative
KGF	Keratinocyte growth factor
KO	Knock out
LPA	Lysophosphatidic acid
LMW	Low molecular weight
MAPK	Mitogen-activated protein kinase
MGO	Methylglyoxal
MRTF	Myocardin-related transcription factor
MCP-1	Monocyte chemoattractant protein-1
MMP	Matrix metalloproteinase
NGS	Normal goat serum
NO	Nitric oxide
PAI-1	Plasminogen activator inhibitor type 1
PAS	Periodic acid-Schiff
PB	Phosphate buffer
PBS	Phosphate buffered saline
PCR	Polymerase chain reaction
PD	Peritoneal dialysis
PDGF	Platelet-derived growth factor
PDGFR	Platelet-derived growth factor receptor

PFA	Paraformaldehyde
PLP	Periodate-lysine-paraformaldehyde
P&P	Pyle-Popovich
PPAR	Peroxisome proliferator-activated receptor
RANTES	Regulated on activation, normal T cell expressed and secreted
RER	Rough endoplasmic reticulum
RFP	Red fluorescent protein
ROR γ t	Retinoic acid receptor-related orphan receptor γ t
SCD-1	Stromal cell-derived factor-1
SDS	Sodium dodecyl sulfate
SES	Supernatant of <i>Staphylococcus epidermidis</i>
SRF	Serum response factor
Stat	Signal transducer and activator of transcription
tdTomato	Tandem dimer Tomato
TGF β 1	Transforming growth factor β 1
T _H 1 / 2/ 17	T helper cells type 1 / 2/ 17
TIMPs	Tissue inhibitors of metalloproteinases
TLR	Toll-liker receptor
tk	Thymidine kinase
TNF- α	Tumor necrosis factor- α
Treg	T regulatory cell
UF	Ultrafiltration
USRDS	United States Renal Data System
VCAM-1	Vascular cell adhesion molecule-1
VEGF	Vascular endothelial growth factor
WT	Wile type
WT1	Wilms tumor-1



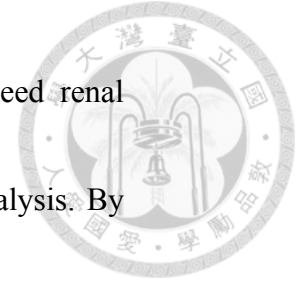


Chapter 1. Introduction

1.1. Chronic kidney disease and end-stage renal disease in

Taiwan

Chronic kidney disease (CKD) population is increasing in the world and is an important issue in public health problem. According to Kidney Disease Outcomes Quality Initiative (KDOQI) ¹ guideline, the definition of CKD is based on presence of kidney damage and level of kidney function, glomerular filtration rate (GFR) less than 60 ml/min/1.73 m² for more than 3 months. Kidney damage is defined as pathological abnormalities or markers of damage, including abnormalities in blood, or urine tests or image studies. The stage of CKD is classification by GFR: stage 1 is GFR \geq 90ml/min/1.73m²; stage 2 is GFR 60~89ml/min/1.73 m²; stage 3 is GFR 30~59ml/min/1.73 m²; stage 4 is GFR 15~29ml/min/1.73 m²; and stage 5 is GFR < 15ml/min/1.73 m². End-stage renal disease (ESRD)



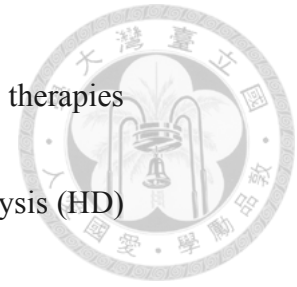
means patients with $GFR < 15 \text{ ml/min/1.73 m}^2$ and they need renal replacement therapy, such as hemodialysis or peritoneal dialysis. By

2001, more than 1 million patients were reported worldwide to receive dialysis treatment alone, with the numbers growing at an annual global average rate of 7% ². The main factors contributing to the continued growth are the universal ageing of populations, multi-morbidity, higher life-expectancy of treated ESRD patients and increasing access of a generally younger patient population to treatment in countries in which access had previously been limited ².

This issue is very important in Taiwan owing to the incidence and prevalence of ESRD in Taiwan is higher than worldwide. According to United States Renal Data System (USRDS) 2014, Taiwan has the highest prevalence and the third greatest incidence of ESRD.

The common causes of CKD and ESRD are Diabetes mellitus, hypertension, chronic glomerulonephritis and polycystic kidney disease, etc. However, herb related nephropathy is another important cause of CKD in Taiwan because of aristolochic acid. Renal

replacement therapy and renal transplantation are life-saving therapies for ESRD patients. And the dialysis modalities are hemodialysis (HD) and peritoneal dialysis (PD).



1.2. Peritoneal dialysis (PD)

Peritoneal dialysis (PD) is a life-sustaining therapy used by > 100,000 patients with ESRD worldwide, accounting for approximately 10 to 15% of the dialysis population ². The number of patients who use PD has increased gradually worldwide, especially in some Asian countries, such as Hong Kong and Thailand. PD patients have better preservation of residual renal function and higher health-related quality of life (HRQoL) ³.

However, PD patients may suffer from some challenges. The complications of PD are 1) infection, such as peritonitis, tunnel infection and exit site infection; 2) hyperglycemia; and 3) peritoneal fibrosis leading to ultrafiltration failure. Actually, peritonitis and hyperglycemia both promote the development of peritoneal fibrosis.




So far, one of the most challenges in PD is the long-term preservation of peritoneal membrane integrity^{4,5}. The incidence rate of peritoneal membrane problems increased from five cases per 100 patient-years initially to 25 cases per 100 patient-years in the third year on PD⁶. The peritoneal membrane preservation is challenged by the vintage on peritoneal dialysis, recurrent peritonitis and use of high glucose PD fluid, etc., which altogether would lead to ultrafiltration failure and peritoneal fibrosis.

1.3. Physiology of peritoneum

Peritoneum is one of serous membranes that also include pericardium, and pleura. Peritoneum covers intra-abdominal organs (visceral peritoneum) and muscle wall (parietal peritoneum).

Peritoneal dialysis is using peritoneum as a semipermeable membrane for diffusion and ultrafiltration. Water, urea, creatinine, uremic toxic agents, albumin and electrolytes could pass through pores over capillaries of peritoneum. According to the three-pore model⁷, the



principal peritoneal exchange route for water and water-soluble substances is a protein-restrictive pore pathway of radius 40-55 Å, accounting for approximately 99% of the total exchange (pore) area and approximately 90% of the total peritoneal ultrafiltration (UF) coefficient (UF coefficient=LpS, hydraulic conductivity surface). For their passage through the peritoneal membrane proteins are confined to so-called "large pores" of radius approximately 250 Å, which are extremely few in number (0.01% of the total pore population) and more or less nonrestrictive with respect to protein transport. The third pathway of the three-pore model accounts for only about 2% of the total LpS and is permeable to water but impermeable to solutes, a so-called "water-only" (transcellular) pathway. In contrast to the classical Pyle-Popovich (P&P) model, the three-pore model can predict with reasonable accuracy not only the transport of water and "small solutes" (molecular radius 2.3-15 Å) and "intermediate-size" solutes (radius 15-36 Å), but also the transport of albumin (radius 36 Å) and larger molecules across the peritoneal membrane.




Fluid transport during PD involves filtration through the capillary wall (also known as transcapillary ultrafiltration), and re-uptake of the filtered and instilled fluid into the lymphatic system (lymphatic absorption). Transcapillary ultrafiltration is greatly enhanced during PD because the dialysis solution contains a LMW (low molecular weight) osmotic agent, usually glucose, which creates an additional crystalloid osmotic pressure gradient, favoring fluid transport from the circulation to the dialysate-filled peritoneal cavity ⁸.

1.3.1. Mesothelial cells (MC)

The mesothelium consists of a single layer of flattened mesothelial cells that lines serosal cavities and the majority of internal organs, playing important roles in maintaining normal serosal integrity and function. Mesothelium is an important barrier against potential pathologic microorganisms in body cavity ⁹.

Mesothelial cells are a monolayer of epithelial-like cells with approximately 25um in diameter, with characteristic surface



microvilli and occasional cilia ¹⁰. They are primitive mesodermal origin, but share characteristics of both epithelial and mesenchymal cells. It is now understood that during human development, the intraembryonic mesoderm on each side of the neural groove differentiates into paraxial, intermediate and lateral mesoderm. Between 5 and 7 weeks, the coelom is sub-divided by a process of septation into a future pericardial cavity, two pleural cavities and a peritoneal cavity. In this phase of development, the mesothelial and submesothelial layers of the coelom are referred to as the pericardium, pleura, and peritoneum respectively, and together as serous membranes. Mesothelial cells are therefore of a primitive mesodermal origin ¹⁰. They display many epithelial characteristics including a polygonal cell shape, cytokeratin and the ability to secrete a basement membrane. And they also show features of mesenchymal cells such as the presence of vimentin, desmin and upon stimulation, alpha smooth muscle actin (α SMA) ¹⁰. And the submesothelial layer is composed of

connective tissue with few fibroblasts, mast cells, macrophages and vessels⁴.



The conventional wisdom about mesothelial cells is that they provide a protective, non-adhesive surface to facilitate intracoelomic movement. But now they are thought that they provide a permeability barrier and a dynamic cellular membrane^{10, 11}. The latest update for functions of mesothelial cells is 1) transport and movement of fluid and particular particulate materials across serosal cavity; 2) regulation of leukocytes migration in response to inflammatory process; 3) synthesis of proinflammatory cytokines, growth factors and extracellular matrix (ECM) molecules; 4) regulation of coagulation, fibrinolysis and antigen presentation¹⁰.

Mesothelial cells participate in serosal inflammation by regulating trafficking of leukocytes into and out of serosal cavities through secreting various immunomodulatory mediators, and changing microvilli density and adhesion molecule expression, in particular intercellular adhesion molecule-1 (ICAM-1) and vascular cell



adhesion molecule-1 (VCAM-1) ¹⁰. Mesothelial cells also produce a multitude of cytokines and growth factors, which can regulate inflammatory responses and stimulate tissue repair. When mesothelial cells were injured, they could produce these inflammatory cytokine, such as interleukin (IL)-1, IL-8, monocyte chemoattractant protein-1 (MCP-1), regulated on activation, normal T cell expressed and secreted (RANTES), growth-related oncogene- α (GRO- α), interferon γ (IFN γ)-inducible protein 10 (IP-10), stromal cell-derived factor-1 (SCD-1) and eotaxin, which recruit neutrophils, monocytes, lymphocytes and eosinophils ¹⁰. But mesothelial cells also secrete anti-inflammatory mediators including prostaglandins, prostacyclin and IL-6 ¹⁰.

Mesothelial cells also release growth factors, which initiate cell proliferation, differentiation and migration of mesothelial and submesothelial cells surrounding a lesion. Transforming growth factor β (TGF β), platelet-derived growth factor (PDGF), fibroblast growth factor (FGF), hepatocyte growth factor (HGF), keratinocyte growth

factor (KGF) and members of the epidermal growth factor (EGF) family are some of the factors likely to regulate these processes



1.4. Peritoneal fibrosis

There are two types of PD related peritoneal fibrosis. Type I is simple peritoneal fibrosis⁴. The injury to peritoneum is mild inflammation and is related to vintage on PD. And the peritoneum could repair itself. Uremia and non-physiologic PD fluid both cause peritoneal membrane thickening⁶.

Type II peritoneal fibrosis is a most severe form and named encapsulating peritoneal sclerosis (EPS). The reported prevalence of EPS within the PD patient population ranges worldwide from 0.7 to 3.7%¹². The onset of EPS is often insidious with non-specific symptoms, such as anorexia, nausea with vomiting, inflammation, weight loss and abdominal discomfort then parietal calcification, fibrin deposits and cocooning intestines^{4, 13}. Patients present nausea with vomiting, abdominal pain, ileus, ultrafiltration failure, bloody-tinged ascites. The consequences of EPS are devastating and



mortality rates exceed 50%, most commonly because of complications related to malnutrition, persistent bowel obstruction, even bowel perforation and prolonged parenteral feeding ^{4, 12}. It is difficult for early diagnosis because of non-specific symptoms ¹⁴. In a prospective study from Japan, the incidence rates and mortality rates increased with vintage on PD ranging from 0% at 3 years to 5.8% at 10 years to 17.2% with 100% mortality in patients on PD for over 15 years ¹⁴. The provisional diagnosis of EPS is usually made by Computer tomography (CT) scan. CT features of EPS¹⁴ are peritoneal thickening, bowel tethering, peritoneal calcification, peritoneal enhancement, loculated fluid collections, thickening of the bowel wall, and bowel dilatation with a change in caliber. In case of clinical suspicion and a negative CT scan, diagnostic surgery (laparoscopy or laparotomy) can provide the diagnosis ¹². It also facilitates taking peritoneal biopsies to detect early EPS or exclude other causes. However, surgical exploration is a challenging decision as extensive peritoneal fibrosis and bowel loops adherent to each other may exist.



1.4.1. Risk factors

Uremia alone could induce fibrotic change in peritoneum⁵. The other risk factors of peritoneal fibrosis are vintage on PD (most important), high glucose PD fluid exposure, age at the start of PD, absence of residual renal function, glucose degradation products (GDPs), fast peritoneal membrane transporter status, and recurrent peritonitis, such as *pseudomonas* and *staphylococcus aureus* infection^{4, 12, 15}.

Vintage on PD and high glucose PD fluid exposure make peritoneal deterioration. Uremia and high glucose PD fluid induce GDPs and advanced glycation end-products (AGE) synthesis. Then GDPs and AGEs stimulate production of extracellular matrix and synthesis of growth factors, such as TGF β 1 and VEGF⁴. These factors induce peritoneal inflammation. The inflammation process to peritoneum is initially loss of mesothelial cells, submesothelial thickness, then angiogenesis, hyalinizing vasculopathy, augmented vessel permeability, accumulation of collagen and fibronectin⁵.



1.4.1.1. Non-physiologic PD fluid

Non-physiologic PD fluid is still a major problem of PD till now. It is low pH, high glucose concentration, high osmotic and high lactate solution. Prolonged exposure of the peritoneum to glucose and acidic pH fluid, the most common osmotic agent in PD fluid, or to Amadori adducts, formed by the condensation between glucose and reactive amino groups of proteins, induces NF- κ B-related inflammatory, fibrogenic, and angiogenic factors synthase, such as tumor necrosis factor- α (TNF- α), IL-1 β , IL-6, cyclooxygenase-2 (COX-2) and nitric oxide (NO), by macrophages and mesothelial cells ^{4, 16}. AGEs are formed by the irreversible cross-linking of proteins, especially collagen, after prolonged incubation with glucose ⁶. The intensity of AGEs is correlated with the severity of peritoneal fibrosis. In long-term PD patients, pentosidine (a biomarker for AGEs) is present submesothelially and in the vascular wall, where it colocalizes with vascular endothelial growth factor (VEGF) ¹⁷. Along with the increase

in peritoneal AGE expression that occurs in PD patients, expression of the AGE receptor RAGE is also increased¹⁸.



1.4.2. The mechanism of peritoneal fibrosis

The mechanism of peritoneal fibrosis is not very clear so far. Devuyst et al.⁵ demonstrated that submesothelial thickening, and angiogenesis of peritoneal biopsy from patients with PD for 5 years. The “two-hit” hypothesis^{14, 19} is a possible mechanism of peritoneal fibrosis: deterioration of the peritoneum as a result of the PD procedure (the first “hit”) and superimposition of inflammatory stimuli such as infectious peritonitis (the second “hit”) are thought to play key roles.

The first hit is the extent of peritoneal damage, such as uremia, high glucose exposure, GDPs synthesis and acidic pH injury peritoneum, and increases with vintage of PD, then 1) induce fibrosis and angiogenesis by increasing TGFβ1 and VEGF; 2) increase plasminogen activator inhibitor type 1 (PAI-1) leads to reduce breakdown of fibrin; 3) loss of mesothelial cells (mesothelial

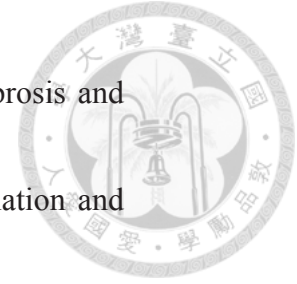


denudation). The first hit induces simple sclerosis through production of fibrinous exudation and increase matrix metalloproteinase (MMP).

In general, it could lysed and resolve spontaneously. The onset of EPS depends on the total intensity of the peritoneal damage and of the superimposed inflammation. If the second hit is on going, such as peritonitis, cessation of peritoneal dialysis, or genetic predisposing, the peritoneum could produce heavy adherence of membrane surface, and increase TNF and IL6. Finally, adhesion of visceral peritoneum is noted then EPS happens.

1.4.2.1. The pathological change in peritoneal fibrosis

The histologic feature of simple fibrosis with increased peritoneal membrane thickness already present in uremic patients at the start of dialysis increases progressively with vintage on PD is more prominent in patients with impaired ultrafiltration capacity and associated with reduction in arteriolar and venular lumen/vessel diameter ratio ¹⁴. On the other hand, histological study of EPS tissue demonstrates mesothelial denudation, increase capillary number (angiogenesis) and



vessel permeability (vasculopathy) as well as interstitial fibrosis and vascular sclerosis^{4, 14}. Additional features include inflammation and fibrin deposition, predominantly affecting the visceral membrane¹⁴.

Macroscopically, advanced cases of EPS typically exhibit a cocoon-like encapsulation of the entire intestine. The intestinal loops are adherent and fixed to one another, and the visceral peritoneum is severely thickened with fibrosis. Adhesions between the visceral and parietal peritoneum are rare, except in cases of severe inflammation. The parietal peritoneum exhibits a similar grayish-white appearance. Fibrin deposition, focal bleeding on the peritoneum, and varying amounts of bloody ascites are observed in many cases. The extent of the intestinal adhesions varies from case to case, depending on the severity and duration of the disease¹⁹.

1.4.2.2. Epithelial-mesenchymal transition (EMT)

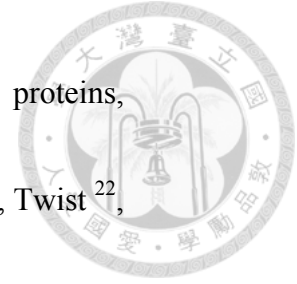
The most famous theory about peritoneal fibrosis is epithelial-to-mesenchymal transition (EMT)¹¹. Many studies support that mesothelial cells progressively lose epithelial phenotype, such as

the expression of E-cadherin and cytokeratin, and then acquire myofibroblast-like characteristics by expression of α SMA during peritoneal injury induce by exposure to high glucose PD solution, long vintage of PD and recurrent peritonitis, etc. Moreover, transdifferentiated mesothelial cells are through to migrate into submesothelial layer, lay down much ECM and lead to scar formation

⁴. EMT is a cellular program consisting of a loss of cell– cell and cell–matrix interaction and cell polarity, cytoskeletal rearrangement, and basement membrane degradation with subsequent migration or invasion ⁵. Invasion is essential in the full EMT process, seen in cancer biology. MMP-2 and MMP-9 have been studied extensively, because they are gelatinases with specificity for basement membrane–associated collagen type IV ⁵.

Biomarkers of EMT process are loss of epithelial adhesion protein E-cadherin and upregulation of mesenchymal markers. E-cadherin expression is regulated at multiple levels, including gene expression and both extracellular and intracellular protein cleavage ⁵. E-cadherin





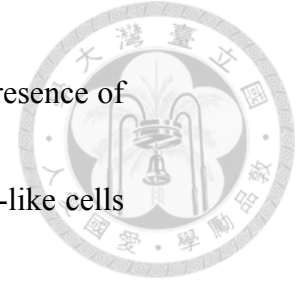
gene expression is suppressed by a family of regulatory proteins, including zinc finger DNA-binding proteins Snail²⁰, Slug²¹, Twist²², ZEB1, and ZEB2²³. These proteins are, in turn, regulated by growth factors such as platelet-derived growth factor (PDGF), TGFβ1, and Wnt proteins^{5, 23}.

Two famous studies disclosing the hypothesis of EMT in human mesothelial cells deserve discussion here. In the first study, Yang et al.⁹ demonstrated that TGFβ1 induced human omental mesothelial cells to transdifferentiate into myofibroblasts in vitro with the characteristic appearance of prominent rough endoplasmic reticulum (RER), conspicuous smooth muscle actin myofilaments, intermediate and gap junctions and active deposition of ECM. Gene expression analysis revealed a complex modulation of gene expression involving cytoskeletal organization, cell adhesion, ECM production, cell proliferation, innate immunity, stress responses and many other essential metabolic processes as the mesothelial cells underwent trans-differentiation. The authors proposed that the differentiated

epithelial cells of the mesothelium convert into myofibroblasts and that the pathological features observed following continuous ambulatory peritoneal dialysis (CAPD) may be due to the recruitment of fibrogenic cells from the mesothelium during serosal inflammation and wound healing⁹.

In the second study, Yáñez-Mo et al.¹¹ demonstrated that human mesothelial cells undergo a transition from an epithelial to mesenchymal phenotype that occurred in patients following serosal injury. Peritoneal mesothelial cells isolated from dialysis fluid effluents displayed a mesenchymal phenotype that appeared to be related to both the duration of PD and to whether peritonitis had occurred. Mesothelial cells lost their epithelial morphology and showed a decrease in the expression of cytokeratin and E-cadherin through induction of the transcriptional repressor snail. They also acquired a migratory phenotype with up-regulation of $\alpha 2$ integrins¹¹. Major profibrotic and inflammatory cytokines, such as TGF β 1 and IL-1 β , were involved in this process. In addition, assessment of





peritoneal biopsy specimens from PD patients showed the presence of mesothelial markers, ICAM-1 and cytokeratin, on fibroblast-like cells embedded in the subserosal layer, suggesting that these cells were derived from a local transition of mesothelial cells ¹⁰.

Moreover, Margetts et al. ²⁴ induced peritoneal fibrosis model using adenovirus-mediated gene transfer of active TGF β 1 to the rat peritoneum. They found that dual-staining α SMA and cytokeratin positive cells in the mesothelial cell layer, with an increase in α SMA-positive cells immediately beneath the mesothelial cells. They thought that they identify cells with both epithelial and myofibroblast characteristics within submesothelial layer supporting EMT. They also found that remnant α SMA-positive cells beneath a single mesothelial cell layer and no evidence of dual-stained cells was seen day 21 after TGF β 1 injection. Fluorescence and ultrastructural studies suggested that migratory behavior, cellular transition, and loss or detachment of mesothelium were maximal at day 7 after TGF β 1

infection. By day 21, there was resolution of these changes suggestive of EMT with evidence of re-mesothelialization.



1.4.2.3. Resident/Submesothelial fibroblasts (SM fibroblasts)

In normal or uremic non-PD peritoneum, submesothelial fibroblasts express CD34, an antigen characteristic of bone marrow stem cells ⁴.

The expression of CD34 disappears gradually in patients with peritoneal fibrosis. The loss of CD34 may be associated with the appearance of myofibroblasts ⁴.

Hirokazu okada et al. ²⁵ depleted fibroblasts with FSP (fibroblast specific protein-1) -1 positive in clohexidine gluconate (CG) induced peritoneal fibrosis model. They used transgenic mice expressing the thymidine kinase (Δtk) gene under the control of the FSP1 promoter (FSP1. Δtk mice) then give gancyclovir to deplete FSP1+ fibroblasts.

They found that depletion of FSP1+ fibroblasts attenuated peritoneal fibrosis. However, FSP-1 is a poor marker of fibroblasts. Lin et al. ²⁶

and the independent group Kisseleva et al. ²⁷ have proved *in vivo* S100A4 (= FSP-1) labeled leukocytes not fibroblasts so FSP cannot



be used to trace fibroblasts. Gancyclovir might deplete macrophages,
not fibroblasts in FSP1. Δ tk mice.

Lysophosphatidic acid (LPA) is a bioactive lipid that mediates diverse cellular responses through interactions with specific G-protein-coupled receptors (GPCRs; LPA1-5), especially LPA-LPA1 signaling is important for the development of fibrosis. LPA-LPA1 signaling contributes to fibroblast accumulation in pulmonary fibrosis by driving fibroblast migration to sites of lung injury²⁸. Sakai et al.²⁹ used CG to induce peritoneal fibrosis model for studying the role of LPA-LPA1 signaling in peritoneal fibroblasts and fibrosis. They found that peritoneal thickness and the number of myofibroblasts after CG challenges were decreased in LPA1-deficient (LPA1-KO) mice and wild type (WT) mice treated with LPA1 antagonist AM095. They also demonstrated that reduced fibroblasts proliferation in the absence of LPA1 signaling contributes to reduction of peritoneal myofibroblast accumulation in LPA1-KO mice following CG challenges. Peritoneal connective tissue growth

factor (CTGF) mRNA expression also decreased in LPA1-deficient (LPA1-KO) mice and WT mice treated with LPA1 antagonist AM095.

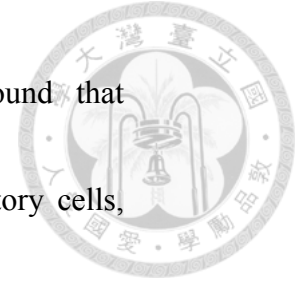


It indicated that LPA-LPA1 signaling is required for the induction of CTGF in peritoneal fibrosis, and it is dependent on myocardin-related transcription factor-A (MRTF-A), MRTF-B, and serum response factor (SRF), not TGF β 1²⁹. These studies pinpointed the important role of fibroblasts in accumulation of peritoneal myofibroblasts and fibrosis.

1.4.2.4. Circulating fibrocytes

Fibrocytes are a small subpopulation of circulating leukocytes that express collagen I, CD45RO, CD13, CD11b, CD34, CD86, and MHC class II, which have been suggested to transform into myofibroblasts when exposed to TGF β 1 in vitro⁴.

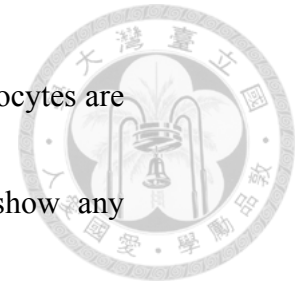
Sekiguchi et al.³⁰ isolated bone marrow cells from green fluorescent protein (GFP) transgenic mice and did bone marrow transplantation to C57Bl/6 mice. These recipient mice were injected intra-peritoneally



with 0.1% CG to induce peritoneal fibrosis. They found that thickening of the peritoneum and infiltration of inflammatory cells, mainly GFP-positive cells, were observed in the submesothelial layer³⁰. Few GFP-positive cells were c-Kit and Sca-1 positive, which are markers of BM multipotential stem cells. Both GFP- and stem cell marker-positive cells were observed in the submesothelium and on the surface day 14 of CG challenge. However, they demonstrated that many GFP- and cytokeratin- positive cells were found in submesothelial layers on day 21. The cytokeratin- and GFP-positive flat-shaped cells appeared on the surface of peritoneum on day 42. They thought that bone marrow-derived cells could transdifferentiate to mesothelial cells for peritoneal repair.

Kokubo, et al.³¹ demonstrated that many fibrocytes positive for dual staining with CD45 and type I collagen infiltrated in injured peritoneum of C57BL/6 mice with CG challenge. And they showed that peritoneal thickness and the number of fibrocytes decreased after treating with a specific inhibitor of p38MAPK (mitogen-activated

protein kinase). Thereafter, they thought that circulating fibrocytes are involved in peritoneal fibrosis. However, they did not show any markers of myofibroblasts in fibrocytes and whether fibrocytes could differentiate into myofibroblasts was still obscure.



1.4.2.5. Monocytes/Macrophages

Tissue-resident macrophages play fundamental roles specific to their microanatomical niche, ranging from dedicated homeostatic functions to immune surveillance. Okada et al.²⁵ used FSP1.Δtk mice to fate tracing fibroblasts and gave gancyclovir to deplete FSP1+ fibroblasts in peritoneal fibrosis model. However, FSP is a marker of macrophages, not fibroblasts^{26, 27}. In their study, macrophages accumulated in injured peritoneum and the number of macrophages decreased after depletion of FSP1+ cells in injured peritoneum. They also found that FSP+ cells could express MCP-1, heat shock protein 47 (HSP47), and VEGF. They thought that these cytokines were partially responsible for macrophage recruitment, matrix production,

and the neoangiogenesis in the subserosal tissue ²⁵. Their result suggested the pro-fibrotic role of macrophages in peritoneal fibrosis.



1.4.2.6. Lymphocytes

The differentiation of T cells is crucial for immune and inflammatory responses and its regulation may be a therapeutic target to control peritoneal damage. It has been found that there are different fates between CD4⁺ and CD8⁺ cells in the peritoneum during PD. It has been postulated that the presence of AGEs is responsible for an increase in the population of CD8⁺ (T cytotoxic) lymphocytes ³². Regarding CD4⁺ (T helper) subsets, in general terms Th1 cells produce high levels of IFN- γ , while Th2 cells secrete predominantly IL-4 ³³. While the predominance of Th17 cells induces the secretion of a large number of proinflammatory cytokines, T regulatory (Treg) cells restrict inflammatory responses and are associated with immunetolerance ³⁴.



Th17 cells represent a subset of T helper cells that secrete mainly IL-17 as well as other proinflammatory cytokines, and they have been related to many autoimmune and chronic inflammatory diseases ³⁵.

There is a balance between Th17 and Treg cells that depends on the activation of the transcription factor ROR γ t (factors retinoic acid receptor-related orphan receptor γ t) and Stat3 (signal transducer and activator of transcription 3), or FoxP3 (forkhead box P3) and Stat5, respectively, which regulate the immune response through the secretion of pro- and anti-inflammatory cytokines. The main cytokines involved in Th17/Treg balance are TGF- β 1 and IL-6 ³⁶.

Rodrigues-Díez et al. ³⁷ demonstrated in both mice and human samples that IL-17 is overexpressed in peritoneal biopsies. This was the first report to demonstrate that IL-17 participates in the typical fibrotic changes suffered in peritoneum during long-term PD (induced fibronectin, α SMA, and FSP-1 expression). Moreover, to better elucidate the effects of IL-17 on peritoneal membrane, intraperitoneal IL-17 was injected in mice, reproducing the changes that abnormally

take place in PD patients. On the other hand, the use of a neutralizing IL-17A antibody injected intraperitoneally in mice exposed to PD fluid for 35 days blockaded the anatomical changes in the peritoneum and reduced peritoneal fibrosis ³⁷.



There is one study focusing on the function of Treg cells on peritoneal damage. This study concluded that rosiglitazone, a PPAR γ (peroxisome proliferator-activated receptor- γ) agonist, augments the intraperitoneal IL-10 levels (Treg-associated cytokine), increases the recruitment of CD4⁺ CD25⁺ FoxP3⁺ (regulatory T cells), and finally attenuates peritoneal fibrosis in an experimental mouse PD model ³⁸.

Peritonitis, and AGEs could stimulate Th17 cells to release IL-17 by activating IL6 and TGF- β 1. The balance between Th17 and Treg cells is guided by proinflammatory cytokines secreted from Th17 cells and anti-inflammatory cytokines produced from regulatory T cells. Any factor that may alter this balance can lead to peritoneal deterioration and finally to peritoneal damage ³⁶.



1.4.3. Cytokines and growth factors involved in peritoneal fibrosis

Many inflammatory cytokines, such as TNF α , IL-1, IL-8, TGF- β 1,

FGF-2 stimulate resident fibroblasts proliferation and ECM

component deposition and by inducing EMT of mesothelial cell. IL-8,

FGF-2, and especially VEGF may induce an increase of peritoneal

capillary number and probably vessel permeability ⁴.

EGF, PDGF and IL1 stimulate to increase collagen production. High

level of TGF β 1 was found in PD patients' effluent. *In vitro*, TGF β 1

could induce human omentum mesothelial cells transdifferentiate into

myofibroblasts ¹⁰. TGF β 1 is the most important growth factor about

peritoneal fibrosis.

Ahmad et al. ³⁹ found that baseline effluent levels of chemokine

ligand (CCL)-18 were also higher in patients who developed EPS

over the subsequent 12 months than in the stable PD group. However,

the effluent concentrations reported by the researchers were consistent

with CCL18 diffusing from the circulation and not by local peritoneal

production ⁶.

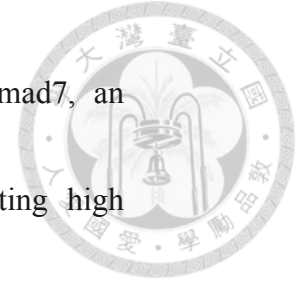


PAI-1 is an important inhibitor of fibrinolysis. The expression of PAI-1 is increased by a number of growth factors including TGF β and VEGF, and by hyaluronan fragments. Krediet et al. ⁶ found a gradual increase in effluent PAI-1 concentration, both cross-sectionally and in a longitudinal analysis, indicating progressive inhibition of local proteinases and fibrinolysis.

1.4.3.1. Transforming growth factor β -1 (TGF β 1)

TGF β 1 is a profibrotic growth factor. It could 1) induce EMT *in vitro*; 2) stimulate myofibroblastic differentiation of resident fibroblasts and recruit fibrocytes; 3) and increase extracellular matrix production ^{4, 40}.

TGF β 1 binds to a specific type I serine-threonine kinase receptor and triggers different Smad-dependent and Smad-independent signaling pathways, which result in a profound molecular reprogramming including the downregulation of the intercellular adhesion molecule E-cadherin and the upregulation of mesenchymal-associated molecules such as Snail, fibronectin, collagen I, and α -SMA ⁴⁰. Yao et al. ⁴¹ found that high glucose in the dialysate could stimulate the



TGF β 1/Smad pathway in peritoneal mesothelial cells. Smad7, an inhibitory factor, attenuate peritoneal fibrosis, by inhibiting high glucose-induced Smad2 and Smad3 activation and type I collagen synthesis^{42, 43}.

Upon ligand binding and TGF β 1 receptor activation, phosphorylation of receptor-regulated Smad2 and Smad3 occurs, which leads to the formation of complexes with Smad4. These complexes then translocate into the nucleus, in which they regulate expression of TGF β 1 responsive genes. TGF β 1 signaling through Smad3 seems to be a crucial element in the signal transduction pathways involved in wound healing and fibrosis.

Patel et al.⁴⁴ demonstrated that EMT occurred in the absence of significant fibrosis in the Smad3^{-/-} mice treated with adenovirus expressing TGF β 1 (AdTGF β 1), suggesting that EMT and fibrosis are independent events and fibrosis requires further Smad3-dependent process to occur. The EMT response in the Smad3^{-/-} mice was attenuated and the cellular invasion was transient. This suggests that



Smad3 is important for some aspects of persisting EMT, and Banh et al.⁴⁵ have suggested that Smad3 may inhibit apoptosis of newly generated myofibroblasts. TGF β 1 is associated with peritoneal dysfunction because its overexpression is correlated with worse PD outcomes^{40, 42}. However the data of EMT is only supported by immunostaining of cytokeratin+ mesothelial cells with co-expression of α SMA, not only lacking direct evidence but also showing high possibility of false positive staining.

1.4.3.2. Vascular endothelial growth factor (VEGF)

VEGF is produced from mesothelial cells⁴. VEGF increases capillary number, and vessel permeability, leading to increase small solute transport then decline of peritoneal function and finally ultrafiltration failure^{4, 14}. [ENREF 9](#) Ada et al. used Bevacizumab, a monoclonal antihuman antibody against VEGF-A, in CG induced peritoneal fibrosis model. They demonstrated that anti-VEGF antibody could reduce fibrosis by preventing neoangiogenesis⁴⁶.



1.4.3.3. Interleukin (IL-6)

Endogenous IL-6 plays a crucial role in local and systemic acute inflammatory responses by controlling the levels of pro-inflammatory, but not anti-inflammatory cytokines¹⁰. IL-6 is produced by various cell types such as T cells, activated monocytes/macrophages, fibroblasts, mesothelial cells, and vascular endothelial cells⁶. Interleukin-6, acting via the latent transcription factors Stat3 and Stat1, plays pivotal roles in governing leukocyte infiltration during acute inflammation.

IL-6 promotes an increase in IFN γ and STAT1 signaling as a consequence of repeat Supernatant of *Staphylococcus epidermidis* (SES) challenge. IFN γ stimulates production of Th1 cells then promote Stat1 enhanced stromal Stat1 signaling as an early prerequisite to the onset of peritoneal fibrosis⁴⁷.

IL-6 and TGF β also regulate Th17 cells and Treg. TGF β in the absence of IL-6 induces FoxP3, thus pushing T-cell differentiation

away from the Th17 transcriptional program and decidedly toward the Treg lineage³⁶.



1.4.3.4. Platelet-derived Growth Factor (PDGF)

PDGF is important in wound healing by inducing cellular proliferation, chemotaxis, expression of growth factors and synthesis of fibronectin and collagen. PDGFR signaling consists of four ligands (PDGF-A, -B, -C, and -D) and two receptors (PDGFR α and PDGFR β). PDGFR possesses tyrosine kinase activity and is autophosphorylated upon ligand binding. Activated signaling will be transduced to activate various proto-oncogenes and immediate-early response genes responsible for particular functions⁴⁸.

Patel et al.⁴⁹ used adenovirus to over-express PDGFB in wild type mice and Smad3^{-/-} mice. They found that PDGF could induce submesothelial thickening, cellular proliferation and angiogenesis in both mice. However, PDGF-B exposure did not lead to mobilization of the mesothelial cells and they remained as a single monolayer



throughout the observation period. Their report showed that PDGF-B effects were independent of TGF β or Smad signaling.

PDGFR subunits α and β were expressed in fibroblasts and myofibroblasts. In our previous study of renal fibrosis, we found that PDGF-PDGFR signaling blockade could inhibit renal fibrosis, decrease proliferation and differentiation of pericytes and activation of myofibroblasts⁵⁰.

1.5. Animal models of peritoneal fibrosis

The ideal animal model of peritoneal fibrosis should be clinically relevant, with clinical characteristics and a disease progression similar to those seen in PD patients. The model should also reflect the clinical histopathology.¹⁵ Animal models of peritoneal fibrosis were mainly rats and mice. Chemical irritation would make peritoneal damage through disruption of mesothelial cells junction, create an inflammatory environment and damage to subserosal tissue.



1.5.1. Supernatant of *Staphylococcus epidermidis* (SES)

This mouse model of acute peritoneal inflammation is induced by injecting intraperitoneally a controlled dose of cell-free supernatant of *Staphylococcus epidermidis* (SES), a major cause of PD-associated peritonitis⁵¹. To lead to peritoneal fibrosis, four sequential rounds of acute SES-induced peritoneal inflammation should be induced at a 7-day interval⁴⁷. This mouse model simulates acute human PD peritonitis, with early activation of proinflammatory cytokines (TNF α , IL-1, and IFN- γ) and subsequent changes in chemokine expression and the rapid recruitment of neutrophils and their subsequent replacement by monocytes⁵¹. Peritoneal fibrosis develops after repetitive acute inflammation.

1.5.2. Overexpression of TGF β 1

TGF β 1 is a profibrotic growth factor and it could induce myofibroblasts differentiation of fibroblasts and recruit monocytes/macrophages. In this model, researchers have achieved a

transient and tissue specific overexpression of TGF β 1 protein similar to the pattern of local cytokine expression likely occurring in humans and animals during fibrogenesis by using adenoviral vectors expressing TGF β 1 intraperitoneally⁵².



1.5.3. Chlorhexidine gluconate (CG)

Chlorhexidine is a chemical antiseptic for both Gram-negative and Gram-positive bacteria. Peritoneal fibrosis is induced by daily intraperitoneal injection with chlorhexidine (0.1% CG in 15% ethanol dissolved in saline) for 3 weeks¹⁵. CG is thought to induce peritoneal injury through disruption of mesothelial cell junctions, with subsequent crystalline damage to the subserosal tissue, creating an inflammatory response that progresses to a fibrosing syndrome¹⁵. CG causes an initial acute sterile peritonitis that progresses to chronic inflammation and peritoneal fibrosis, and that culminates in the formation of the abdominal cocoon¹⁵. CG also makes high level of TGF β 1 in effluent, increased submesothelial thickness, angiogenesis and significantly decreased ultrafiltration volume.

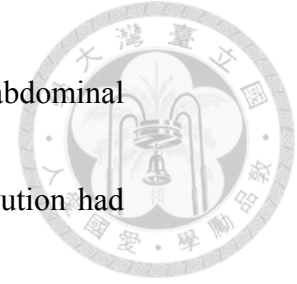


1.5.4. Sodium hypochlorite (NaOCl, bleach)

Another chemical irritation is sodium hypochlorite. The animals received intra-peritoneal injection bleach (5.25% sodium hypochlorite diluted 1:100 – 1:200 in saline) to stimulate chemical peritonitis. Sodium hypochlorite would induce fibrous thickening of the intestinal mucosa with an infiltrate of mononuclear cells and a few polymorphonuclear cells⁵³. The combination of sodium hypochlorite and whole blood resulted in inflammatory, profibrotic, and procoagulant processes that led to cocoon formation¹⁵.

1.5.5. Low-pH solution

A low-pH solution also proved effective in causing abdominal cocoon. In the relevant study, rats received daily intraperitoneal injection PD fluid containing 1.35% glucose at pH 3.8, pH 5.0, or pH 7.0 for 40 days. The pathology seen in the pH 3.8 group was the most severe and similar to that seen in EPS patients: decreased body weight, loss of the mesothelial cell layer, monocyte and fibroblast proliferation,



extracellular matrix deposition, vascular sclerosis, and abdominal cocoon formation. The animals treated with the pH 5.0 solution had less severe damage: slight subserosal thickening and partial adhesion of the peritoneum, but no cocoon formation. No significant changes were observed in the pH 7.0 group. However, the pH of PD fluid used in peritoneal dialysis is around pH 5.2 to 6.0^{15, 54}.

1.5.6. **High glucose PD fluid with and without Methylglyoxal (MGO)**

This is a mouse model of PD fluid exposure. Mice are implanted with a peritoneal access and received 0.2 ml of saline with 1 IU/ml of heparin for 7 days to facilitate wound healing. Then these mice were daily instilled with 1.5-2ml of high glucose PD fluid for 5 weeks⁴⁰. Histologic analysis of parietal peritoneum biopsies from animals exposed to PD fluid showed a loss of the mesothelial cell monolayer and an increase in the peritoneal membrane thickness when compared with mice exposed to saline solution⁴⁰.

1.5.6.1. Methylglyoxal (MGO)

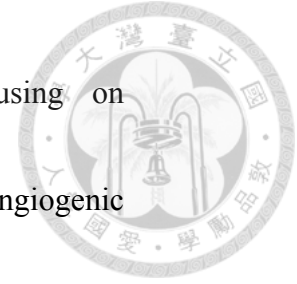


Methylglyoxal is one of GDPs in PD fluid. MGO stimulates VEGF synthesis by peritoneal mesothelial and endothelial cells, which implies that GDPs may contribute to the vascular proliferation in the peritoneal membrane ⁵⁵.

1.6. Prevention and treatment of peritoneal fibrosis

The potential to preserve peritoneal membrane and prevent peritoneal fibrosis through the use of PD solutions that are more biocompatible must be evaluated. Icodextrin, a new PD solution with polyglucose component and significantly reduced levels of glucose degradation products shows improved biocompatibility in in vitro studies, animal models, and clinical studies ¹².

Physioneal is another new PD solution with low GDP and neutral pH due to bicarbonate/lactate buffer. In vivo studies demonstrated that physioneal could better preserve peritoneal integrity than standard PD fluids, such as maintain ultrafiltration, decrease submesothelial fibrosis, MGO, VEGF, AGE and RAGE ^{55, 56}.



Therapies to halt down peritoneal fibrosis are focusing on inflammation and fibrosis. Antifibrotic and anti-angiogenic compounds, anti-inflammatory agents, and inhibitors of the renin-angiotensin system have been shown in the experimental protocol to determine their effects on adhesion formation and encapsulation¹².

1.6.1. Corticosteroid

Corticosteroid is so far the principal medication to treat the most carastrophic form of peritoneal fibrosis, EPS, because it could inhibit fibrosis progression through inhibiting inflammation, collagen synthesis and maturation¹². Although the optimum dose and duration of steroid therapy have not been established by a controlled trial, most publications support a regimen of prednisolone 0.5 to 1.0 mg/kg/day or a pulse dose of 500 to 1000 mg methylprednisolone for two to three days in EPS patients¹². The dose of prednisolone needs to be approximately 0.5 to 1.0 mg/kg/day during the first month, 0.25 to 0.5 mg at months 2 and 3 and thereafter tapered to 10 mg at six months¹². Treatment with steroids must be continued for at least one year. It is

important to prolong the period of high-dose steroids in a responding patient with a persistently elevated CRP (C-reactive protein) level as dose reduction may result in recurrence of intestinal obstruction and inflammation, responding to retreatment with prednisolone.



1.6.2. Tamoxifen

Tamoxifen is a selective estrogen receptor modulator used in breast cancer and is also used to treat some fibrotic disorder, such as retroperitoneal fibrosis. Tamoxifen is proved to inhibit TGF β 1-induce collagen and CTGF then decrease collagen deposition⁵³. Most reports show improvement of the intestinal function and a decrease in inflammation and fibrosis. Most studies in EPS report a tamoxifen dose between 20 and 40 mg/day. A favorable course is an initial dose of 20 mg twice daily for at least one year¹².



1.6.3. ACEi (inhibitors of angiotensin-converting enzyme) and ARB

(Angiotensin II receptor blockers)

ACEi (inhibitors of angiotensin-converting enzyme) and ARB

(Angiotensin II receptor blockers) could also reduce level of TGF β

and VEGF then attenuate submesothelial thickness. Angiotensin II can

upregulate several profibrotic genes including TGF β , PDGF, and FGF

¹². Pharmacologic inhibition of Angiotensin II, a potent EMT

promoter, could attenuate EMT and reduce renal fibrosis.

1.6.4. Other antifibrotic medications

Antifibrotic drugs, including pentoxifylline, dipyridamole,

troglitazone, have direct inhibitory effects on ECM protein synthesis

or on TGF β 1 expression and activity in mesothelial cell ⁴. These focus

primarily on treating underlying inflammation and suppression of

inflammatory cell activity using anti-inflammatory therapies in

conjunction with immune-modulating drugs ⁵⁷.



1.6.5. Surgery (Enterolysis)

Surgery is indicated after the inflammation has subsided and if ileus symptoms become pervasive ¹². Sometimes the encapsulation is very localized and in these cases, it tends to be at the ileocecal part of the intestines. These EPS patients benefit most from a relatively easy to perform localised peritonectomy. Some complications after surgical intervention include recurrent intestinal obstruction, formation of fistulas, or sepsis due to a perforated intestinal wall.

1.7. Mesothelial repair

Mesothelial repair or mesothelial remodeling is another important issue about peritoneal fibrosis. The process of mesothelial remodeling is thought to include several pathways: proliferation of cells lying on the margin of the tissue defect, the layer of mesothelial cells on the opposite surface of the peritoneum, immature mesothelial cells circulating in the serous liquid and mesenchymal precursor cells located in the peritoneal interstitial layer, as well as transformation of

bone marrow(BM)-derived cells infiltrating from the peripheral blood

³⁰. The role of mesothelial cells in mesothelial remodeling is very important but still need more studies to clarify the mechanism of mesothelial remodeling.



1.8. The aim of my study

1.8.1. Identify the cell source of myofibroblasts during peritoneal

fibrosis.

1.8.2. Identify the cell source of mesothelial repair and regeneration.

1.8.3. Clarify the cross talk between mesothelial cells, submesothelial

cells and macrophages in injured peritoneum.



Chapter 2. Material and Method

2.1. Materials

2.1.1. Animals

2.1.1.1. Colla1-GFP transgenic mice

Colla1-GFP^{Tg} transgenic mice are generated and validated as previously described on the C57BL/6 background whose fibroblasts express eGFP²⁶.

2.1.1.2. Colla2-CreERT transgenic mice

Colla2-CreERT transgenic mice are generated using a 6-kb procollagen I a2 enhancer to drive the expression of a cDNA encoding CreERT whose Cre recombinase activity were activated in fibroblasts under tamoxifen induction⁵⁸.

2.1.1.3. WT1^{CreERT2/+} mice

WT1^{CreERT2/+} (Wilms tumor-1) mice were generated by knocking in CreERT2 complementary DNA into the endogenous WT1 start codon

whose WT1-expressing cells express Cre recombinase under tamoxifen induction (JAX#010912)⁵⁹.



2.1.1.4. Csf1r-Cre/Esr1 transgenic mice


Csf1r (Colony stimulating factor 1 receptor)-Cre/Esr1 transgenic (Csf1r-Cre/Esr1^{Tg}) mice were generated by expressing the tamoxifen-inducible MerCreMer fusion protein under control of the macrophages specific mouse Csf1r promoter at the background of FVB/N (JAX#019098).

2.1.1.5. B6.Cg-Gt(ROSA)26Sor^{tm14(CAG-tdTomato)Hze}/J reporter mice

B6.Cg-Gt(ROSA)26Sor^{tm14(CAG-tdTomato)Hze}/J reporter mice (hereafter referred as ROSA26^{stdTomato}) were obtained from The Jackson Laboratory (Bar Harbor, ME) (JAX#007914). Specific cells in the reporter mice express red fluorescence protein (RFP) tdTomato once Cre recombinase removes stop sequence.

2.1.1.6. C57BL/6-Gt(ROSA)26Sor^{tm1(HBEGF)Awai}/J reporter (iDTR) mice

C57BL/6-Gt(ROSA)26Sor^{tm1(HBEGF)Awai}/J reporter mice were obtained from The



Jackson Laboratory (Bar Harbor, ME) (JAX#007900). Simian HBEGF cDNA is the same as simian diphtheria toxin receptor (DTR) so this reporter mice are referred as inducible DTR (iDTR) mice. The Cre-inducible expression of DTR in these iDTR mutant mice render cells susceptible to ablation following Diphtheria toxin (DT) administration.

2.1.1.7. C57BL/6-Tg (CAG-EGFP) 10sb/J transgenic mice

C57BL/6-Tg (CAG-EGFP) 10sb/J transgenic mice referred as CAG-EGFP^{Tg} (JAX#003291). This transgenic mouse line with an "enhanced" GFP (EGFP) cDNA under the control of a chicken beta-actin promoter and cytomegalovirus enhancer makes all of the tissues, with the exception of erythrocytes and hair, appear green under excitation light.

All studies were carried out under a protocol approved by Institutional Animal Care and Use Committee, National Taiwan University College of Medicine.

2.1.2. Tamoxifen administration

Tamoxifen base (T5648, Sigma) in peanut oil (P2144, Sigma-Aldrich) (10 mg/ml) were prepared by sonication. Mice were administered with 250µl



(2.5 mg) daily through oral gavage for 5 days every week at the age of 10 and 11 weeks. After washing period for 2 weeks, mice were subjected to peritoneal injury ⁶⁰.

2.1.3. Imatinib administration

Imatinib mesylate (50 mg/kg; Novartis Pharmaceuticals Co., Basel, Switzerland) through oral gavage 2 hours before an intraperitoneal injection of 100 ml/kg body weight of normal saline with 0.05% sodium hypochlorite, and then once a day until analysis on day 10.

2.1.4. Diphtheria toxin (DT)

Diphtheria toxin (0.5mg/vial; Sigma-Aldrich Co. LLC., St. Louis, MO, USA). Mice were administered through intraperitoneal (ip) injection with dose from 0, 25 to 50ng/g of body weight every other day for totally 3 times ⁶¹.

2.1.5. Chemicals

Name	Information
------	-------------

100 bp DNA ladder	Cat. ADM100.500, Arrowtec Limited, Berkshire, RG46XJ, UK
Agarose	Cat. A9539, Sigma-Aldrich Co. LLC., St. Louis, MO, USA
BD IMag TM buffer (10X)	Cat. 552362, BD Biosciences, San Jose, CA, USA
Bovine serum albumin (BSA)	Cat. ALB001, BioShop Canada Inc., Burlington, Ontario, Canada
Chloroform: Isoamylalcohol 24:1	Cat. C0549, Sigma-Aldrich Co. LLC., St. Louis, MO, USA
4',6'-Diamidino-2-phenylindole dihydrochloride (DAPI)	Cat. D1306, Molecular Probes, Life Technologies, Thermo Fisher Scientific Inc., USA
Diethyl pyrocarbonate (DEPC)	Cat. D-5758, Sigma-Aldrich Co. LLC., St. Louis, MO, USA
DNase I recombinant	Cat. 04-536-282-001, Roche Diagnostics GmbH, Roche Applied





	Science, Werk Penzberg, Germany
Dullbecco's modified eagle medium (DMEM)	Cat. 12100-046, Gibco, Life Technologies, Thermo Fisher Scientific Inc., USA
Dullbecco's modified eagle medium, a nutrient mixture F-12 powder (DMEM/F12)	Cat. 12400-024, Gibco, Life Technologies, Thermo Fisher Scientific Inc., USA
Ethelenediaminetetraacetic acid (EDTA)	Cat. E-5134, Sigma-Aldrich Co. LLC., St. Louis, MO, USA
Ethanol absolute	Cat. 32221, Sigma-Aldrich Co. LLC., St. Louis, MO, USA
Fetal bovine serum (FBS)	Cat. 26140-079, Gibco, Life Technology, Green Island, NY, USA
Formalin solution, neutral buffered, 10%	Cat. HT501128, Sigma-Aldrich Co. LLC., St. Louis, MO, USA
iQ TM SYBR [®] green supermix	Cat. 170-8882AP, Bio-Rad Laboratories Inc., Hercules, CA, USA

iScript™ cDNA synthesis kit	Cat. 170-8891, Bio-Rad Laboratories Inc., Hercules, CA, USA
Isoflurane	Panion & BF Biotech Inc., Taoyuan, Taiwan
Isopropanol	Cat. A10335-0500, Bionovas Biotechnology Co. Ltd., Toronto, Ontario, Canada
Ketalar® injection 50 mg/mL	Pfizer Inc., New York, NY, USA
Liberase TL research grade	Cat. 05-401-020-001, Roche Diagnostics GmbH, Mannheim, Germany
L-Lysine monohydrochloride (Lysine: HCl)	Cat. L-5626, Sigma-Aldrich Co. LLC., St. Louis, MO, USA
Normal goat serum (NGS)	Cat. 005-000-121, Jackson ImmunoResearch Laboratories Inc., West Grove, PA, USA
Normal mouse serum	Cat. 015-000-120, Jackson





	ImmunoResearch Laboratories Inc., West Grove, PA, USA
Paraformaldehyde (PFA)	Cat. 441244, Sigma-Aldrich Co. LLC., St. Louis, MO, USA
Phosphate buffer solution (PBS) pH7.4 (10X)	Cat. 70011-044, Gibco, Life Technologies, Thermo Fisher Scientific Inc., USA
Potassium chloride (KCl), crystal	Cat. 3040-01, J.T. Baker [®] , Avantor Performance Materials Inc., Phillipsburg, NJ, USA
Potassium phosphate (KH ₂ PO ₄)	Cat. CK-CP1580153, One-Star Biotechnology Co. Ltd., Taipei, Taiwan
ProLong [®] Gold antifade reagent	Cat. P36934, Molecular Probes, Life Technologies, Thermo Fisher Scientific Inc., USA
Proteinase K	Cat. V3021, Promega Corporation,



	Madison, WI, USA
RNeasy [®] mini kit	Cat. 74106, Qiagen GmbH, Hilden, Germany
Sodium dodecyl sulfate (SDS)	Cat. 75746, Sigma-Aldrich Co. LLC., St. Louis, MO, USA
Sodium azide (NaN ₃)	Cat. S-8032, Sigma-Aldrich Co. LLC., St. Louis, MO, USA
Sodium chloride (NaCl), crystal	Cat. 3624-05, J.T. Baker [®] , Avantor Performance Materials Inc., Center Valley, PA
Sodium (meta) periodate	Cat. S1878, Sigma-Aldrich Co. LLC., St. Louis, MO, USA
Sodium phosphate dibasic (Na ₂ HPO ₄)	Cat. S3264, Sigma-Aldrich Co. LLC., St. Louis, MO, USA
Sodium phosphate monobasic (NaH ₂ PO ₄)	Cat. S3139, Sigma-Aldrich Co. LLC., St. Louis, MO, USA
Sucrose	Cat. AS1560-1000, Bionovas



	Biotechnology Co. Ltd., Toronto, Ontario, Canada
SyBR [®] safe DNA gel stain	Cat. S33102, Invitrogen [™] , Life Technologies, Thermo Fisher Scientific Inc., USA
Taq DNA polymerase 2x master mix RED	Cat. A180306, Ampliqon A/S, Odense M, Denmark
Tissue-Tek [®] O.C.T Compound	Cat. 4583, Sakura Finetek USA., Inc., Torrance, CA, USA
Tris (base)	Cat. 4109-02, J. T. Baker, Avantor Performance Materials, Inc., Center Valley, PA, USA
Tris hydrochloride (Tris-HCl)	Cat. 4103-02, J. T. Baker, Avantor Performance Materials, Inc., Center Valley, PA, USA
TRIZol [®] reagent	Cat. 15596018, Ambion, Life Technologies, Thermo Fisher



	Scientific Inc., USA
VECTASHIELD [®]	Cat. H-1000, Vector Laboratories, Inc., Burlingame, CA, USA
Xylazine hydrochloride	Cat. X1251, Sigma-Aldrich Co. LLC., St. Louis, MO, USA


2.1.6. Buffer

FACS Buffer

Chemicals and reagent	Quantity	Final concentration
10x PBS	100 mL	1x
FBS	50 mL	5 %
10 % NaN ₃	10 mL	0.1 %
ddH ₂ O	Add to 1 L	

FACS Wash Buffer

Chemicals and reagent	Quantity	Final
-----------------------	----------	-------



		concentration
10x PBS	100 mL	1x
BSA	1 g	0.1 %
10 % NaN ₃	10 mL	0.1 %
ddH ₂ O	Add to 1 L	

Periodate-lysine-paraformaldehyde (PLP) solution 200mL

Chemicals and reagent	Quantity	Final concentration
10x PBS	100 mL	1x
BSA	1 g	0.1 %
10 % NaN ₃	10 mL	0.1 %
ddH ₂ O	Add to 1 L	

Phosphate buffer (PB) 0.1M 200mL

Chemicals and reagent	Quantity	Final concentration
------------------------------	-----------------	--------------------------------



0.2 M NaH_2PO_4	19 mL	19 mM
0.2 M Na_2HPO_4	81 mL	81 mM
ddH ₂ O	Add to 200 mL	

Phosphate buffered saline (PBS) (10x) 1L

Chemicals and reagent	Quantity	Final concentration
NaCl	80 g	1.37 M
Na_2HPO_4	14.2 g	0.1 M
KCl	2 g	26.8 mM
KH_2PO_4	2.4 g	17.6 mM
HCl	Adjust to pH 7.4	
ddH ₂ O	Add to 1 L	

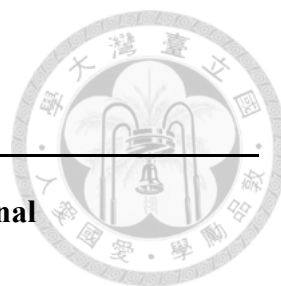


Sorting Buffer 50mL

Chemicals and reagent	Quantity	Final concentration
0.5 M EDTA	200 μ L	2 mM
FBS	0.5 mL	1 %
1x PBS pH 7.4	Add to 50 mL	

Tail Lysis Buffer 200mL

Chemicals and reagent	Quantity	Final concentration
10 % SDS	4 mL	0.2 %
1 M Tris pH 8.5	20 mL	0.1 M
0.5 M EDTA pH 8.0	2 mL	5 mM
NaCl	2.36 g	200 mM



TE Buffer 50mL

Chemicals and reagent	Quantity	Final concentration
0.5 M EDTA pH 8	0.1 mL	1 mM
1 M Tris-HCl pH 7.5	0.5 mL	10 mM
ddH ₂ O	Add to 50 mL	

2.1.7. Antibodies

Primary antibodies

Name	Host	Information
Anti-CD11b	Rat	1:200, Cat. 14-0112, 0.5 mg/mL eBioscience, Inc., San Diego, USA
Anti-wide spectrum cytokeratin antibody	Rabbit	1:200, Cat. Ab9377, Sigma-Aldrich
Anti-Ki67 antibody	Rabbit	1:200, Cat. 15580,



1mg/mL

Abcam, Inc.,
Cambridge, UK

Anti-Laminin antibody

Rabbit

1:400, Cat. L9393,

0.5 mg/mL

Sigma-Aldrich Co.
LLC., St. Louis, MO,
USA

Anti-mouse CD45

Rat

1:200, Cat. 45-0451

PerCP-Cy5.5

eBioscience, Inc.,

0.2mg/mL

San Diego, USA

Anti-mouse F4/80

Rat

1:200, Cat.

0.2 mg/mL

MF48000,
Invitrogen™, Life
Technologies,
Thermo Fisher
Scientific Inc., USA

Anti-Nidogen

Rat

1:200, Cat.

0.2mg/mL

Sc-33706 Santa Cruz



Biotechnology,

SantaCruz,CA

Anti-PDGFR β

Rabbit

1:500,

gift from Dr.

Stallcup

Anti-Vimentin

Rat

1:200, Cat sc7557,

0.2mg/mL

Santa Cruz

Biotechnology,

SantaCruz,CA

Secondary antibodies

Name

Information

Alexa Fluor[®] 488

1:400, Cat. 112-545-167,

conjugated AffiniPure

ImmunoResearch Laboratories Inc.,

Goat Anti-Rat IgG (H+L)

West Grove, PA, USA

Alexa Fluor[®] 488

1:400, Cat. 111-545-144,

conjugated AffiniPure

ImmunoResearch Laboratories Inc.,



Goat Anti-Rabbit IgG West Grove, PA, USA

(H+L)

Alexa Fluor[®] 647 1:400, Cat. 111-606-144,

conjugated AffiniPure ImmunoResearch Laboratories Inc.,

Goat Anti-Rabbit IgG West Grove, PA, USA

(H+L)

CyTH 3-conjugated 1:400, Cat. 112-165-167,

AffiniPure Goat Anti-Rat ImmunoResearch Laboratories Inc.,

IgG (H+L) West Grove, PA, USA


CyTH 3-conjugated 1:400, Cat. 111-165-144,

AffiniPure Goat ImmunoResearch Laboratories Inc.,

Anti-Rabbit IgG (H+L) West Grove, PA, USA

Fluorescence-conjugated primary antibodies

Name	Information
α SMA-Cy3	1:200, C6198
mouse	Sigma-Aldrich Co. LLC., St. Louis,

	MO, USA	
α SMA-FITC	1:200, F3777	
mouse	Sigma-Aldrich Co. LLC., St. Louis,	
	MO, USA	
Fluorescein labeled Lotus	1:500, Cat. FL-1321, Vector	
Tetragonolobus Lectin	Laboratories, Inc., Burlingame, CA,	
2 mg/mL	USA	
Fluorescein lebeled	1:200, Cat. FL-1031, Vector	
Dolichos Biflorus	Laboratories, Inc., Burlingame, CA,	
Agglutinin	USA	
2 mg/mL		

2.1.8. Instruments

Name	Information
BD FACS Aria TM IIIu	BD Biosciences, San Jose, CA, USA
BD IMag TM Cell Separation	BD Biosciences, San Jose, CA, USA



Magnet	
CFX Connect™ Real-Time PCR Detection System	Cat. 185-5201, Bio-Rad Laboratories, Inc., Hercules, CA, USA
Cryostat	Leica CM 1950, Leica Microsystems GmbH, Wetzlar, Germany
Homeothermic Blanket System	Cat. 50300, Stoelting Co., IL, USA.
Leica TCS SP5	Cat. DM5000B, Leica Microsystems GmbH, Wetzlar, Germany
My iQ™ Single Color Real-Time PCR Detection System	Cat. 170-9740, Bio-Rad Laboratories, Inc., Hercules, CA, USA
MultiGene Thermal Cycler	Cat. TC9600-G, Labnet International, Inc., Edison, NJ, USA
NanoDrop 2000 UV-Vis Spectrophotometer	Cat. ND-2000, Thermo Fisher Scientific Inc., Waltham, MA, USA
T100™ Thermal Cycler	Cat. 186-1096, Bio-Rad Laboratories,

Inc., Hercules, CA, USA

Zeiss Axio Imager

Carl Zeiss, Jena, Germany

A1 Microscope with

AxioVision Software

Zeiss Laser Scanning

Carl Zeiss, Jena, Germany

780 Microscope with Zen

2011 Software

Zeiss Laser Scanning

Carl Zeiss, Jena, Germany

880 Microscope with Zen

2011 Software

2.2. Methods

2.2.1. Peritoneal fibrosis model

2.2.1.1. Sodium hypochlorite model

Adult (>14 weeks) mice received once intraperitoneal injection of 50

ml/kg of sodium hypochlorite (1:100 in normal saline) ⁵³. Mice were analyzed at day 4, 7, 10 and 14 after injury.



2.2.1.2. Peritoneal dialysis model

Adult (>12 weeks) mice received daily intraperitoneal injection of 50 ml/kg of 4.25% PD fluid (Baxter Healthcare, Singapore) with 40 mM methylglyoxal (Sigma-Aldrich, St. Louis, MO) for 14 days. This model is the most close to the clinical situation that patients develop peritoneal fibrosis after long-term PD with high concentration of glucose and glucose degradation product. Mice were analyzed at day 7, and 14 after initiating injury.

2.2.1.3. Overexpression of TGF β 1 model

Adult (>12 weeks) mice received once intraperitoneal injection of purified Ad TGF β 1 at a dose of 1.5×10^8 plaque forming units diluted in 100 ml PBS ²⁴. Mice were analyzed at D4, 7, and 14 after injury. Control virus at the same dose was used as the control.



2.2.2. Chimeric mice model

2.2.2.1. Parabiosis model

The CAG-EGFP^{Tg} and C57BL/6 mice were shaved and unilateral flank skin incision from elbow to the knee joints were created. The skin edge of CAG-EGFP^{Tg} mice was sutured together with C57BL/6 mice by clips ⁶².

2.2.2.2. Bone marrow transplantation (BMT)

Coll1a1-GFP^{Tg} male mice were donor mice. Femur and tibia bone of Coll1a1-GFP^{Tg} male mice were collected after sacrifice and the bone marrow cells were wash out with 1x PBS. After centrifugation, the cell pellet was resuspended with 1x PBS. C57BL/6 female mice were recipient mice and received 1000rad irradiation at first.

Bone marrow cells from donor mice were injected through tail veins of recipient mice ⁶³.



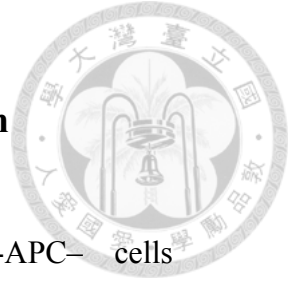
2.2.3. Sample preparation

2.2.3.1. Great omentum, liver and anterior abdominal wall collection

When mice were sacrificed, great omentum, liver, and anterior abdominal wall were collected for pathology, RNA, and protein preparation²⁶.

2.2.3.2. Isolation of mesothelial cells and submesothelial fibroblasts

Two weeks after the last dose of tamoxifen, $WT1^{CreERT2/+}; ROSA26^{fstdTomato}$ mice were injected intraperitoneally with 10 ml of 0.125% trypsin and 0.05% EDTA (Life Technologies, Carlsbad, CA). After digestion for 30 minutes, the intraperitoneal cell suspension was collected by syringe. After centrifugation, cells were resuspended in 5 ml of PBS/1% BSA, and filtered (40 μ m). MCs were purified by isolating $WT1-RFP^+$; $PDGFR\beta-APC^-$ cells (eBioscience, San Diego, CA) using a FACS Aria cell sorter (BD Biosciences, San Jose, CA). $Coll1a1-GFP^+$ SM fibroblasts were purified from peritoneal cells of normal $Coll1a1-GFP^{Tg}$ mice after intraperitoneal injection with trypsin/EDTA as described above. Purified cells were then cultured in DMEM containing 10% FBS.



2.2.4. Fluorescence-activated cell sorting (FACS) system

MCs were purified by isolating WT1-RFP+; PDGFR β -APC- cells (eBioscience, San Diego, CA) using a FACSAria cell sorter (BD Biosciences, San Jose, CA). Colla1-GFP+ SM fibroblasts were purified from peritoneal cells of normal Colla1-GFP^{Tg} mice after intraperitoneal injection with trypsin/EDTA as described above. Purified cells were then cultured in DMEM containing 10% FBS.

2.2.5. Immunofluorescence stain

Primary antibodies against the following proteins were used for immunolabeling in 5 mm-thick cryosections: α SMA-Cy3, α SMA-FITC, laminin, and cytokeratin (Sigma-Aldrich), as well as Ki67 (Abcam, Inc., Cambridge, UK), vimentin and nidogen (Santa Cruz Biotechnology, Santa Cruz, CA), and PDGFR β (gift from Dr. Stallcup). Fluorescence conjugated secondary antibody labeling (Jackson ImmunoResearch Laboratories, West Grove, PA), colabeled with 4',6-diamidino-2-phenylindole, and mounting with Vectashield were carried out as previously described^{26, 64}.

Conventional and confocal images were taken with an Zeiss Axio Imager A1
Microscope with AxioVision Software and a Zeiss Laser Scanning 780
Microscope with Zen 2011 Software, respectively (Carl Zeiss, Jena, Germany).

Images were processed using Adobe Photoshop software.

2.2.6. Masson's trichrome stain

Masson's trichrome stain was performed in 4-mm-thick paraffin sections and the peritoneal membrane thickness on the liver surface was measured in 10 sections from every 10th section for each mouse (five randomly selected images per section).

2.2.7. Isolation of bone marrow cells and measurement of

engraftment efficiency

We used QIAGEN DNeasy® Blood and Tissue Kit to get DNA of recipient mice. Engraftment efficiency was confirmed by duplex qPCR using specific detection probes for Y-chromosome Y6 and autosomal GAPDH primer amplicons in bone marrow of recipient ⁶⁵. Successful engraftment in bone marrow of the female recipient was defined by the result of Y-chromosome Y6

qPCR more than 75% shown in bone marrow of male donor.



2.2.8. Statistical analysis


Data is expressed as mean \pm s.e.m. Statistical analyses are carried out using GraphPad Prizm (GraphPad Software). The statistical significance is evaluated by one-way ANOVA.



Chapter 3. Result

3.1. Expanded population of myofibroblasts in models of peritoneal fibrosis

Using *Coll1a1-GFP^{Tg}* mice expressing enhanced green fluorescent protein (GFP) under the regulation of the *Coll1a1* promoter and enhancers, we studied the collagen-producing cells in normal and injured peritoneum. *Coll1a1-GFP*-positive cells were cytokeratin-, PDGF receptor- β (PDGFR β)+, and vimentin+, and lay beneath the nidogen+ basal lamina (Figure 1, A– C). We called these cells SM fibroblasts. Seven days after hypochlorite injury, the population of *Coll1a1-GFP*+ cells expanded in the peritoneum of the liver, omentum, and abdominal wall (Figure 2). In addition, we noted diffuse thickening of the basal lamina to become scar tissue (Figure 1, D and E). Because the preparation of peritoneum covering solid organs for immunofluorescence study was easier, we showed the findings of peritoneal covering of liver unless otherwise specified. After hypochlorite injury, cytokeratin+ staining was not



detected at many surfaces of the peritoneum, suggesting the loss of MCs. At peritoneal surfaces in which MCs remained attached after injury, the cytokeratin+ MCs could now be seen to express Colla1-GFP, in sharp contrast with the healthy state (Figure 1, A, D, and F). Cytokeratin+ MCs did not express detectable α SMA (Figure 1F). Myofibroblasts, defined by coexpression of α SMA and Colla1-GFP, accumulated markedly within the thickened basal lamina between MCs and SM fibroblasts (Figure 1, E and F), and expressed both PDGFR β and vimentin (Figure 1, G and H). The observations that injured cytokeratin+ MCs generated Colla1 transcripts and that α SMA+ myofibroblasts accumulated in the thickened laminin+ scar were reproduced in *Colla1-GFP^{Tg}* mice 10 days after intraperitoneal injection of AdTGF- β 1 (Figure 3).


3.2. The fate marker activated in *WT1*^{CreERT2/+} mice



identified MCs and a small population of SM

fibroblasts

Permanent expression red fluorescence protein (RFP) was activated in WT1-expressing cells by somatic DNA recombination in adult *WT1*^{CreERT2/+}; *ROSA26*^{fstdTomato} (WT1-RFP) mice. Activation was induced conditionally by oral tamoxifen administration so that a cohort of cells was permanently labeled only during tamoxifen exposure (Figure 4A). On the peritoneal surface, 83.3% of the cytokeratin⁺ MCs underwent somatic recombination and were referred to as WT1-RFP⁺ MCs (Figure 4, B and C, Figure 5). In addition, WT1-RFP⁺; cytokeratin⁻ cells, representing 23.6% of all WT1-RFP⁺ cells, were seen beneath the mesothelium in keeping with labeling of SM fibroblasts (Figure 4B). In addition to notable expression in SM fibroblasts, vimentin was detectable in normal WT1-RFP⁺ MCs (Figures 1C and 4D), suggesting that MCs normally expressed this mesenchymal protein. To confirm that WT1-RFP⁺ cells beneath the mesothelium were SM



fibroblasts, we generated $WT1^{CreERT2/+};ROSA26^{fstdTomato};Coll1a1-GFP^{Tg}$ mice. Of the $Coll1a1-GFP^+$ SM fibroblasts, 17.6% expressed WT1-RFP, indicating that CreERT2 at the *WT1* locus activated $ROSA26^{fstdTomato}$ in a small population of SM fibroblasts (Figure 4E). Furthermore, 74.8% of all WT1-RFP+ cells were $Coll1a1-GFP^-$ and were on the peritoneal surface, in keeping with them being MCs (Figure 4E). FACS analysis showed similar results (Figure 4F).

3.3. Injured peritoneum was remesothelialized by

WT1-RFP+ MCs

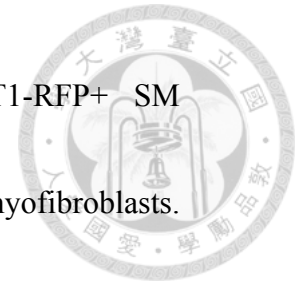
Peritoneal fibrosis was initiated by hypochlorite in $WT1^{CreERT2/+};ROSA26^{fstdTomato}$ mice 2 weeks after the last dose of tamoxifen and the fate of the cohort of WT1-RFP+ cells was mapped (Figure 6A). Within 10 days after injury, peritoneal surfaces were partially covered by WT1-RFP+ or cytokeratin+ MCs (Figure 6 B and C), but many surfaces were devoid of MCs (Figure 6B). WT1- RFP expression was noted in 85.6% of cytokeratin MCs (Figure 6B). There was no dilution of the proportion of

cytokeratin+ MCs with the fate marker WT1-RFP before and after injury (Figures 4B and 6B). Active proliferation in WT1-RFP+ MCs was confirmed by positive Ki67 staining (Figure 6D). No recombination of somatic DNA in the absence of tamoxifen administration was detected before and after injury (Figure 7).

In contrast with the active involvement of surviving MCs in remesothelialization after hypochlorite injury (Figure 6B–D), only a few WT1-RFP+ cells coexpressing α SMA were found within the thickened laminin+ scar (Figure 6, E and F, Figure 8). Most of the WT1-RFP+; α SMA– cells were found on the peritoneal surfaces, indicating that they were MCs as those observed in (Figures 4 and 6C), the others were beneath the thickened scar and therefore SM fibroblasts (Figure 6, E and F, Figure 8). The percentage of α SMA+ cells expressing WT1-RFP was 15.9%, representing a proportion similar to that of Colla1-GFP+ SM fibroblasts expressing WT1-RFP (Figures 4, E and F, and 6, E and F). Furthermore, WT1-RFP+ cells within and beneath the thickened scar expressed PDGFR β , but WT1-RFP+ MCs did not (Figure 9),



collectively suggesting that the minor population of WT1-RFP+ α SMA+ fibroblasts is the source of the minor population of WT1-RFP+ myofibroblasts.



To validate the fate of WT1 lineage of cells in peritoneal injury, we studied a second model of peritoneal fibrosis induced by daily intraperitoneal injection, for 2 weeks, of dialysis solution containing 4.25% glucose and 40 mM of the glucose degradation product methylglyoxal (Figure 10A). Although the injury was much milder than that induced by hypochlorite, α SMA+ myofibroblasts was detectable (Figure 10B). Similar to the observation in the hypochlorite-induced model, WT1-RFP+ cells were noted on the peritoneal surface or beneath the thickened scar (Figure 10, B and C). A low percentage (16.5%) of α SMA+ myofibroblasts coexpressing WT1-RFP was detected within the laminin+ scar (Figure 10B). Similar to the findings in the hypochlorite-induced model, >85% of the cytokeratin+ MCs at the peritoneal surface were WT1-RFP+ before and after injury (Figure 10C).



3.4. TGF- β 1 upregulated α SMA in WT1-RFP+ MCs in

vitro but not in vivo

We induced a third model of peritoneal fibrosis by intraperitoneal injection of AdTGF- β 1 in *WT1^{CreERT2/+};ROSA26^{fltdTomato}* mice (Figure 11A). Before AdTGF- β 1 administration, 82.6% of cytokeratin+ MCs were labeled with the WT1-RFP fate marker. Ten days after AdTGF- β 1 administration, marked accumulation of α SMA+ myofibroblasts was seen in the peritoneum (Figure 11, B and C). In addition to WT1-RFP+; α SMA- SM fibroblasts beneath the thickened laminin+ scar, occasional scattered WT1-RFP+ ; α SMA+ myofibroblasts were noted within the thickened scar but these amounted to only 14.6% of α SMA+ myofibroblasts (Figure 11, B and C). α SMA was not detected in WT1-RFP+ MCs on the peritoneal surface (Figure 11C). In peritoneal areas in which coverage by MCs remained intact, >85% of cytokeratin+ MCs were WT1-RFP+ (Figure 11D).

To determine whether primary MCs had the capacity to express α SMA in vitro, which some investigators have used to define the mesothelial EMT process,

we isolated and cultured WT1-RFP+; PDGFR β -APC- MCs from *WT1^{CreERT2/+}; ROSA26^{fstdTomato}* mice after tamoxifen pretreatment (Figure 12).



MCs in culture medium alone lacked detectable α SMA (Figure 11E). In the presence of TGF- β 1 for 2 days, cultured MCs activated expression of α SMA (Figure 11E), indicating that although MCs in vivo do not express α SMA, they are capable of activating this protein in vitro. In contrast with the upregulation of mesenchymal genes (*Acta2* and *Colla1*) by TGF- β 1 in cultured MCs, TGF- β 1 suppressed *Gpm6a* (glycoprotein6a, a MC marker) (Figure 13). However, *Krt8* (cytokeratin8) was upregulated by TGF- β 1 (Figure 13).

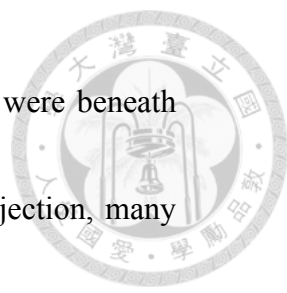
3.5. SM fibroblasts were the major precursors of peritoneal myofibroblasts

To determine whether SM fibroblasts were the primary source of α SMA+ myofibroblasts, we generated *Colla2-CreERT^{Tg}; ROSA26^{fstdTomato}; Colla1-GFP^{Tg}* mice in which cells expressing the *Colla2* chain of collagen I could undergo somatic recombination to express the tdTomato RFP permanently after tamoxifen


administration (Colla2-RFP+ cells). Dynamic expression of the Colla1 chain reported by the Colla1-GFP transgene was used to define SM fibroblasts.



The cohort of Colla1-GFP+ SM fibroblasts induced by tamoxifen to express Colla2-RFP was 64.2% in *Colla2-CreERT^{Tg}; ROSA26^{stdTomato}; Colla1-GFP^{Tg}* mice (the numbers of Colla2-RFP+ cells and Colla1-GFP+ cells were 2.8 and 4.4 cells per field at x 630 magnification, respectively) (Figure 14, A, B, and D). Two weeks after cohort labeling, hypochlorite injury was induced. After 1 week, the numbers of Colla2-RFP+ cells and Colla1-GFP+ cells increased (11.7 and 18.5 cells per field at x 630 magnification, respectively); the proportion of Colla1-GFP+ cells that coexpressed Colla2-RFP was 63.0% (Figure 14, A, C, and D). The absence of a significant decrease in the proportion of Colla1-GFP+ cells coexpressing Colla2-RFP indicated that SM fibroblasts, rather than other cell sources, were the major precursors of collagen-producing cells in the injured peritoneum. To be sure that these SM fibroblasts became α SMA+ myofibroblasts, we induced peritoneal fibrosis by hypochlorite injection in *Colla2-CreERT^{Tg}; ROSA26^{stdTomato}* mice 2 weeks after tamoxifen treatment to label a 64.2% cohort of SM fibroblasts (Figure



15A). Before hypochlorite injury, *Coll1a2*-RFP+ SM fibroblasts were beneath cytokeratin+ MCs (Figure 16). Seven days after hypochlorite injection, many *Coll1a2*-RFP+ cells entered the cell cycle evidenced by expression of Ki67 (Figure 15B). *Coll1a2*-RFP+ cells accumulated within the thickened peritoneum and accounted for 60% of α SMA+ myofibroblasts, confirming SM fibroblasts as the major precursors of peritoneal myofibroblasts (Figure 15, C and D, Figure 17) and also supporting WT1- RFP+ SM fibroblasts as the progenitors of WT1-RFP+; α SMA+ myofibroblasts in *WT1^{CreERT2/+}; ROSA26^{fstdTomato}* mice after peritoneal injury (Figures 6, E and F, and 11, B and C, Figures 8– 10). Although remesothelialization occurred, no cytokeratin+ MCs coexpressed *Coll1a2*-RFP, indicating that the injured peritoneum is not remesothelialized by SM fibroblasts (Figure 15, E and F, Figure 18) and also excluding the possible contribution of WT1-RFP+ SM fibroblasts to remesothelialization (Figure 6, B and C). Without cohort labeling by tamoxifen, <0.01% of cells expressed RFP before or after hypochlorite injury, indicating that “leaky” somatic recombination could not be responsible for the appearance of *Coll1a2*- RFP+ cells after injury (Figure19).



In separate cohorts of *Colla2-CreERT^{Tg};ROSA26^{stdTomato}* mice, we induced a second model of fibrosis by AdTGF- β 1 injection (Figure 20A). Ten days after viral administration, we observed marked expansion of the *Colla2-RFP+* SM fibroblasts, which again accounted for 62.5% of myofibroblasts, indicating in this second model that SM fibroblasts are the major source of myofibroblasts during peritoneal fibrosis (Figure 20B).

To determine whether primary SM fibroblasts had the capacity to express α SMA in vitro, we isolated and cultured *Colla1-GFP+* SM fibroblasts from normal *Colla1-GFP^{Tg}* mice (Figure 21A). SM fibroblasts in culture medium alone lacked detectable α SMA (Figure 21B). In the presence of TGF- β 1 for 2 days, SM fibroblasts activated expression of α SMA (Figure 21B). Quantitative PCR (QPCR) showed the increase of *Acta2* and *Colla1* by TGF- β 1 (Figure 21C).



3.6. Imatinib reduced peritoneal myofibroblasts and fibrosis

Because SM fibroblasts, not MCs, express PDGFR β and SM fibroblasts are the precursors of scar-forming myofibroblasts, we blocked PDGFR signaling during the hypochlorite model using the PDGFR tyrosine kinase inhibitor imatinib (Figure 22A). Imatinib significantly attenuated peritoneal adhesion, thickening of fibrotic peritoneum, and accumulation of α SMA+ myofibroblasts despite no change in the remesothelialization induced by hypochlorite (Figure 22, B– E).

3.7. Chimeric mice are created by parabiosis and bone marrow transplantation

To study role of circulating fibrocytes in peritoneal fibrosis, we used bone marrow transplantation²⁶ and parabiosis⁶² to create chimeric mice.

In the parabiosis, development of cross-circulation between *CAG-EGFP^{Tg}* mice and wild type C57BL/6 mice was analyzed by flow cytometric analysis of the

peripheral blood at day 16 after surgery. Flow cytometric analysis revealed that 50.39% of the CD45⁺ cells in peripheral blood of C57BL/6 mice were GFP⁺, suggesting the development of cross-circulation in the parabiont (Figure 23B).

The bone marrow cells of male *Colla1-GFP^{Tg}* mice were injected through tail vein to sublethally irradiated female wild type C57BL/6 mice. Engraftment efficiency was checked by QPCR using specific detection probes for Y-chromosome Y6 and successful engraftment was defined by the presence of Y chromosome in bone marrow of female recipient mice more than 75% of that shown in bone marrow of male donor. (Figure 23C)

Therefore we used C57BL/6 wild type mice with parabiosis from *CAG-EGFP^{Tg}* mice and BMT chimerism from *Colla1-GFP^{Tg}* mice to study the recruitment of CAG-EGFP⁺ leukocytes and Colla1-GFP⁺ fibrocytes into peritoneum after injury.






3.8. Circulating fibrocytes do not transform to myofibroblasts in peritoneal fibrosis

Parabiosis mice, including *CAG-EGFP^{Tg}* and C57BL/6 mice, were all induced peritoneal fibrosis by intraperitoneal hypochlorite. Fourteen day after hypochlorite injury, some CAG-EGFP⁺; CD45⁺; CD11b⁻ leukocytes were found in injured peritoneum of parabiont C57BL/6 mice (Figure 24, B and D).

This indicated that cross circulation was created and maintained at least 35 day after surgery. However, these CAG-EGFP⁺; CD45⁺ leukocytes did not express α SMA after peritoneal injury (Figure 24C). This indicated that these CAG-GFP⁺ leukocytes in injured peritoneum did not transit into myofibroblasts.

For further clarify the CAG-GFP⁺; CD45⁺ leukocytes in injured peritoneum, BMT chimera from *Coll1a1-GFP^{Tg}* mice were created.

BMT chimeric mice were also induced peritoneal fibrosis by hypochlorite injury. Only few Coll1a1-GFP⁺ cells were found in fibrotic peritoneum (Figure 25B-D). And these Coll1a1-GFP⁺ cells all expressed CD45⁺ and




CD11b-, indicating they were of hematopoietic lineage, circulating fibrocytes (Figure 25, B and D). However, these Colla1-GFP+ cells did not express α SMA (Figure 25C), suggesting circulating fibrocytes do not transit into myofibroblasts in injured peritoneum. Compared to the cell number of α SMA+ myofibroblasts (cells/HPF), the cell number of Colla1-GFP+ fibrocytes (cells/HPF) was very few (Figure 25E).

3.9. Macrophages accumulated in injured peritoneum but do not produce collagen

Numerous CD11b+ cells accumulated in fibrotic peritoneum of wild type C57BL/C mice with parabiosis from *CAG-GFP^{Tg}* mice and bone marrow chimera from *Colla1-GFP^{Tg}* mice (Figure 24D and 25D). No CD11b+ cells expressed Colla1-GFP, suggesting that macrophages themselves do not produce collagen during peritoneal injury (Figure 25D).

To study the role of accumulated macrophages in the fibrogenesis of injured peritoneum, we generated *Csf1r-Cre/Esr1^{Tg};ROSA26^{stdTomato}* mice in which cells expressing the *Csf1r* could undergo somatic recombination to express



the tdTomato RFP permanently after tamoxifen administration (*Csf1r*-RFP+ cells). We then generated *Csf1r-Cre/Esr1^{Tg};ROSA26^{stdTomato};Colla1-GFP^{Tg}* mice to further clarify whether macrophages produce collagen during peritoneal injury. Our data showed that *Csf1r*-RFP+ macrophages did not express *Colla1*-GFP in neither normal nor fibrotic peritoneum (Figure 26), confirming that macrophages do not produce collagen even in neither healthy nor injured peritoneum.

3.10. Animal model of conditional ablation of macrophages

Although accumulated macrophages did not produce collagen by themselves, they might promote fibrosis through cross talk with collagen-producing cells. We then performed conditional ablation of macrophages in mice subjected to peritoneal injury to understand whether macrophages contributed to fibrosis. Identification of the human receptor for diphtheria toxin (DT), also known as heparin-binding epidermal growth factor (HBEGF), provided an opportunity for a unique ablation strategy ⁶⁶. The murine form of HBEGF binds DT poorly, but mouse cells can be rendered sensitive through transgenic expression of human HBEGF ⁶¹. In transgenic mice expressing human



HBEGF lineage specifically, cell ablation results following DT injection. In addition, DT is a protein synthesis inhibitor and kills both mitotic and terminally differentiated cells ⁶¹.

After tamoxifen administration, *Csf1r*-expressing cells expressed diphtheria toxin receptor (DTR) in *Csf1r-Cre/Esr1^{Tg};iDTR* mice. FACS analysis revealed ablation efficiency induced by DT injection (Figure 27).

3.11. Ablation of macrophages could attenuate peritoneal fibrosis

We generated *Csf1r-Cre/Esr1^{Tg};ROSA26^{stdTomato};iDTR* mice to ablate macrophages ⁶¹. Peritoneal fibrosis was induced by intraperitoneal injury of hypochlorite and diphtheria toxin (DT) was injected intraperitoneally every other day for 3 times from day 2 after peritoneal injury (Figure 28A). Immunofluorescence showed that cell number of α SMA+ myofibroblasts was reduced when RFP+ macrophages were ablated (Figure 28B and C). Masson's trichrome stain showed that thickness of injured peritoneum was reduced markedly after macrophages ablation (Figure 28D-G). These

experiments confirmed that macrophages play a role in the accumulation of α SMA+ myofibroblasts and extracellular matrix during peritoneal fibrosis.

These experiments also suggested that macrophages may cross talk with SM fibroblasts to promote their transition into myofibroblasts in peritoneal fibrosis.





Chapter 4. Discussion

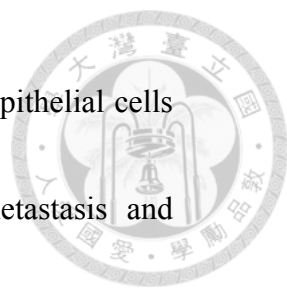
These studies report an extensive population of $\text{Col1a1}^+; \text{Col1a2}^+; \text{PDGFR}\beta^+$ SM fibroblasts lying below the basal lamina of the normal peritoneal membrane, which produce collagen protein in healthy states. By mapping the fate of cohorts of conditional, somatically labeled SM fibroblasts, our studies show that they transdifferentiate into an expanding population of $\text{Col1a1}^+; \text{Col1a2}^+; \text{PDGFR}\beta^+; \alpha\text{SMA}^+$ myofibroblasts in the region of pathologic matrix production. These cells thus are a major source of myofibroblasts in three different models of peritoneal fibrosis and are an important new cellular target for fibrosing diseases of the peritoneum. Our labeling strategies did not label all SM fibroblasts, but we successfully labeled cohorts of approximately 65% of these discrete SM fibroblast cells and they expanded in disease settings to become approximately 65% of all myofibroblasts. The fact that the proportion of cells did not change from healthy to disease states suggests that the vast majority of myofibroblasts in these peritoneal fibrosis models derive from SM fibroblast precursors, rather

than from an alternate cell precursor. Although conditional labeling of all SM fibroblasts would be desirable, the labeling of 65% of cells is the technical limit of labeling using these genetic tools in adult mice.



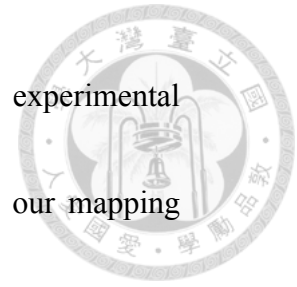
We mapped the fate of MCs using a similar strategy to that for mapping the fate of SM fibroblasts. The transcriptional regulator WT1 is expressed by adult MCs and therefore the conditional Cre enzyme knocked into the WT1 locus was used to map MCs. Our conditional labeling strategy resulted in labeling a cohort of > 80% of all MCs. It also labeled a minor population (approximately 15%) of SM fibroblasts. In response to peritoneal injury, the cohort of somatically labeled WT1+ cells did not expand. In fact, there was a reduction in cell number. The proportion of myofibroblasts that derived from WT1-labeled cells was approximately 15%, a number consistent with these myofibroblasts deriving from the WT1-labeled SM fibroblasts in the normal adult, rather than from the cohort of WT1-labeled MCs.

Although our data did not support the transition of MCs to myofibroblasts *in vivo*, MCs were found to express *Colla1* after peritoneal injury. Therefore, the role of MCs in peritoneal fibrosis cannot be excluded because they produced



Col1a1 after injury. Although EMT results in differentiation of epithelial cells to migratory mesenchymal cells in the setting of cancer metastasis and development, recent fate mapping experiments in mice using conditional somatic recombination techniques led to a reappraisal of the importance of EMT as an explanation for the appearance of myofibroblasts in multiple organs as well as to a new appreciation for discrete mesenchymal cells known as resident fibroblasts or pericytes as the major origin of myofibroblasts in many tissues, including the liver, muscle, skin, intestine, lung, spinal cord, and kidney^{26, 27, 64, 67-71}. Our studies stand in contrast with previous studies that reported MCs as an important source of peritoneal myofibroblasts^{9, 11, 24, 72}; rather, our studies support SM fibroblasts as the major source of myofibroblasts during peritoneal fibrosis. Our studies represent an advance of the previous studies that analyzed MC responses to peritoneal injury for two reasons. First, we used conditional labeling of cohorts of cells with robust Cre-expressing mouse lines, whereas previous studies used less robust methods including immunohistochemistry and cell culture *in vitro*. Second, we described a poorly appreciated population of SM fibroblasts that were not

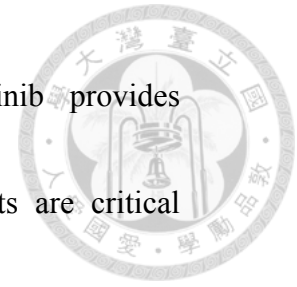
considered in those previous studies. Although variations in experimental conditions cannot be excluded as a cause for differing results, our mapping strategy provides the most robust approach reported to date.



Some studies thought that circulating fibrocytes are also the origin of myofibroblasts. However, our study did not support this. Chimeric mice of parabiosis and bone marrow transplantation are so far most common used animal models to study circulating fibrocytes, such as renal fibrosis ^{26, 63}, or acute myocardia injury ⁶². In chimeric model, these Coll1a1-GFP+ cells could be transferred successfully into recipient mice and parabiont mice. Only few Coll1a1-GFP+; CD45+ circulating fibrocytes were seen in fibrotic peritoneum. These Coll1a1-GFP+ fibrocytes did not express α SMA staining during peritoneal fibrosis. Our report proved that circulating fibrocytes could not transit into myofibroblasts during peritoneal fibrosis.

PDGFR β signaling by myofibroblasts was shown to be pathologic in models of kidney, liver, and lung fibrosis ^{27, 50, 73}. The restricted expression of PDGFR β to SM fibroblasts and myofibroblasts in peritoneal fibrosis suggested that PDGFR β blockade might be an attractive therapeutic strategy. Blockade of

PDGFR β signaling by the tyrosine kinase-inhibitor imatinib provides supportive evidence that SM fibroblast-derived myofibroblasts are critical cells in fibrogenesis, and provides new avenues for therapeutic discovery.



However, we emphasize that the result is far more applicable to EPS than to the vast majority of peritoneal dialysis patients in whom fibrosis is a late clinical event.

Our data indicate that the injured peritoneum was remesothelialized by surviving MCs, not by SM fibroblasts. These studies did not support WT1-labeled SM fibroblasts as stem cells for mesothelial repair. This mechanism of mesothelial regeneration is similar to kidney epithelial regeneration, which was previously shown to be from intrinsic surviving tubular epithelial cells rather than epithelial progenitors. Because MCs express different growth factor receptors from SM fibroblasts and myofibroblasts (e.g., EGF receptor, as previously reported⁷⁴), interventions that activate specific receptor signaling for mesothelial repair may promote more effective remesothelialization after injury.



We found that numerous macrophages were recruited in injured peritoneum.

We found that thickness of fibrotic peritoneum was reduced following

macrophages were depleted. At the same time, the number of myofibroblasts

was also reduced when macrophages were depleted. Our results suggested that

macrophages could cross talk with SM fibroblasts during peritoneal fibrosis.

We thought that macropahges could stimulate SM fibroblasts to transit into

myofibroblasts through secreting cytokines or growth factors.

In response to distinct inflammatory signals, macrophages can differentiate

into classically activated (M1) macrophages or other activated macrophages

often referred to under an umbrella term 'alternatively activated' or 'M2'

macrophages. Classically activated M1 macrophages are stimulated by

Toll-like receptor (TLR) ligands and Th1 immune factors, such as IFN- γ , and

mediate host defense from various pathogens including bacteria, viruses or

protozoa. In contrast, alternatively activated M2 macrophages are considered

to have anti-inflammatory functions and promote tissue repair and remodeling

M2 macrophages produce growth factors to stimulate fibroblasts, including TGFβ1, PDGF and insulin-like growth factor 1 (IGF-1)^{76, 77}.

Macrophage-derived TGFβ1 contributes to tissue regeneration and wound repair by promoting fibroblast differentiation into myofibroblasts, by enhancing expression of TIMPs that block the degradation of ECM and by directly stimulating the synthesis of interstitial fibrillar collagens in myofibroblasts^{78, 79}. Macrophage-derived PDGF also stimulates the proliferation of activated ECM-producing myofibroblasts^{74, 80} [ENREF 78](#).

Bellón et al.⁸¹ have previously reported on the phenotype of peritoneal effluent macrophages and demonstrated the capacity of CD163+CD14+ cells to stimulate proliferation of human fibroblasts. The capacity of peritoneal macrophages to stimulate fibroblast proliferation correlated strongly with chemokine ligand 18 (CCL18) mRNA levels. Additionally, they showed that an increased concentration of CCL18, a pro-fibrotic chemokine produced by M2 macrophages, was found in the peritoneal effluent of patients who later developed EPS.

Chapter 5. Conclusion and future prospects



In conclusion, we used comprehensive genetic lineage analysis to clarify the role of MCs and SM fibroblasts in the repair of mesothelium and generation of myofibroblasts during peritoneal fibrosis. And we use two chimeric models to study circulating fibrocytes during peritoneal fibrosis and found circulating fibrocytes did not transit into myofibroblasts. We provide lineage tracing evidence that SM fibroblasts are the major myofibroblast precursors in peritoneal fibrosis and surviving MCs are the principal cells for remesothelialization after injury (Figure 29A).

We also used genetic lineage analysis to clarify the role of macrophages during peritoneal fibrosis. And we found that macrophages could stimulate SM fibroblasts to transit into myofibroblasts in injured peritoneum (Figure 29B).

However, we still need to clarify the process of macrophages stimulate SM fibroblasts to transit into myofibroblasts.

These findings need to be recapitulated in more clinically relevant models. We need clarify EMT and the role of MCs during peritoneal fibrosis. Now we are generating transgenic mice for specific markers of MCs. Then we could

specifically deplete MCs and SM fibroblasts during peritoneal fibrosis and survey their functions.



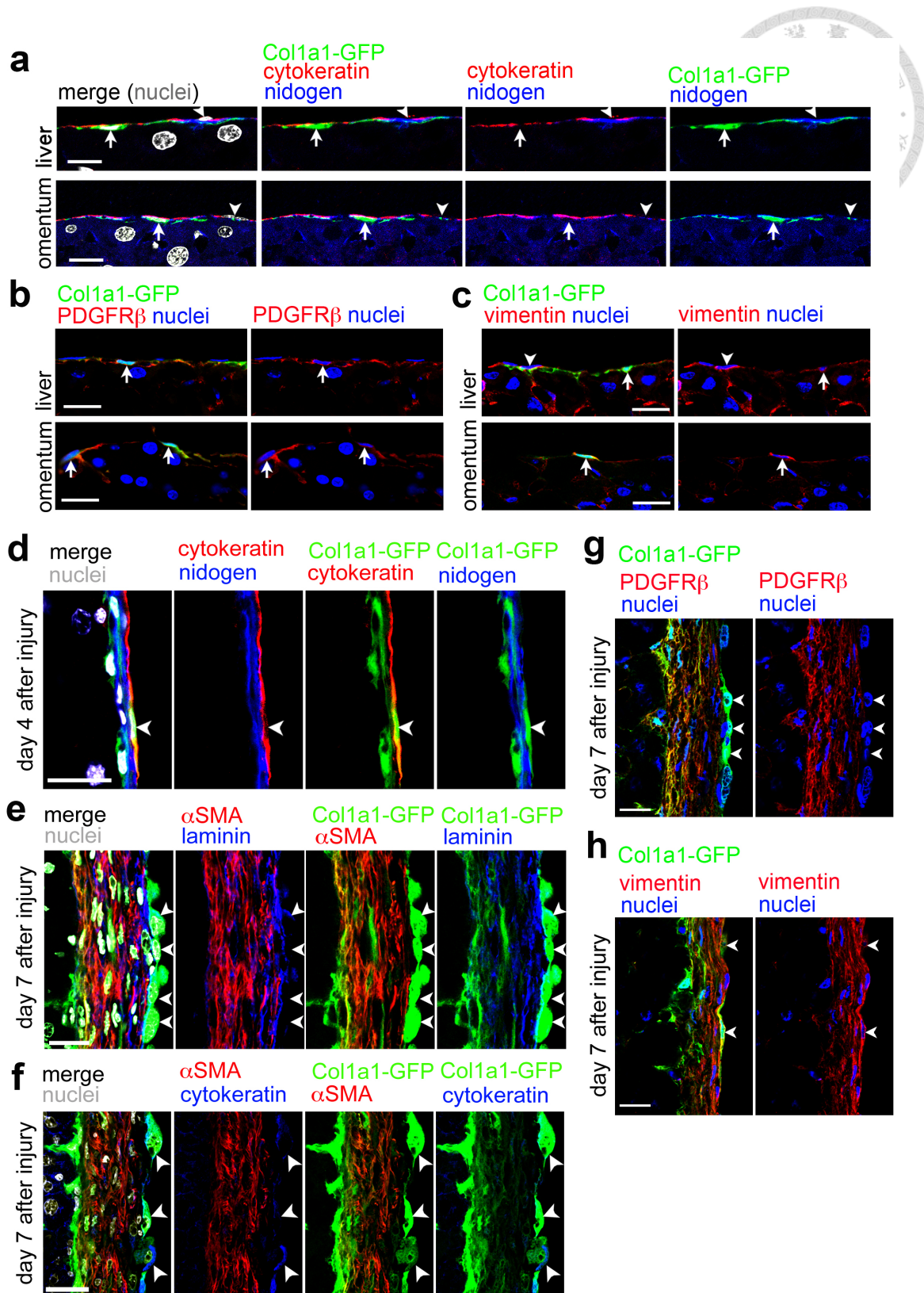
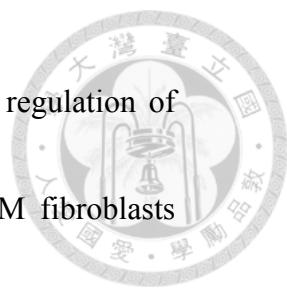


Figure 1

Col1a1-GFP identifies collagen-producing cells in normal and injured peritoneum.



(A) Collagen-producing cells expressing enhanced GFP under the regulation of the *collagen type I (α1) (Colla1)* promoter and enhancers are SM fibroblasts (arrows), not cytokeratin+ MCs (arrowheads), in normal peritoneum of *Colla1-GFP^{Tg}* mice. (B and C) *Colla1-GFP^{Tg}* SM fibroblasts (arrows) express PDGFR β and vimentin in normal peritoneum. Cells (arrowheads) above *Colla1-GFP^{Tg}* SM fibroblasts, suggesting MCs are PDGFR β - and weak vimentin+. (D) Cell numbers of *Colla1-GFP^{Tg}* collagen- producing cells and thickness of the nidogen+ scar in *Colla1-GFP^{Tg}* mice increase within 4 days after intraperitoneal injection of hypochlorite. Cytokeratin+ MCs after hypochlorite injury (arrowheads) also express *Colla1-GFP*. (E) Myofibroblasts, characterized by α SMA+ and *Colla1-GFP^{Tg}* coexpression, accumulate in the thickened laminin+ scar 7 days after hypochlorite injury. *Colla1-GFP^{Tg}* cells on the peritoneal surface, suggesting injured MCs (arrowheads), do not express α SMA. (F) Cytokeratin+ MCs (arrowheads) express *Colla1-GFP*, not α SMA, 7 days after hypochlorite injury. (G) *Colla1-GFP^{Tg}* cells on the peritoneal surface, suggesting injured MCs (arrowheads), do not express PDGFR β 7 days after hypochlorite injury. (H) Vimentin is expressed in *Colla1-GFP^{Tg}* cells 7 days after hypochlorite

injury. Arrowheads indicate Col1a1-GFP+ cells on the peritoneal surface, suggesting injured MCs. All images are taken at the original magnification from the peritoneal covering of the liver unless otherwise specified. Bar, 20 μ m.

Original magnification, x630.



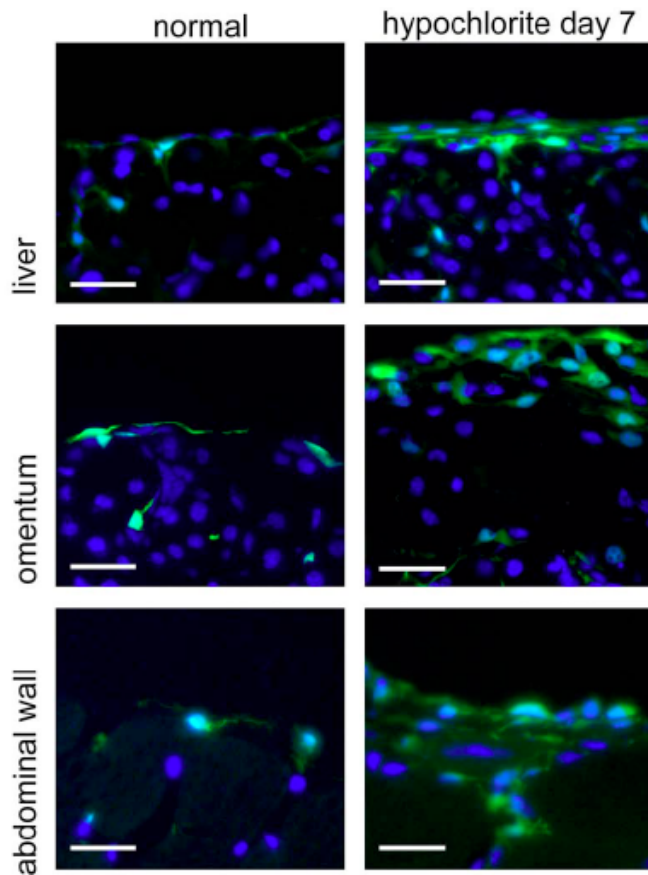


Figure 2

Colla1-GFP+ cells expand in the peritoneum of *Colla1GFP^{Tg}* mice 7 days after hypochlorite injury. Magnification x400. Scale bar = 25 μ m.

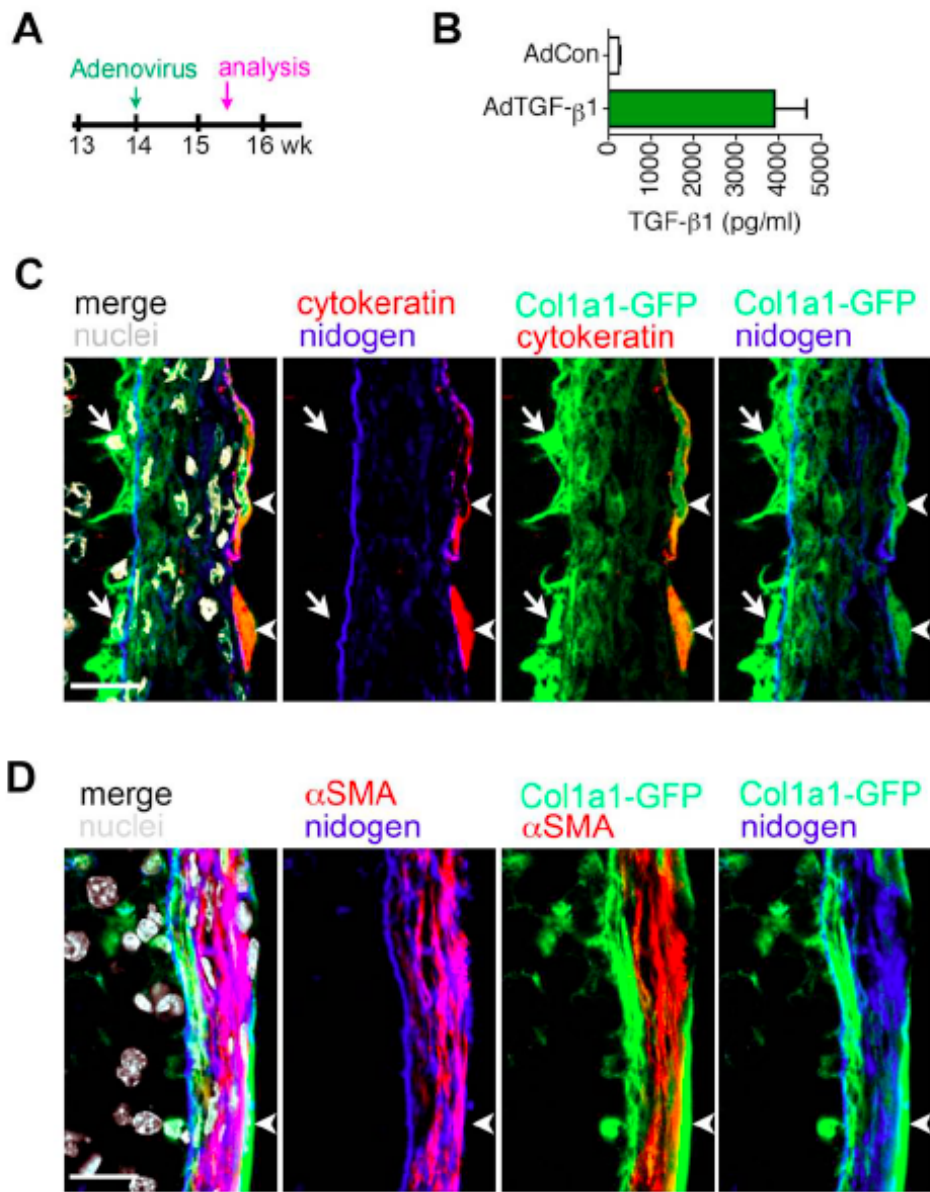


Figure 3

Colla1-GFP⁺ cells expand in the peritoneum of *Colla1-GFP^{Tg}* mice 10 days after intraperitoneal injection of TGF- β 1-producing adenovirus. **(A)** Experimental schema for adult mice with intraperitoneal injection of adenovirus expressing TGF- β 1

(AdTGF- β 1) or control virus (AdCon). Mice are analyzed 10 days after virus injection. **(B)** Ten days after adenovirus injection, mice with AdTGF- β 1 have increased concentration of total TGF- β 1 in the peritoneal effluent (n = 6/group). **(C)**

In addition to Col1a1-GFP+ cells within and beneath thickened nidogen+ scar, cytokeratin+ MCs (arrowheads) also express Col1a1-GFP. Arrows indicate SM fibroblasts. **(D)** α SMA+;Col1a1-GFP+ myofibroblasts accumulate within thickened nidogen+ scar. The Col1a1-GFP+ cells (arrowhead) on the peritoneal surface do not express α SMA, suggesting injured MCs. Magnification x630. Scale bar = 20 μ m.

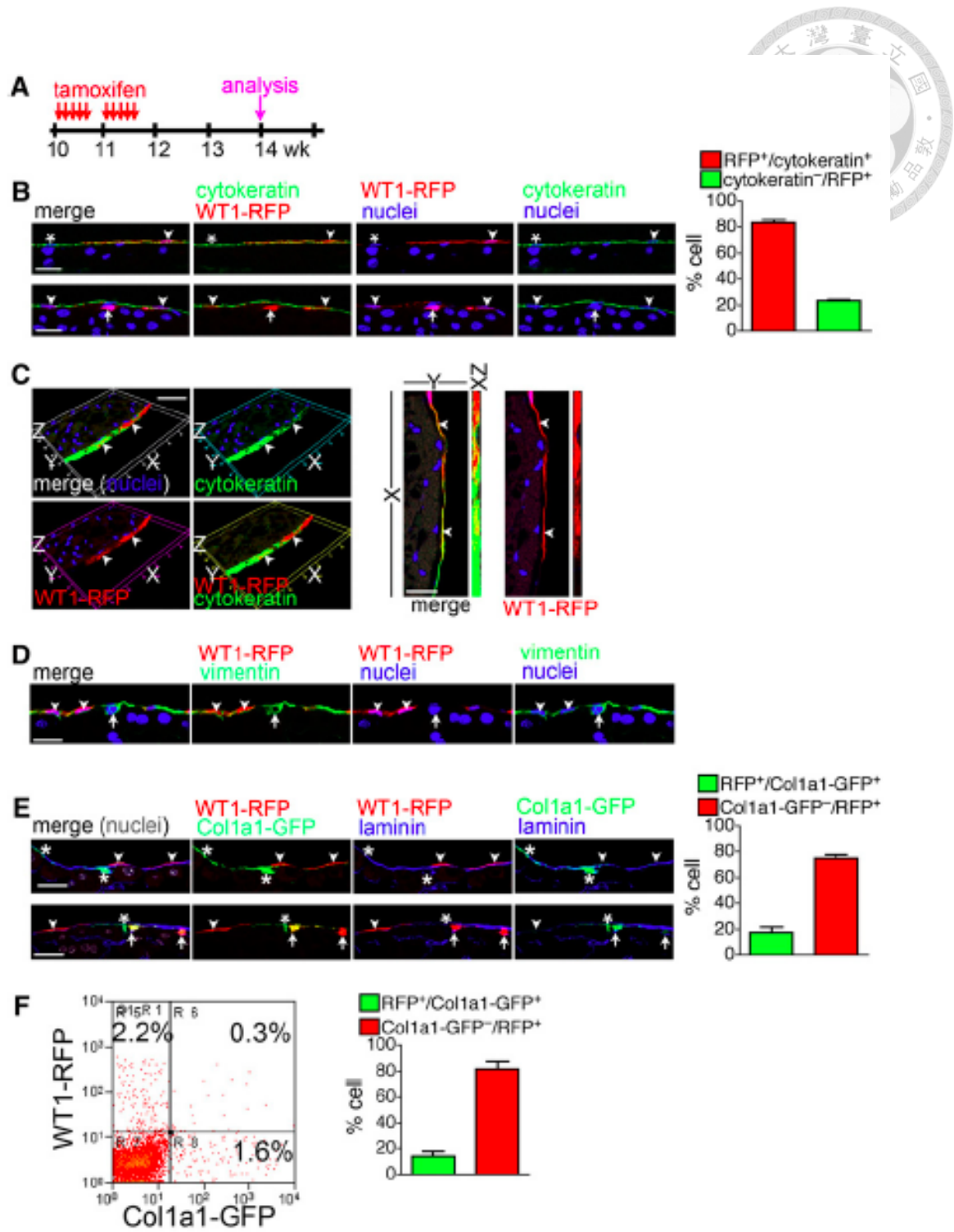
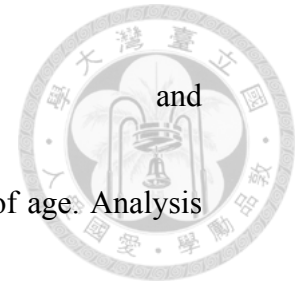


Figure 4

WT1 expression in the adult peritoneum enables efficient labeling of MCs as well as a minor population of SM fibroblasts. (A) Experimental schema for cohort

labeling in $WT1^{CreERT2/+};ROSA26^{fstdTomato}$ and

$WT1^{CreERT2/+};ROSA26^{fstdTomato};Colla1-GFP^{Tg}$ mice from 10 weeks of age. Analysis



is performed on the peritoneal covering of liver 2 weeks after cohort labeling. (B)

Cytokeratin+;WT1-RFP+ (arrowheads) and cytokekeratin+;WT1-RFP-MCs

(asterisks) are shown in normal peritoneum of $WT1^{CreERT2/+};ROSA26^{fstdTomato}$ mice.

Cytokeratin-;WT1-RFP+ cells (arrows) are occasionally seen. The graph shows the

percentage of cytokekeratin+ MCs labeled with WT1-RFP and the percentage of

WT1-RFP+ cells without cytokekeratin expression (mean±SEM, n=6). (C)

Three-dimensional images with XZ stacks show cytokekeratin+;WT1-RFP+ MCs

(arrowheads) on the surface of normal peritoneum of $WT1^{CreERT2/+};ROSA26^{fstdTomato}$

mice. (D) Vimentin is expressed by both WT1-RFP+ cells (arrowheads, suggesting

MCs) and WT1-RFP- cells (arrows, suggesting SM fibroblasts) in normal


peritoneum of $WT1^{CreERT2/+};ROSA26^{fstdTomato}$ mice. (E) WT1-RFP+;Coll1a1-GFP-

MCs (arrowheads) and WT1-RFP-;Coll1a1-GFP+ SM fibroblasts (asterisks)

separated by the laminin+ basal lamina are shown in normal peritoneum of

$WT1^{CreERT2/+};ROSA26^{fstdTomato};Colla1-GFP^{Tg}$ mice. WT1-RFP+;Coll1a1-GFP+ SM

fibroblasts (arrow) are occasionally seen. The graph shows the percentage of



Coll1a1-GFP⁺ SM fibroblasts labeled with WT1-RFP and the percentage of WT1-RFP⁺ MCs without Coll1a1-GFP expression (n=6). (F) Representative plot shows FACS analysis of peritoneal cells prepared from *WT1^{CreERT2/+}; ROSA26^{fltdTomato}; Coll1a1-GFP^{Tg}* mice after intraperitoneal retention of trypsin-EDTA. The graph shows the percentage of Coll1a1-GFP⁺ SM fibroblasts labeled with WT1-RFP and the percentage of WT1-RFP⁺ MCs without Coll1a1-GFP expression (n=3). Bar=20 μ m. Original magnification, x630.

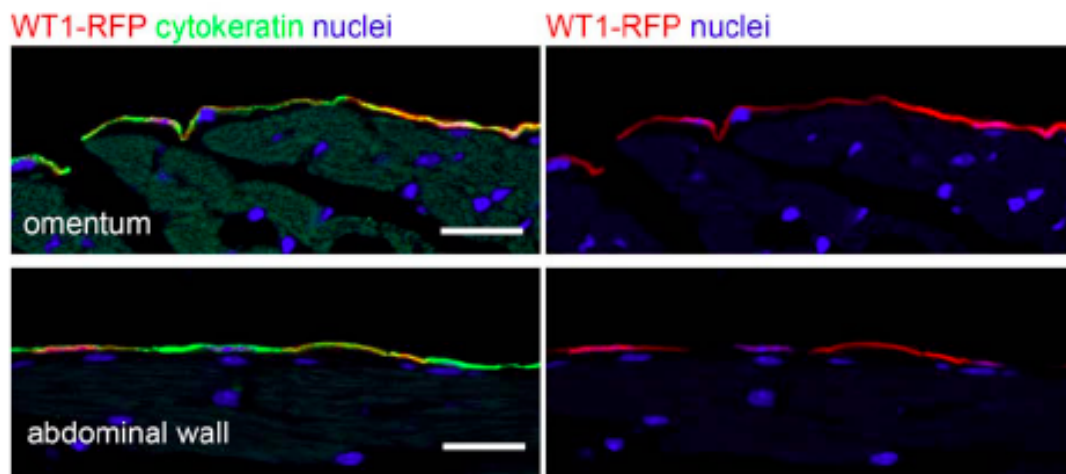


Figure 5

WT1 expression in the adult peritoneum enables efficient labeling of cytokeratin+ MCs. Schema indicating cohort-labeling of WT1-expressing cells in normal peritoneum of $WT1^{CreERT2/+}; ROSA26^{fstdTomato}$ mice is described in Figure 4A.

Magnification x630. Scale bar = 20 μm .

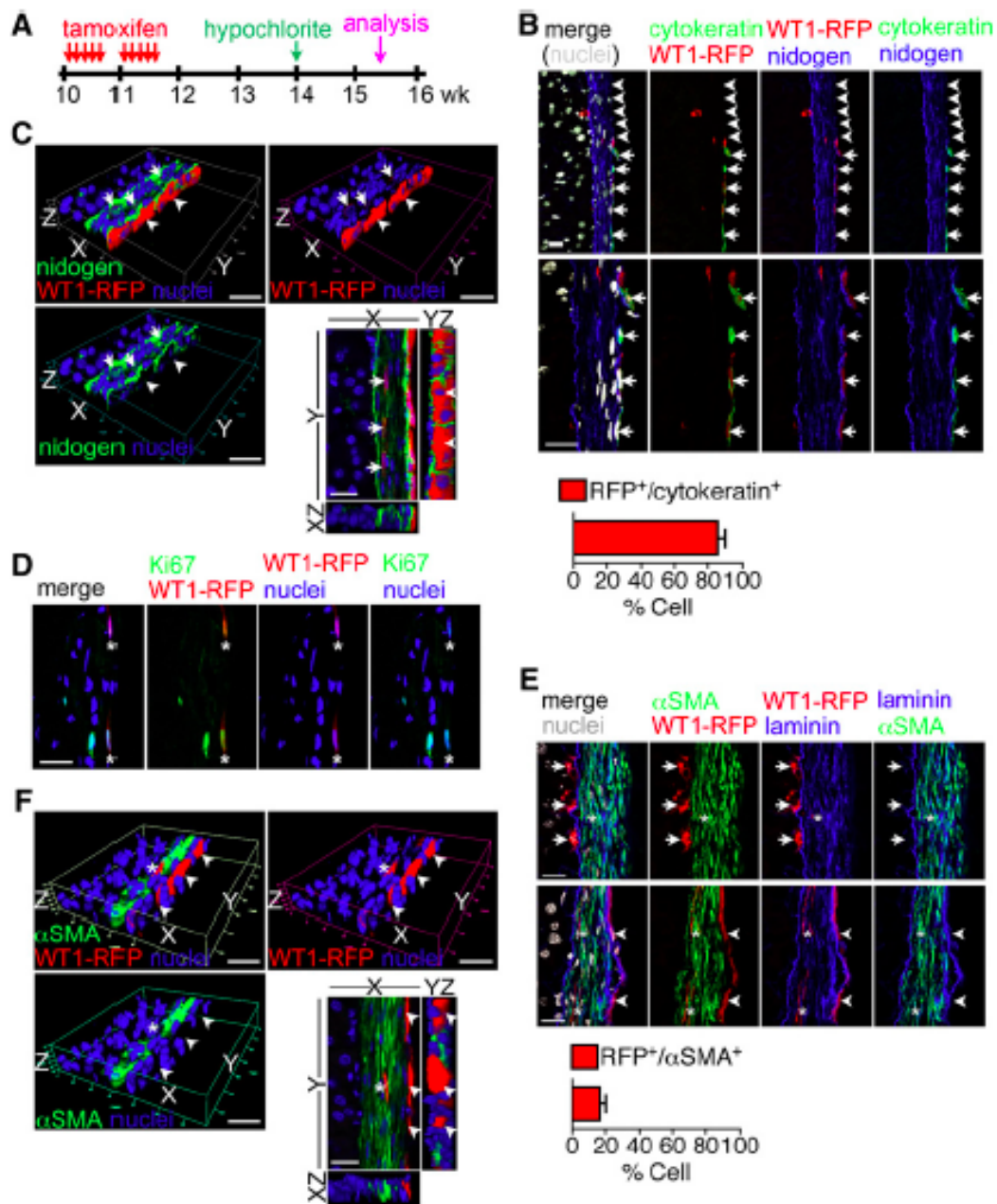
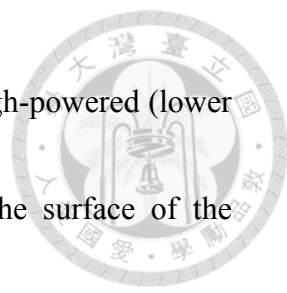


Figure 6

Injured peritoneum is remesothelialized by surviving MCs. (A) The experimental schema shows cohort labeling followed by hypochlorite injury in *WT1^{CreERT2/+}; ROSA26^{stdTomato}* mice. Analysis is performed on the peritoneal covering



of liver 10 days after injury. (B) Low-powered (upper panel) and high-powered (lower panel) images show cytokeratin⁺;WT1-RFP⁺ MCs (arrows) on the surface of the thickened nidogen⁺ scar. Arrowheads indicate the denuded peritoneum. Only rare WT1-RFP⁺ cells are noted within or beneath the nidogen⁺ scar. The graph beneath shows the percentage of cytokeratin⁺ MCs labeled with WT1-RFP at this time point (n=6). (C) Three-dimensional images with YZ and XZ stacks show WT1-RFP⁺ MCs (arrowheads) on the surface of the thickened nidogen⁺ scar. Only rare WT1-RFP⁺ cells (arrows) are noted within the nidogen⁺ scar. (D) Active proliferation of WT1-RFP⁺ MCs after injury is shown by Ki67 expression (asterisks). (E) Images show that most of WT1-RFP⁺ cells are found above (MCs, arrowheads) or below (SM fibroblasts, arrows) the thickened laminin⁺ scar after injury. Extremely rare WT1-RFP⁺;αSMA⁺ myofibroblasts (asterisks) are within the thickened laminin⁺ scar. The graph beneath shows the percentage of αSMA⁺ myofibroblasts coexpressing WT1-RFP (n=6). (F) Three-dimensional images with YZ and XZ stacks show that most of WT1-RFP⁺ cells are on the peritoneal surface (MCs, arrowheads) after injury. WT1-RFP⁺;αSMA⁺ myofibroblasts (asterisks) are extremely rare. Bar= 20μm. Original magnification, x200 in B upper panel; x630 in B lower panel and C–F.

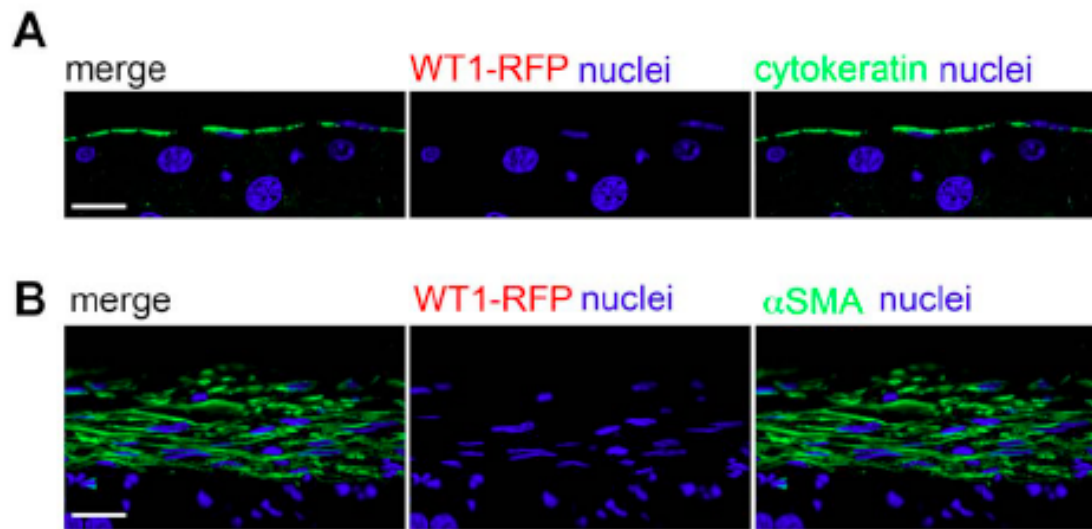


Figure 7

No labeling of WT1-expressing cells with RFP occurs in the peritoneum of *WT1^{CreERT2/+}; ROSA26^{stdTomato}* mice in the absence of tamoxifen activation of CreERT2 fusion protein. (A) Normal peritoneum. (B) Peritoneum 10 days after hypochlorite injury. Magnification x630. Scale=20um.

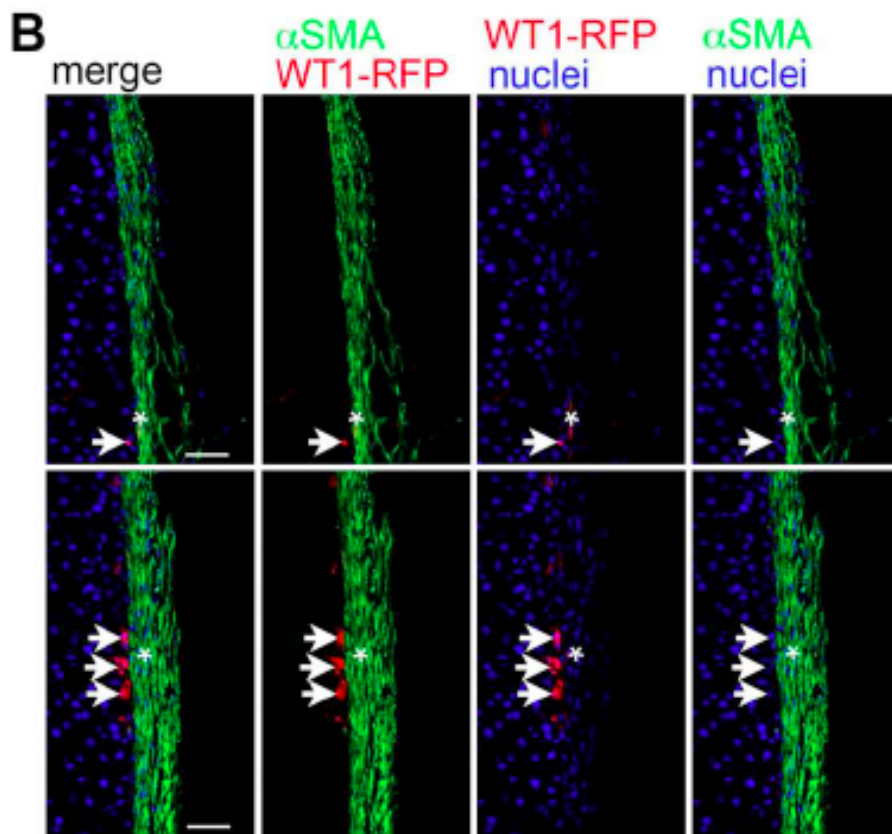
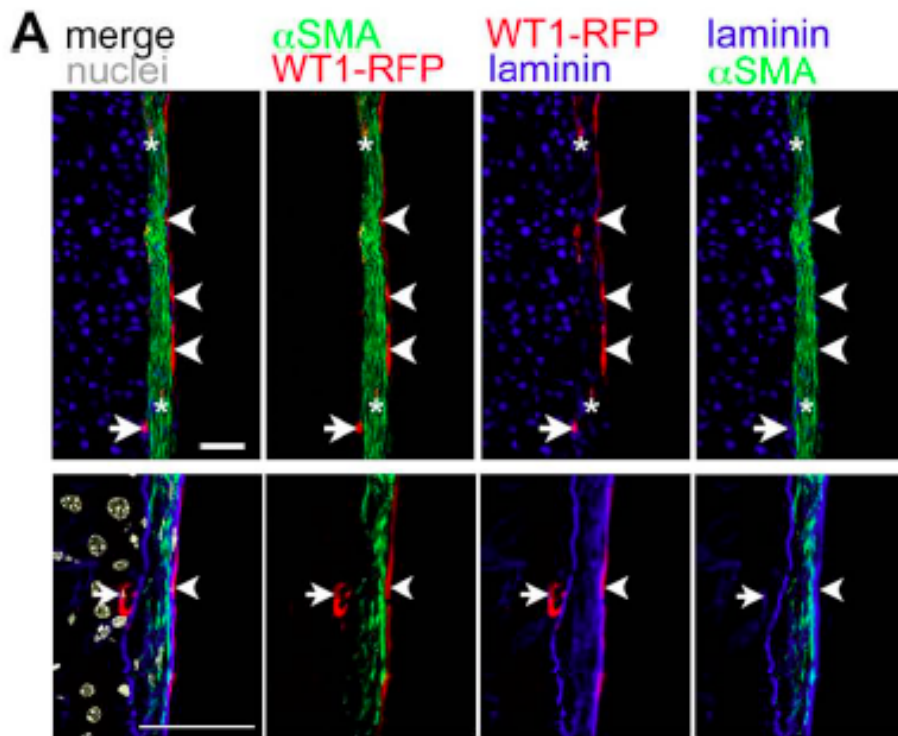




Figure 8

Cohort-labeled WT1-RFP+ cells contribute little to the appearance of myofibroblasts in peritoneum after hypochlorite injury. **(A)** Low-powered (upper panel, magnification x200) and high-powered (lower panel, magnification x 630) images showing that most of WT1-RFP+ cells are found above (MCs, arrowheads) or below (SM fibroblasts, arrows) the thickened laminin+ scar day 7 after hypochlorite injury. Extremely rare WT1-RFP+; α SMA+ cells (asterisks) are within the thickened laminin+ scar. **(B)** In thickened peritoneum devoid of coverage of WT1-RFP+ MCs on the surface, low-powered (magnification x200) images showing most WT1-RFP+ cells are found beneath (SM fibroblasts, arrows) the accumulation of α SMA+ myofibroblasts. Rarely, WT1-RFP+ cells (asterisk) are found within the accumulation of α SMA+ myofibroblasts. The percentage of α SMA+ cells expressing WT1-RFP is 15.9% as described in Figure 6E. Scale bar = 50 μ m

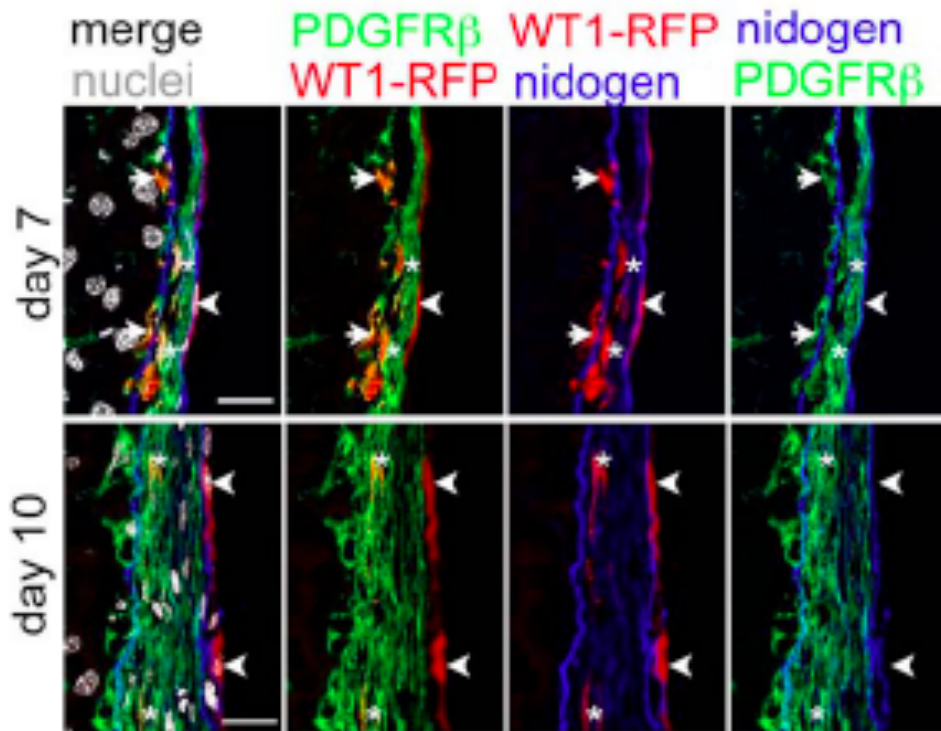


Figure 9

WT1-RFP+ cells within (asterisks) and beneath (arrows) the thickened nidogen+ scar, not WT1-RFP+ MCs (arrowheads) on the peritoneal surface, express PDGFR β .

Magnification x630. Scale bar = 20 μ m.

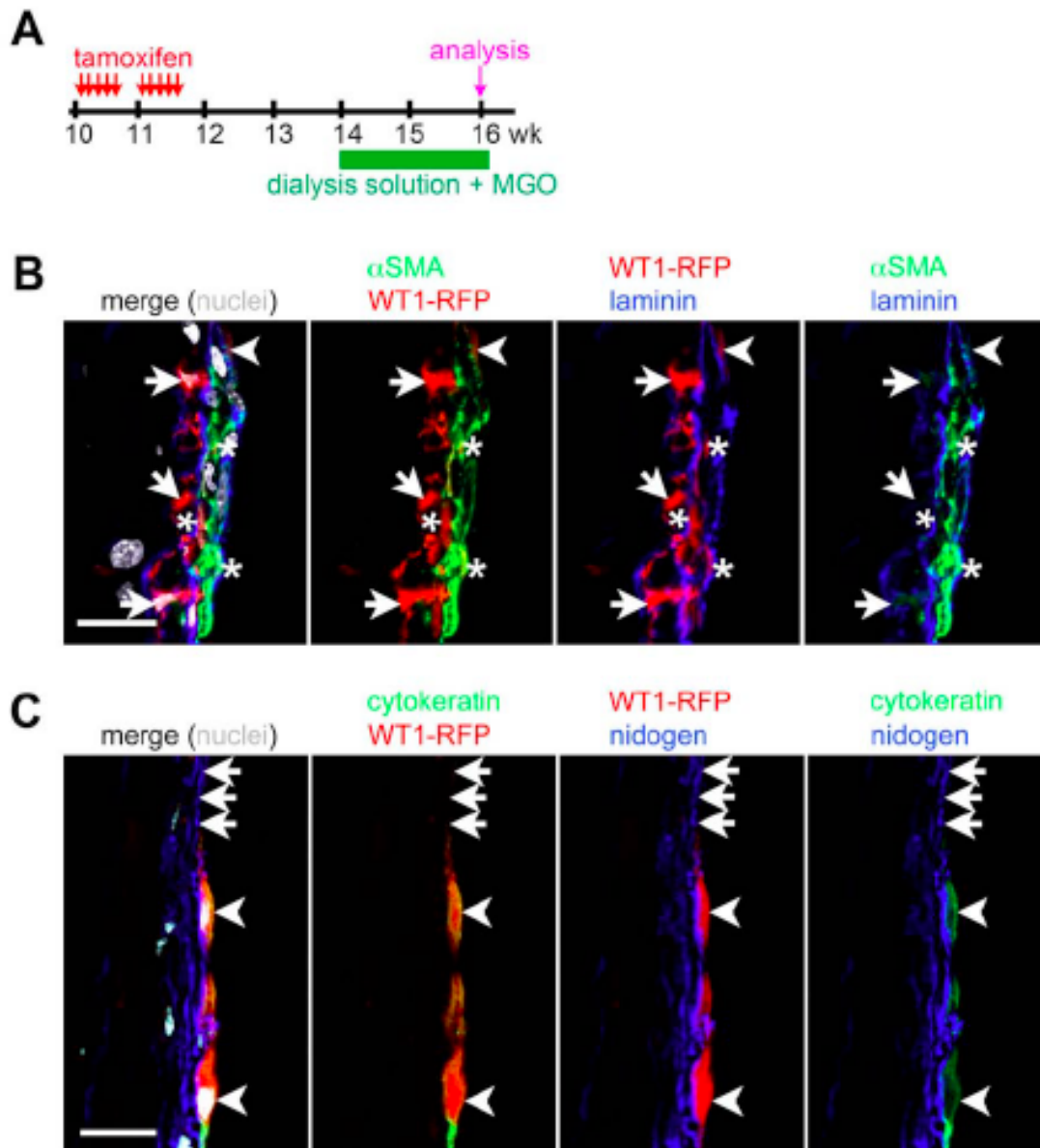
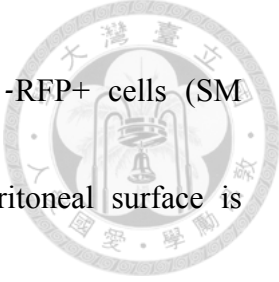


Figure 10

WT1-RFP+ cells contribute little to the appearance of myofibroblasts in peritoneum after injury induced by hyperglycemic dialysis solution. (A) Experimental schema for cohort-labeling of WT1-expressing cells prior to injury and induction of peritoneal injury by dialysis solution containing 4.25% glucose and 40 mM methylglyoxal (MGO)



in *WT1^{CreERT2/+};ROSA26^{stdTomato}* mice. **(B)** The majority of WT1-RFP⁺ cells (SM fibroblasts, arrows) lie beneath thickened laminin⁺ scar. The peritoneal surface is partially covered by WT1-RFP⁺ cells (MCs, arrowhead). Occasional WT1-RFP⁺ cells (asterisks) are found in 16.5% of α SMA⁺ myofibroblasts within thickened laminin⁺ scar. **(C)** Cytokeratin⁺ MCs are WT1-RFP⁺ on the peritoneal surface (arrowheads). Arrows indicate area of peritoneal surface without cytokeratin⁺ or WT1-RFP⁺ MCs.

Magnification x630. Scale bar = 20 μ m.

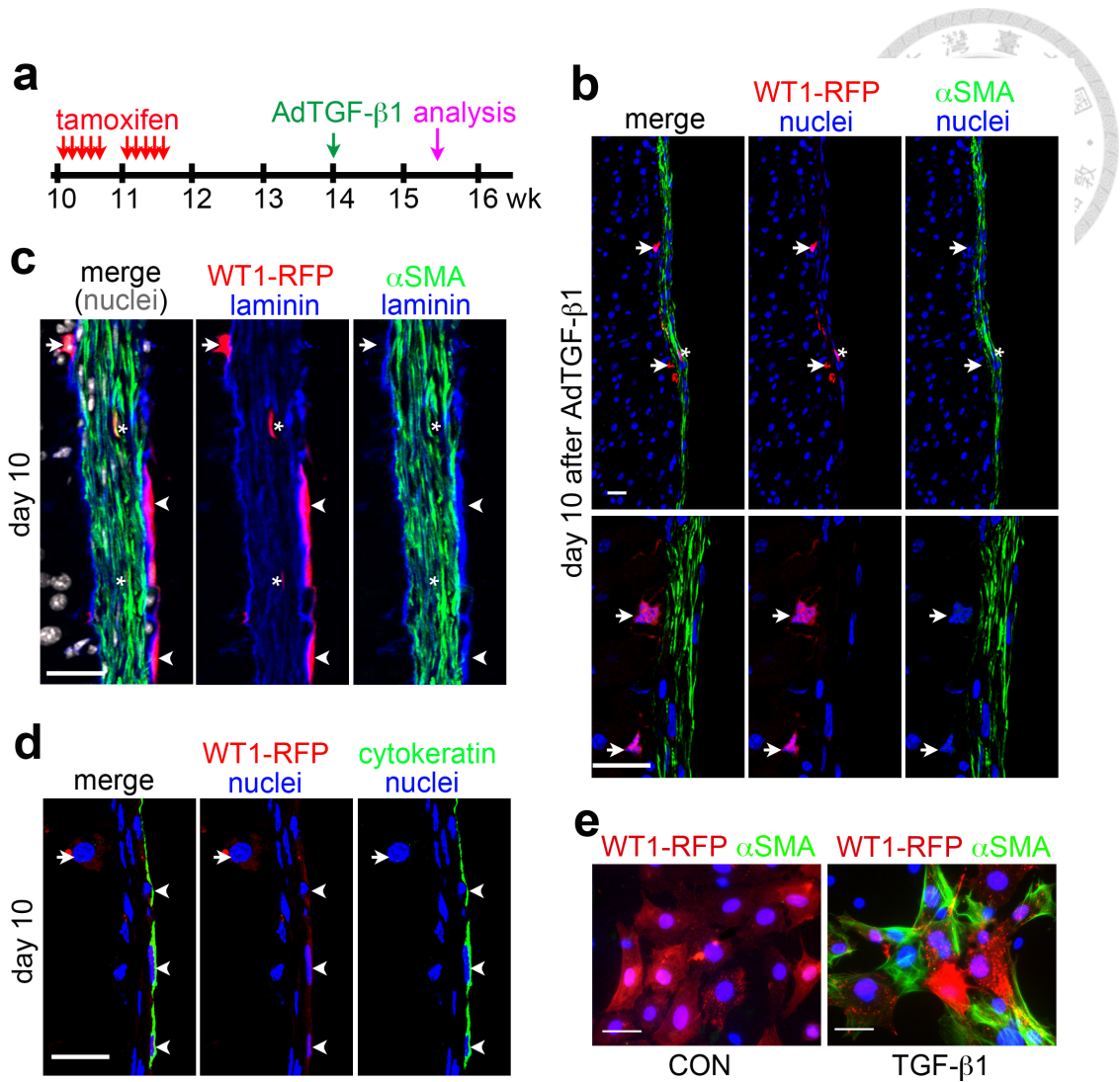



Figure 11

Overexpression of TGF- β 1 in the peritoneum induces peritoneal fibrosis in *WT1^{CreERT2/+};ROSA26^{stdTomato}* mice. (A) Experimental schema for cohort labeling in *WT1^{CreERT2/+};ROSA26^{stdTomato}* mice followed by injection of AdTGF- β 1 transgenic expression. Analysis is performed on the peritoneal covering of liver 10 days after AdTGF- β 1. (B) Low-powered (upper panel) and high-powered images (lower panel)



show large areas of the peritoneal surface devoid of WT1-RFP+ MCs. Occasional WT1-RFP+ cells (SM fibroblasts, arrows) are found beneath the accumulated α SMA+ myofibroblasts. Rare WT1-RFP+; α SMA+ myofibroblasts (asterisks) are identified. (C) Surviving WT1-RFP+ MCs (arrowheads) on the surface of injured peritoneum do not express α SMA. Rare WT1-RFP+; α SMA+ myofibroblasts (asterisks), amounting to 14.6% of α SMA+ myofibroblasts, are seen exclusively within the thickened laminin+ scar. WT1-RFP+; α SMA–SM fibroblast (arrows) is located beneath the scar. (D) Images show WT1-RFP+;cytokeratin+ MCs on the peritoneal surface after AdTGF- β 1 (arrowheads). A WT1-RFP+;cytokeratin– SM fibroblast (arrows) is seen. (E) MCs isolated and cultured from peritoneal WT1-RFP+;PDGFR β -APC– cells of *WT1^{CreERT2/+};ROSA26^{stdTomato}* mice after cohort labeling lack expression of α SMA in culture medium alone (CON), whereas activate expression of α SMA in the presence of TGF- β 1 for 2 days. Scale bar, 20 μ m. Original magnification, x200 in B upper panel; x630 in B lower panel and C–E.

WT1-RFP⁺;PDGFR β ⁻ MCs

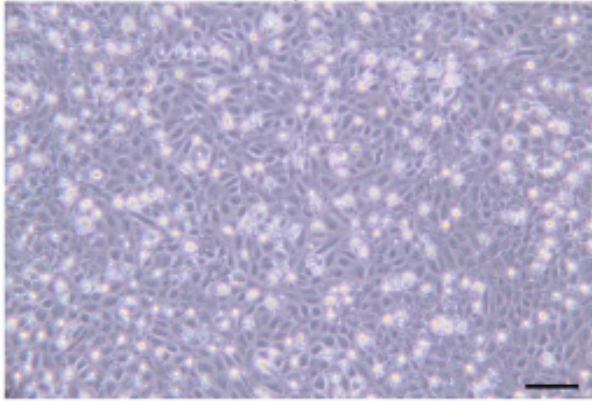


Figure 12

Bright-field image shows primary cultured MCs at passage 2. Magnification x200.

Scale bar = 25 μ m.

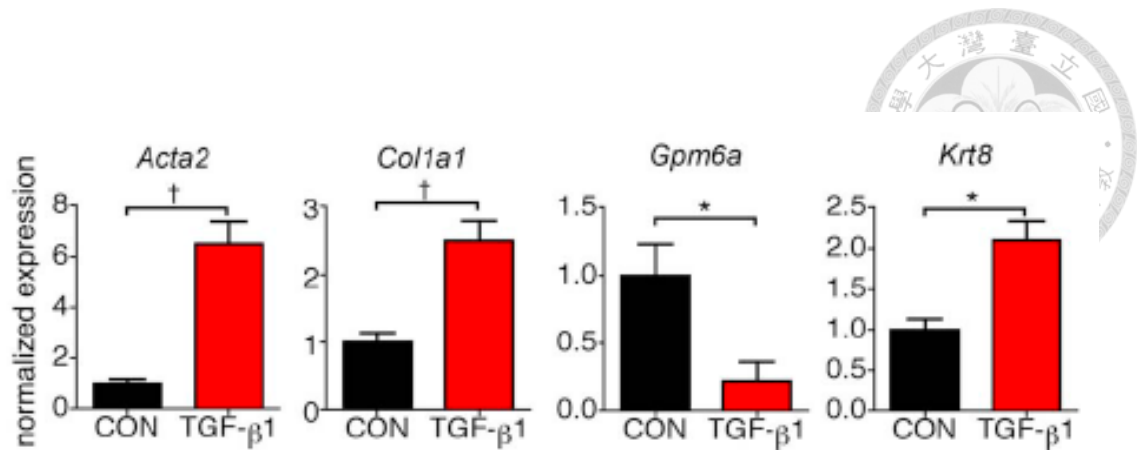


Figure 13

TGF-β1 upregulates the mesenchymal genes of cultured MCs. Primary WT1-RFP+;PDGFRβ-APC- MCs are cultured in the presence or absence of TGF-β1 for 24 hours. Gene expression is assessed by quantitative polymerase chain reaction (QPCR). TGF-β1 induces the expression of mesenchymal markers (*Acta2* and *Col1a1* encoding αSMA and α1 chain of collagen-I respectively). TGF-β1 downregulates the gene expression of MC marker *Gpm6a* (encoding glycoprotein m6a). However *Krt8* (encoding cytokeratin8) was upregulated by TGF-β1. The expression levels are normalized by *Gapdh* (encoding glyceraldehydes 3-phosphate dehydrogenase) and expressed as mean +/- s.e.m. (n = 3). *P < 0.05, †P < 0.01.

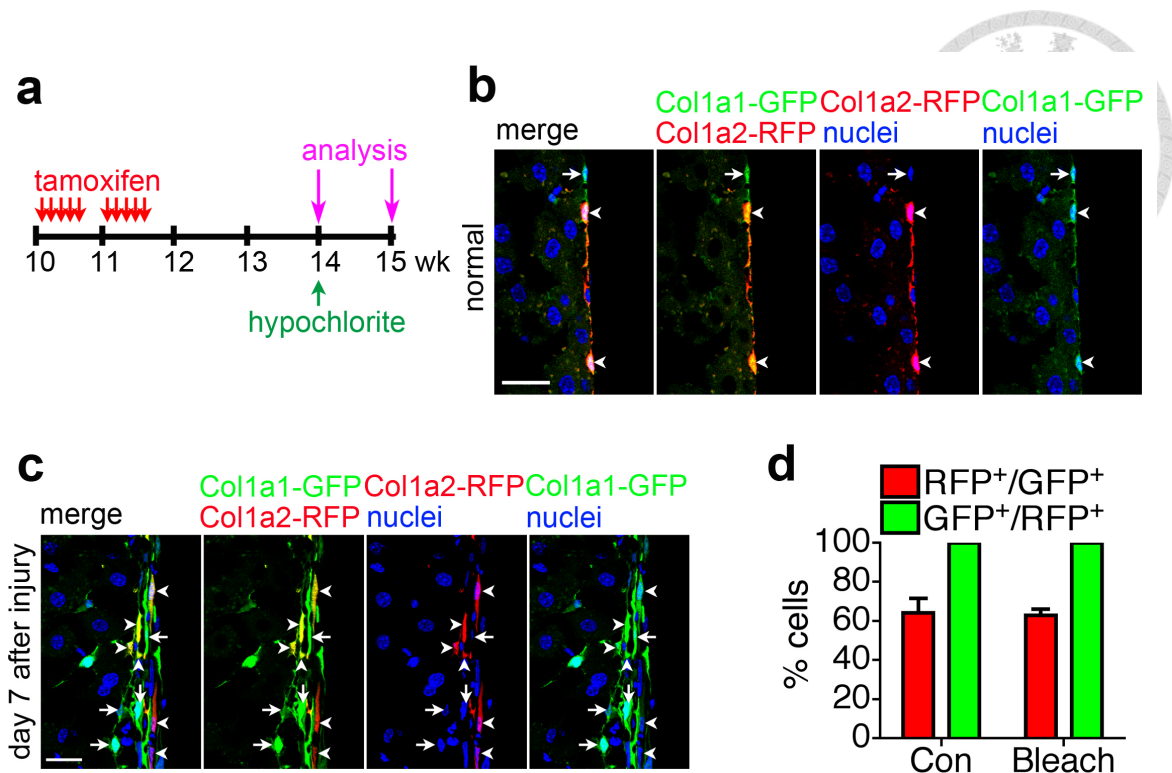
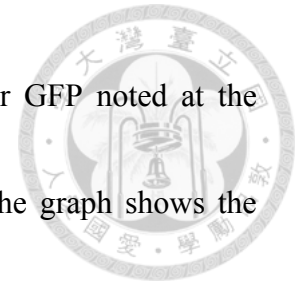


Figure 14

SM fibroblasts are the major precursors of collagen-producing cells during peritoneal fibrosis after hypochlorite injury. (A) Experimental schema for cohort labeling of *Col1a2*⁺ cells and hypochlorite peritoneal injury in *Col1a2-CreERT^{Tg}; ROSA26^{fstdTomato}; Col1a1-GFP^{Tg}* mice. Analysis is performed on the peritoneal covering of liver before and 7 days after hypochlorite injury. (B and C) Images show tamoxifen-induced cohort labeling of *Col1a1-GFP*⁺ SM fibroblasts with *Col1a2-RFP* before (B) and 7 days after hypochlorite injury (C). Arrowheads and arrows indicate *Col1a1-GFP*⁺ with and without coexpression of *Col1a2-RFP*,

respectively. Numerous DAPI+ nuclei without labeling of RFP or GFP noted at the surface of normal peritoneum suggest MCs (asterisks) (B). (D) The graph shows the percentages of Col1a1-GFP+ cells that coexpress the fate reporter Col1a2-RFP and the proportion of Col1a2-RFP+ cells that coexpress Col1a1-GFP before (Con) and 7 days (Hypochlorite) after injury (n=6 per group). DAPI, 4',6-diamidino-2-phenylindole. Bar =20 μ m. Original magnification, x630.



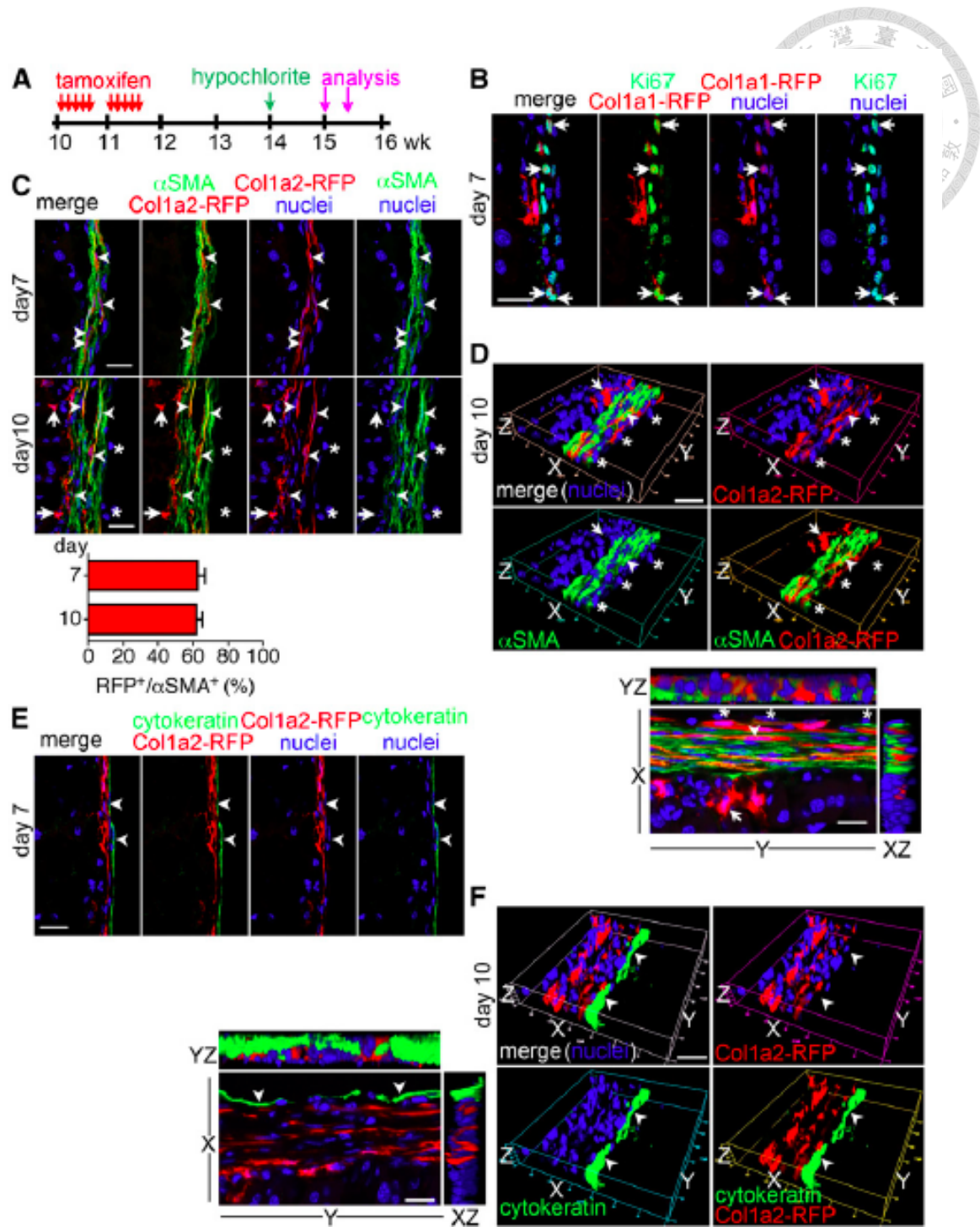
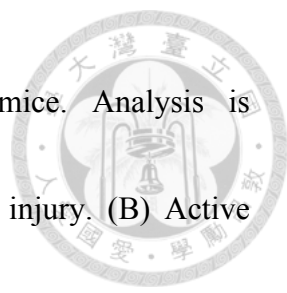


Figure 15

Col1a2-RFP+ fate-mapped SM fibroblasts are the major precursors of myofibroblasts in the peritoneum after hypochlorite injury. (A) Experimental schema for cohort labeling



and hypochlorite injury in *Colla2-CreERT^{Tg};ROSA26^{stdTomato}* mice. Analysis is performed on the peritoneal covering of liver 7 or 10 days after injury. (B) Active proliferation of *Colla2-RFP+* SM fibroblasts after injury is shown by Ki67 expression (arrows). (C) Images show numerous *Colla2-RFP+;αSMA+* myofibroblasts (arrowheads) after injury. *Colla2-RFP+;αSMA-* SM fibroblasts and *DAPI+;Colla2-RFP-;αSMA-* MCs at the peritoneal surface are indicated by arrows and asterisks, respectively. The graph beneath shows the percentage of *αSMA+* myofibroblasts coexpressing the fate marker *Colla2-RFP* (n=6 per group). (D) Three-dimensional images with YZ and XZ stacks show numerous *Colla2-RFP+;αSMA+* myofibroblasts after injury. Cells are indicated as in C. (E) Images show that cytokeratin+ MCs (arrowheads) do not express the fate marker *Colla2-RFP*. (F) Three-dimensional images with YZ and XZ stacks show numerous *Colla2-RFP+* cells beneath cytokeratin+ MCs after injury. Cytokeratin+ MCs (arrowheads) do not express the fate marker *Colla2-RFP*. DAPI, 4',6'-diamidino-2-phenylindole. Bar, 20μm. Original magnification, x630.

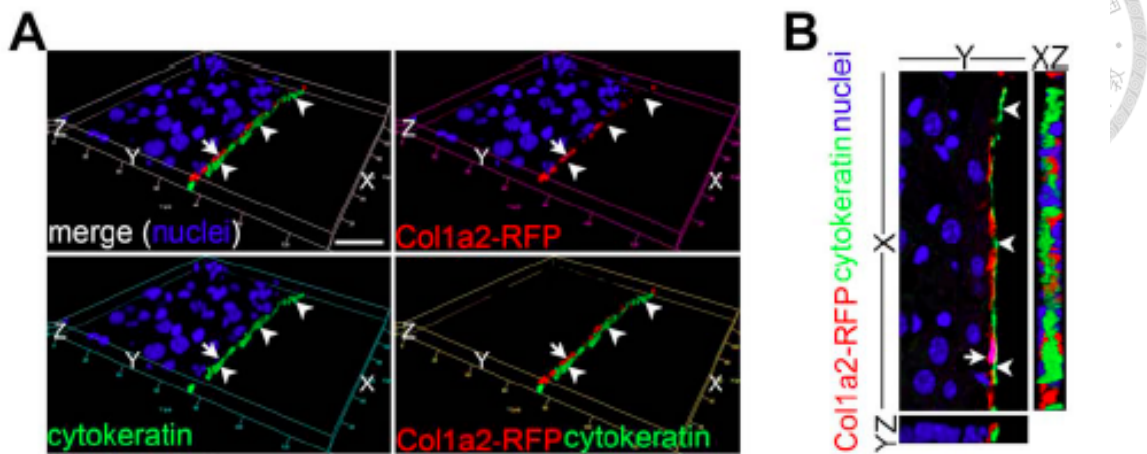


Figure 16

3D images with YZ and XZ stacks showing Col1a2-RFP+ cells are beneath cytokeratin+ MCs in normal peritoneum. Arrowheads and arrows indicate cytokeratin+ MCs and Col1a2-RFP+ SM fibroblasts respectively. Magnification x630. Scale bar = 20 μ

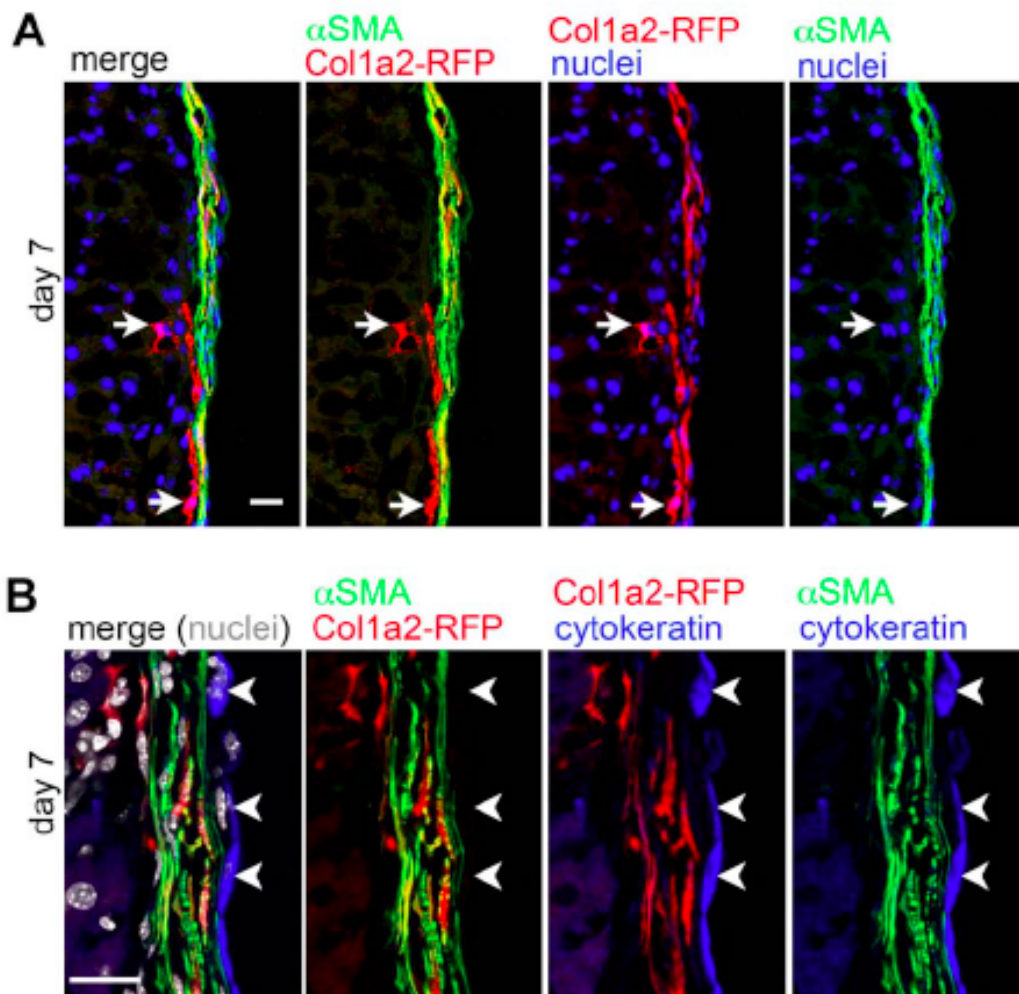


Figure 17

Cohort-labeled Col1a2-RFP+ SM fibroblasts are the major precursors of peritoneal myofibroblasts but not those of repaired mesothelium following hypochlorite injury.

Schema indicating cohort-labeling of Col1a2-expressing cells in normal peritoneum

followed by hypochlorite injury in *Col1a2CreERT^{Tg}; ROSA26^{stdTomato}* mice is described

in Figure 15A. **(A)** Low-powered images taken at 200x magnification showing numerous Coll1a2-RFP+ cells co-expressing α SMA 7 days after hypochlorite injury.

Coll1a2-RFP+; α SMA– SM fibroblasts (arrows) beneath the accumulation of Coll1a2-

RFP+; α SMA+ myofibroblasts are shown. **(B)** High-powered images taken at 630x

magnification showing numerous Coll1a2-RFP+ cells co-express α SMA, but not cytokeratin. Arrowheads indicate cytokeratin+ MCs. Scale bar = 20 μ m.



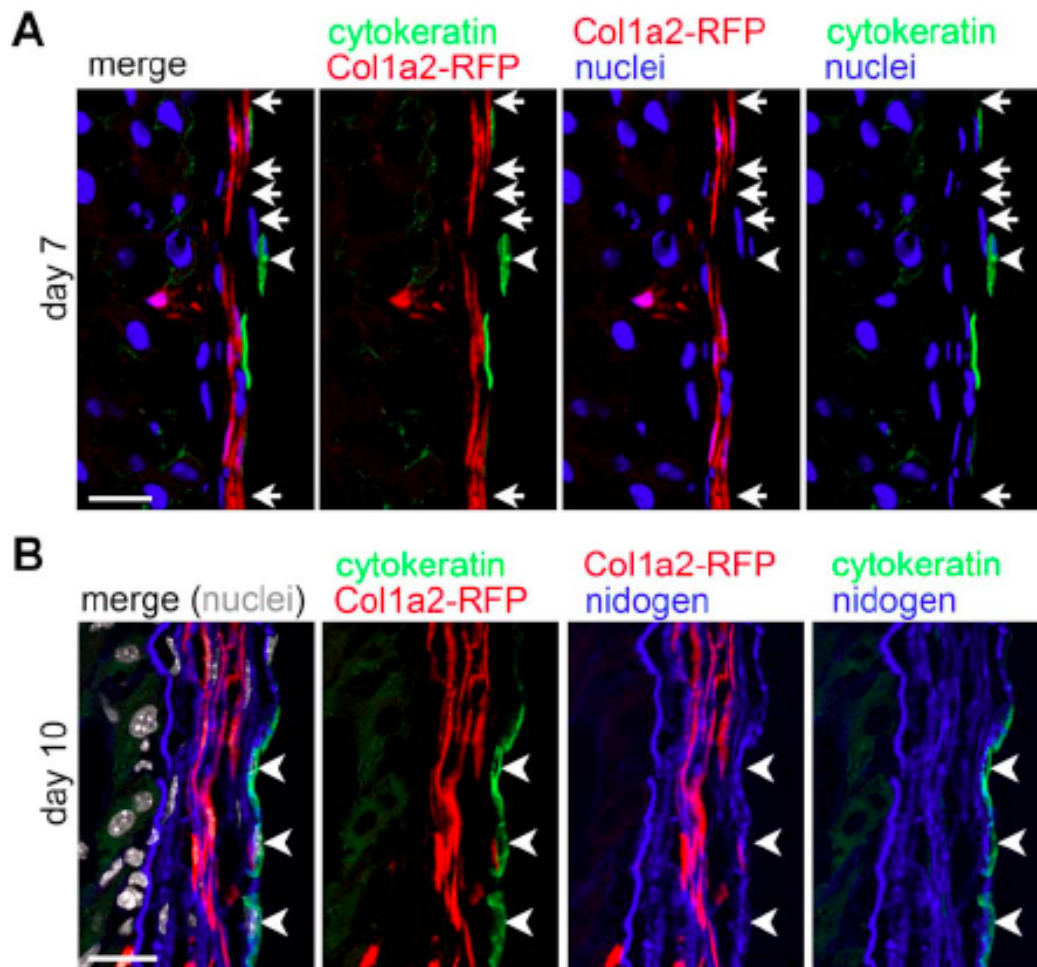


Figure 18

Cohort-labeled *Col1a2*-RFP⁺ SM fibroblasts are not the precursors of repaired mesothelium following hypochlorite injury. Schema indicating cohort-labeling of *Col1a2*-expressing cells in normal peritoneum followed by hypochlorite injury in *Col1a2CreERT^{Tg}; ROSA26^{fstdTomato}* mice is described in Figure 15A. (A) Numerous

Colla2-RFP+ cells accumulate in the area beneath cytokeratin+ MCs 7 days after hypochlorite injury. Arrowheads indicate cytokeratin+ MCs. Peritoneal surface without cytokeratin+ MCs is indicated by arrows. **(B)** Numerous Colla2-RFP+ cells accumulate within the thickened nidogen+ scar 10 days after hypochlorite injury. Cytokeratin+ MCs (arrowheads) do not co-express Colla2-RFP. Magnification x630. Scale bar = 20 μ m.



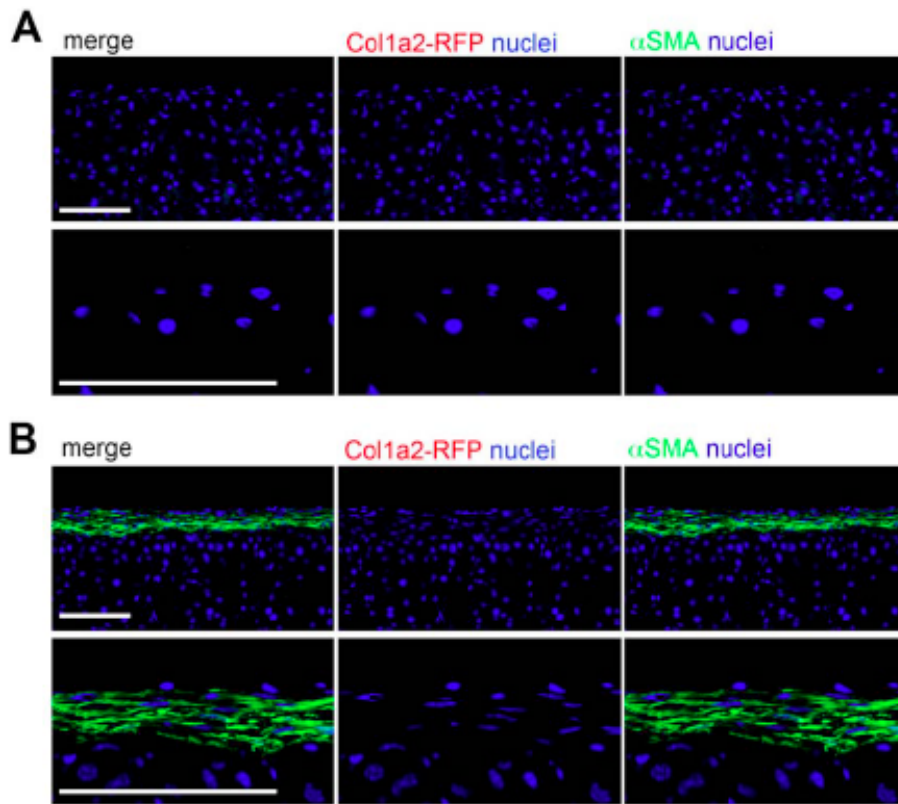
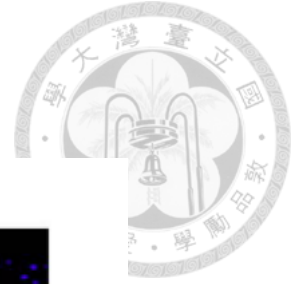


Figure 19

Representative images showing no labeling of Col1a2 expressing cells with the RFP reporter occurs in the peritoneum of *Col1a2CreERT^{Tg}; ROSA26^{fltdTomato}* mice in the absence of tamoxifen administration. **(A)** Normal peritoneum. **(B)** Peritoneum 10 days after hypochlorite injury. Upper and lower panels are taken at magnifications x200 and x630 respectively. Scale bar = 100 μm .

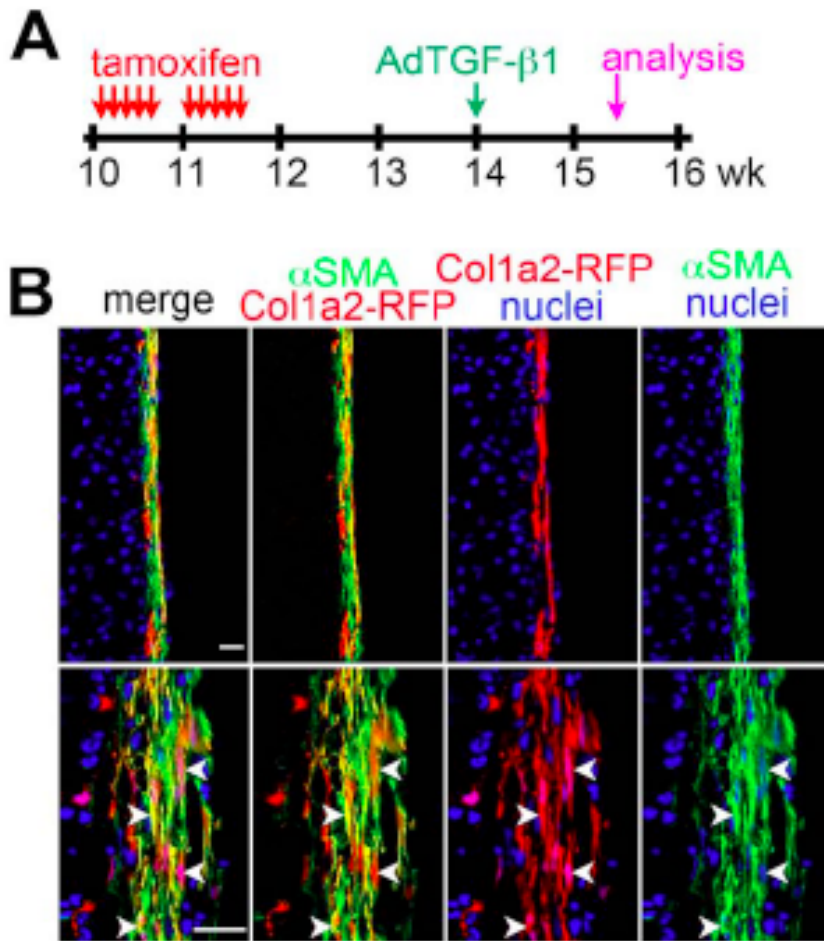


Figure 20

Col1a2-RFP⁺ fate-mapped SM fibroblasts are the major source of myofibroblasts in peritoneal fibrosis induced by intraperitoneal injection of TGF- β 1-producing adenovirus. **(A)** Experimental schema for cohort-labeling in *Col1a2CreERT^{Tg}*; *ROSA26^{stdTomato}* mice followed by intraperitoneal injection of AdTGF- β 1. **(B)** Low-powered (upper panel, magnification x200) and high-powered (lower panel, magnification x630.) images showing Col1a2-RFP⁺ cells co-expressing α SMA

(arrowheads) day 10 after transgenic peritoneal overexpression of TGF- β 1. Scale bar =

20 μ m.



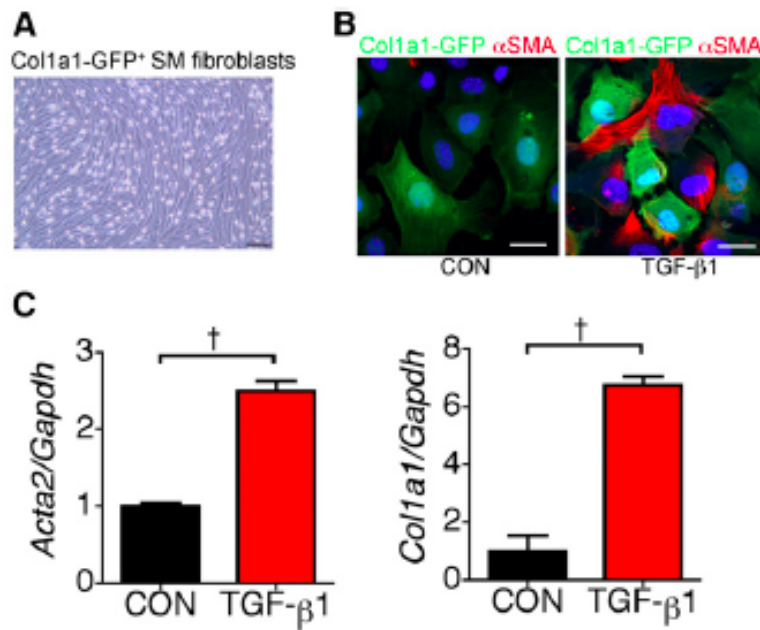


Figure 21

TGF- β 1 induces α SMA expression in cultured SM fibroblasts. (A) Peritoneal Coll1a1-GFP⁺ SM fibroblasts are isolated and cultured from normal *Coll1a1-GFP^{Tg}* mice after intraperitoneal retention of trypsin-EDTA. The bright-field image shows SM fibroblasts at passage two cultured in the treated cell culture dish. (B) Coll1a1-GFP⁺ SM fibroblasts cultured in the chamber slide lack expression of α SMA in culture medium alone (CON), whereas they activate expression of α SMA in the presence of TGF- β 1 for 2 days. (C) Coll1a1-GFP⁺ SM fibroblasts are cultured in the presence or absence of TGF- β 1 for 24 hours. Quantitative PCR shows that *Acta2* and *Colla1* are upregulated by TGF- β 1. The expression levels are normalized by *Gapdh* and expressed as the

mean&SEM (n=3). †P<0.01. Bar, 25 μm in A; 20 μm in B. Original magnification,
x200 in A; x630 in B.



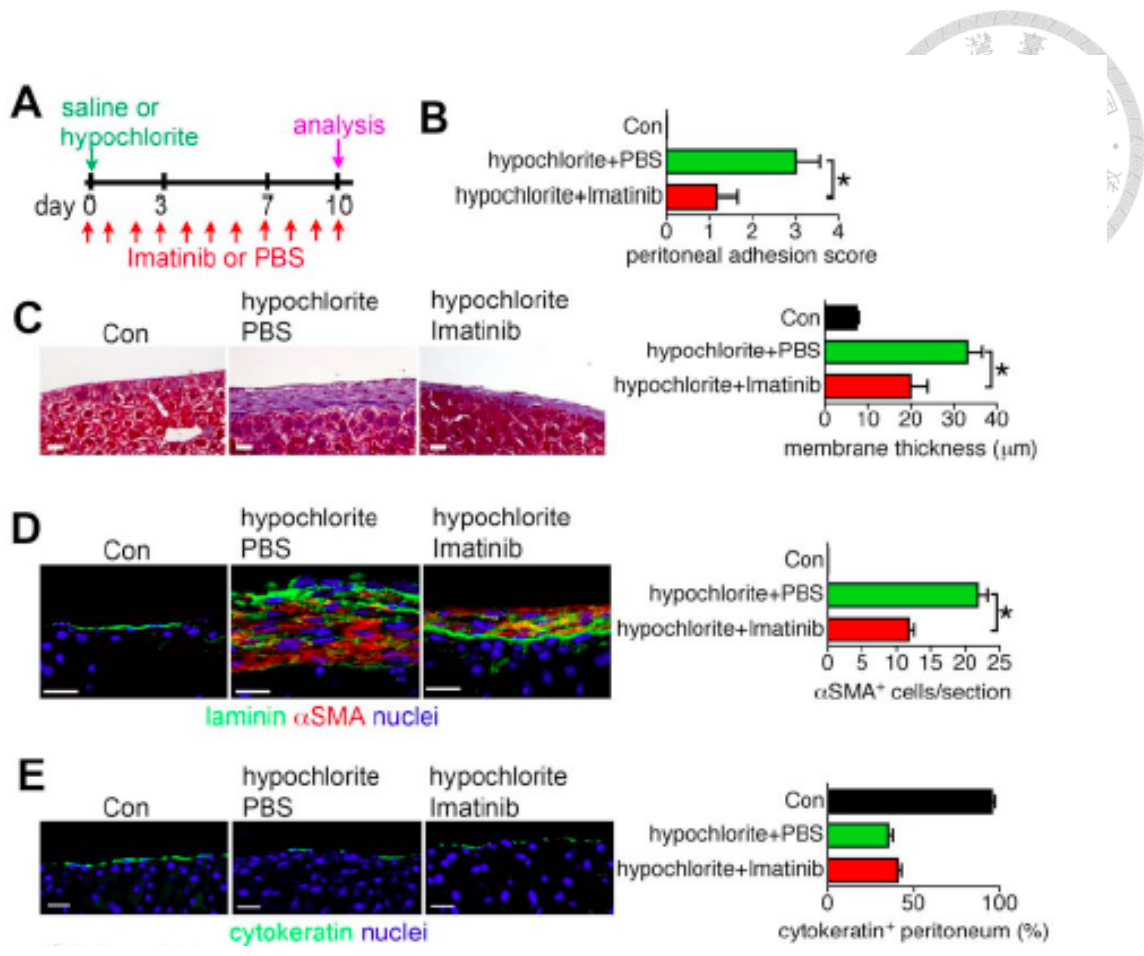
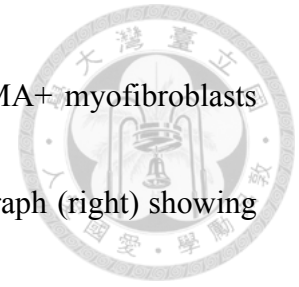


Figure 22

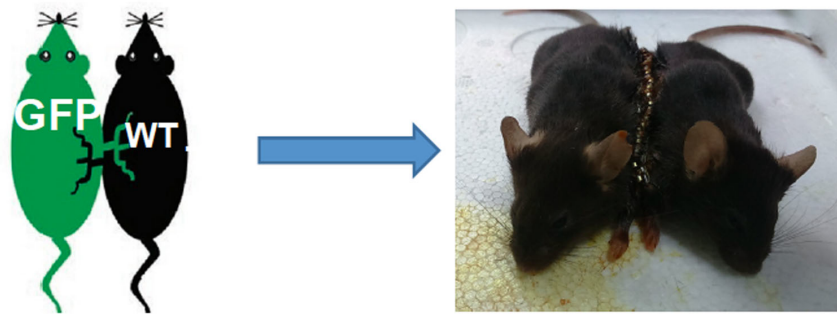
Imatinib reduces peritoneal myofibroblasts and fibrosis. **(A)** Schema showing Imatinib or PBS administration and hypochlorite-induced peritoneal fibrosis. Saline injection on day 0 and then PBS administration serves as control (Con). **(B)** Graph showing peritoneal adhesion induced by bleach in the presence of Imatinib or PBS. **(C)** Images (left, magnification x400) and graph (right) showing the extent of Masson's trichrome blue/green stained fibrotic peritoneal membrane overlying the liver. **(D)** Images (left,

magnification x630) and graph (right) showing the number of α SMA+ myofibroblasts in fibrotic peritoneum. **(E)** Images (left, magnification x400) and graph (right) showing cytokeratin+ MCs and the % of peritoneal surface with cytokeratin+ MCs. Scale bar = 20 μ m. Data in graph is expressed as mean + s.e.m.. *P < 0.05

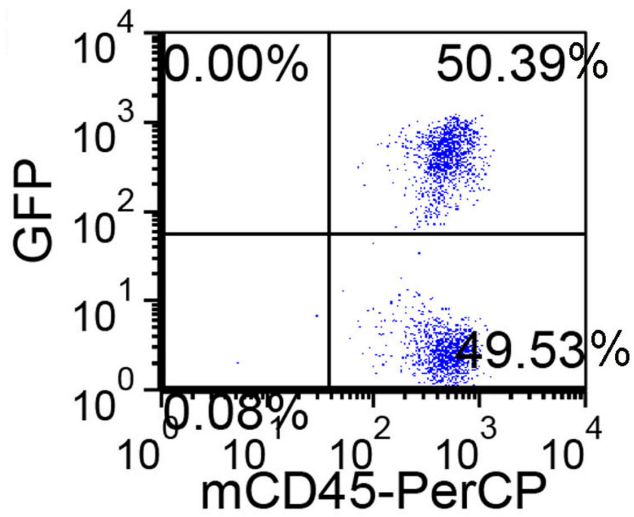




A



B



C

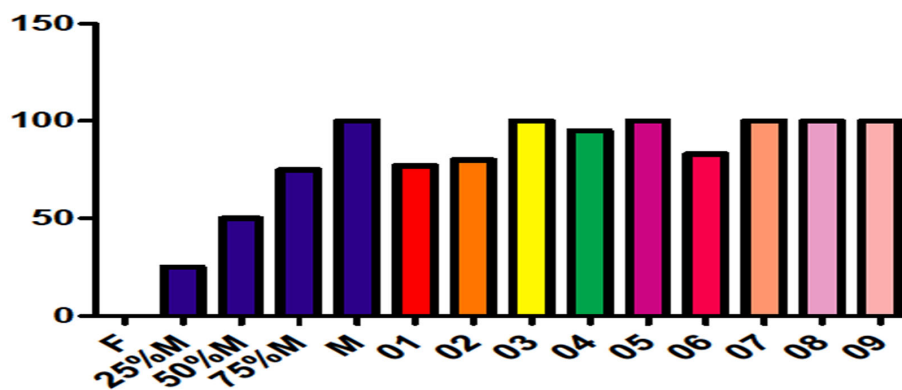


Figure 23



Parabiosis and bone marrow transplantation were used to create chimeric mice. (A)

The *CAG-EGFP^{Tg}* and C57BL/6 mice were shaved and unilateral flank skin incision

from elbow to the knee joints were created. The skin edge of *CAG-EGFP^{Tg}* mice was

sutured together with C57BL/6 mice by clips. Parabiosis models were made

successfully from *CAG-EGFP^{Tg}* and C57BL/6 mice for more than 21 days then they

were induced peritoneal fibrosis by hypochlorite injury. (B) In the parabiosis,

development of cross-circulation between *CAG-EGFP^{Tg}* mice and C57BL/6 mice was

analyzed by flow cytometric analysis of the peripheral blood at day 16 after surgery.

Flow cytometric analysis showed that 50.39% of CD45+ cells in peripheral blood of

C57BL/6 mouse are GFP+. It indicated that cross-circulation in parabiont mice was

developed successfully (C) The bone marrow cells of male *Colla1-GFP^{Tg}* mice were

injected through tail vein to sublethally irradiated female wild type C57BL/6 mice.

Engraftment efficiency was checked by QPCR using specific detection probes for

T-chromosome Y6 and successful engraftment was defined by the presence of Y

chromosome in bone marrow of female recipient mice more than 75% of that shown in

bone marrow of male donor.

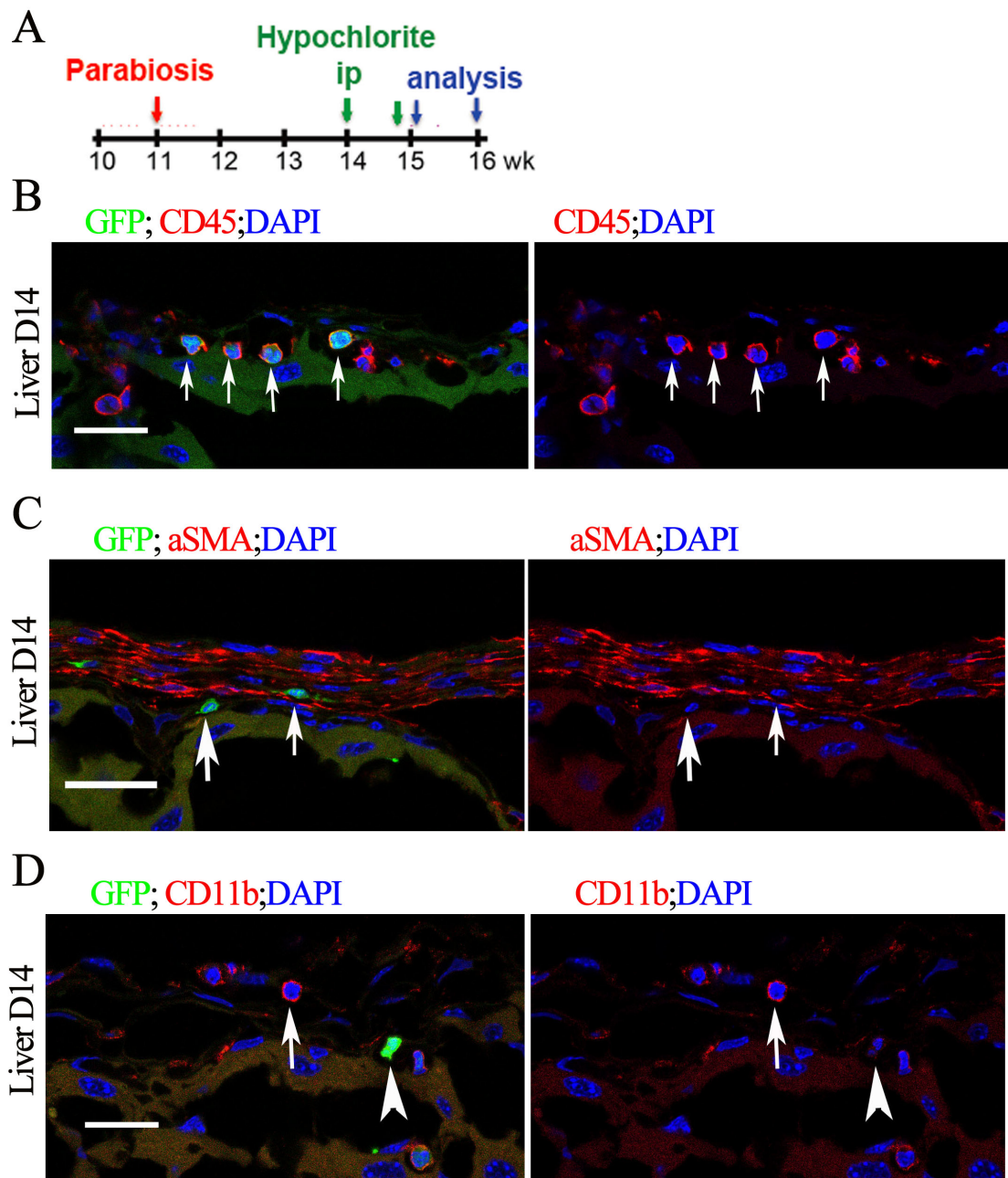
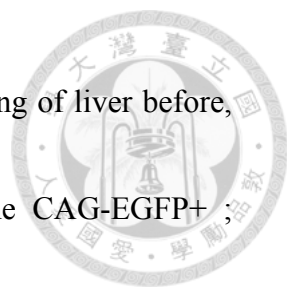


Figure 24

Some CAG-EGFP+ leukocytes were recruited in fibrotic peritoneum but they did not transit into myofibroblasts.

(A) Experimental schema for hypochlorite injury in *CAG-EGFP^{Tg}* and C57BL/6 mice



of parabiosis model. Analysis is performed on the peritoneal covering of liver before, 7, and 14 days after hypochlorite injury. (B) Images show some CAG-EGFP⁺; CD45⁺ leukocytes (arrows) in parabiont after injury, confirming cross-circulation was developed successfully. (C) Images show numerous α SMA + myofibroblasts accumulated and few CAG-EGFP⁺ cells in fibrotic peritoneum. But the CAG-EGFP⁺ cells (arrows) did not express α SMA. It indicates that leukocytes did not transit into myofibroblasts during peritoneal fibrosis. (D) Many CD11b⁺ cells (arrowhead) accumulated in fibrotic peritoneum. But the CAG-EGFP⁺ cell (arrow) did not express CD11b, suggesting the CAG-EGFP⁺ cell was not macrophages. DAPI, 4',6'-diamidino-2-phenylindole. Bar= 20 μ m. Original magnification, x630.

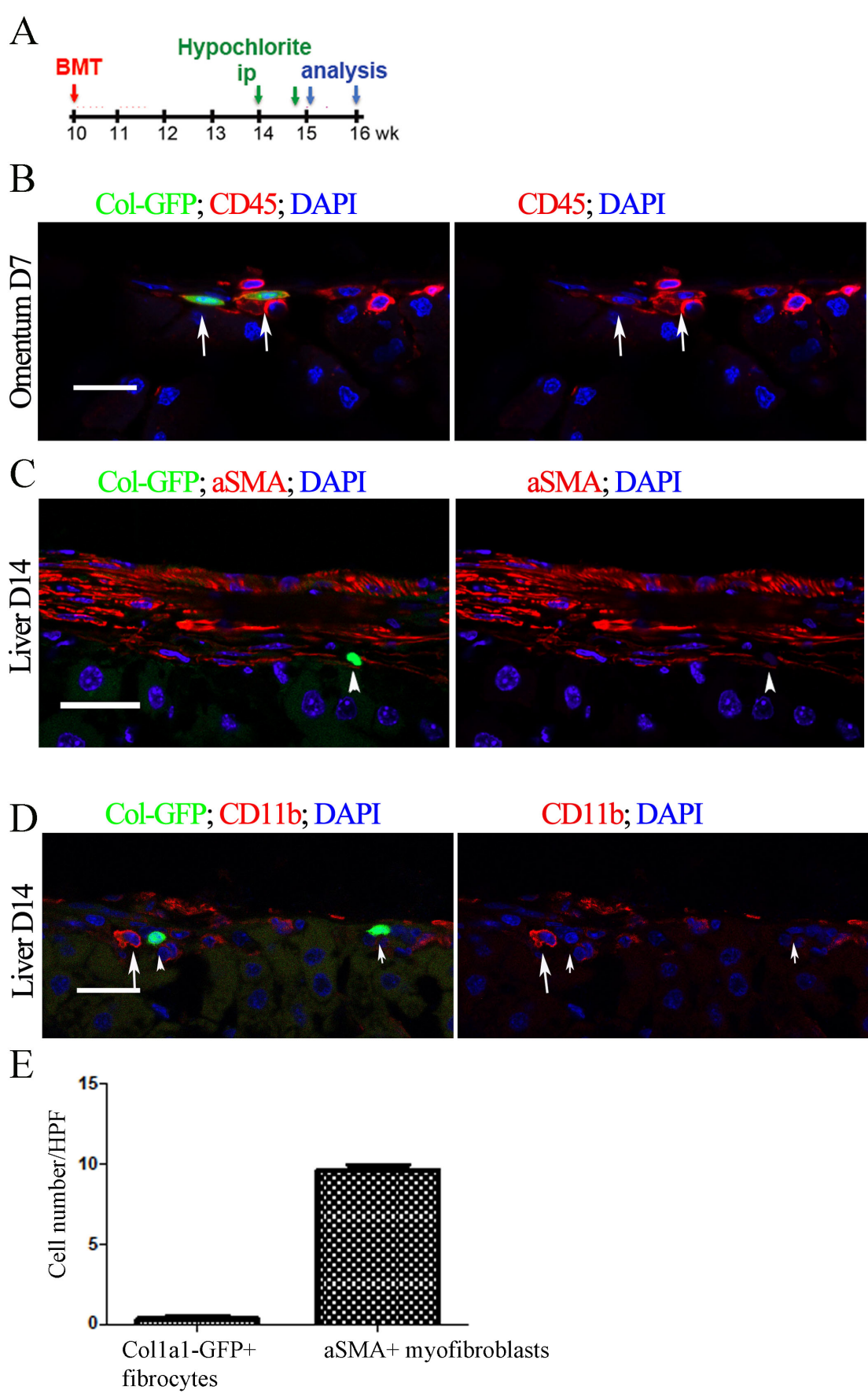




Figure 25

Circulating fibrocytes did not transit into myofibroblasts during peritoneal fibrosis and macrophages accumulated during peritoneal fibrosis.

(A) Experimental schema for hypochlorite injury in BMT chimera. Analysis is performed on the peritoneal covering of omentum and liver before, 7 and 14 days after hypochlorite injury. (B) Images show only few Colla1-GFP+; CD45+ fibrocytes (arrows) after injury, suggesting engraft was created successfully and the Colla1-GFP+ fibrocytes are hematopoietic origin. (C) Images show numerous α SMA + myofibroblasts accumulated in fibrotic peritoneum. But the Colla1-GFP+ cell (arrowhead) did not express α SMA. It indicates that circulating fibrocytes did not transit into myofibroblasts during peritoneal fibrosis. (D) Numerous CD11b+ macrophages accumulated in fibrotic peritoneum. But these CD11b+ macrophages (arrow) did not express Colla1-GFP+ (arrowheads), It suggested that macrophages did not produce type I collagen. DAPI, 4',6'-diamidino-2-phenylindole. Bar= 20 μ m. Original magnification, x630.

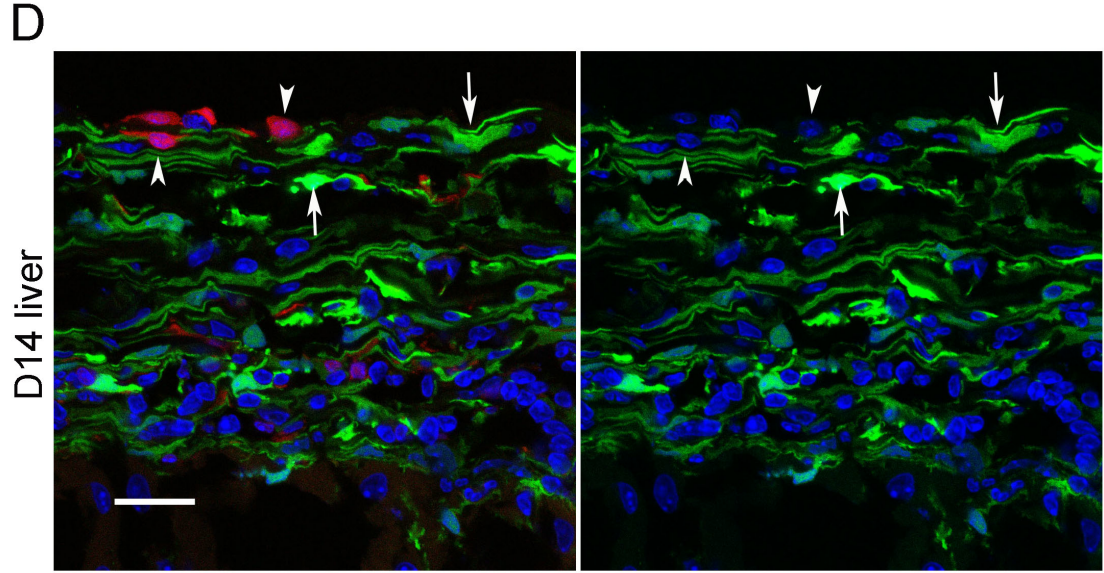
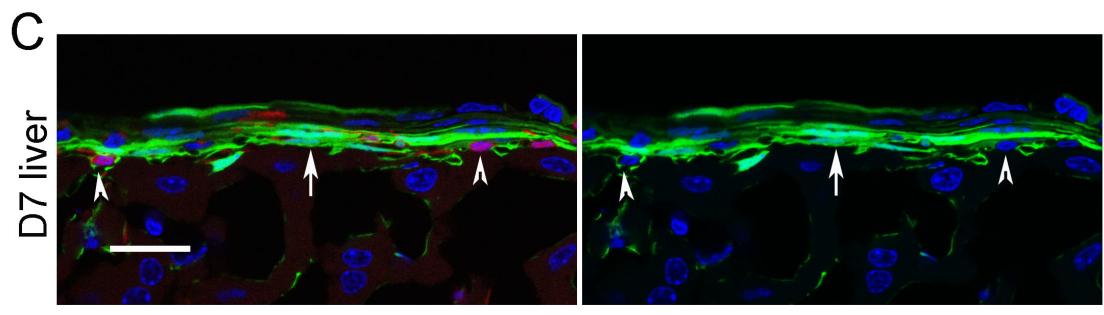
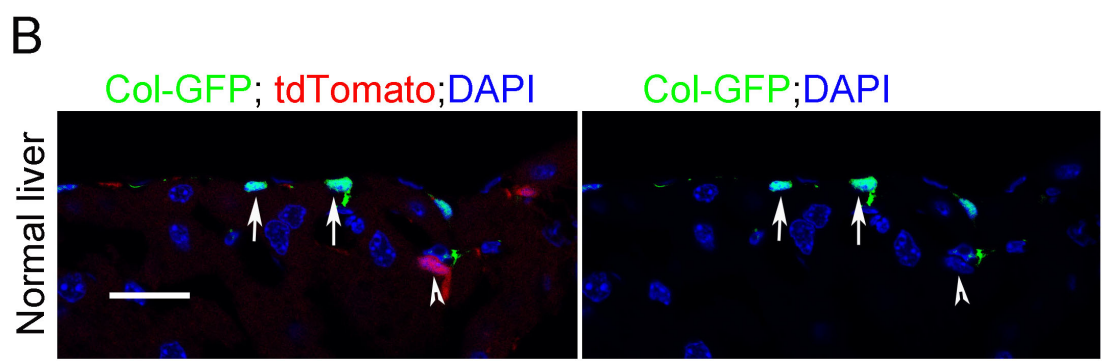
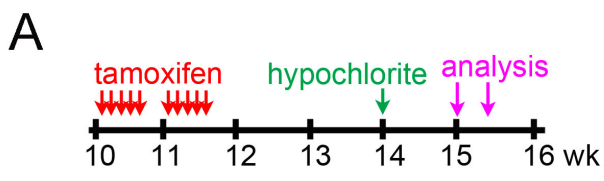




Figure 26

Numerous macrophages accumulated in peritoneal fibrosis but they did not produce

type I collagen. (A) Experimental schema for cohort labeling of Csf1r-RFP+ cells and

hypochlorite peritoneal injury in *Csf1r-Cre/Esr1^{Tg};ROSA26^{fstdTomato};Colla1-GFP^{Tg}* mice.

Analysis is performed on the peritoneal covering of liver before, 7 and 14 days after

hypochlorite injury. (B) Images show few Colla1-GFP+ fibroblasts (arrows) and only

one Csf1r-RFP+ macrophage (arrowhead) in normal peritoneum. (C-D) The number of

Colla1-GFP+ cells and Csf1r-RFP+ macrophages are increased after hypochlorite

injury and they accumulated in fibrotic peritoneum 7 and 14 days after hypochlorite

injury. However, Csf1r-RFP+ macrophages did not expression Colla1-GFP even in

normal peritoneum nor injured peritoneum. It indicated that macrophages do not

produce collagen in neither normal nor fibrotic peritoneum. (n=6 per group). DAPI,

4',6-diamidino-2-phenylindole. Bar, 20 μ m. Original magnification, x630.



Tamoxifen 3mg ip x2 days, D1 DT ip, D2 PBMC

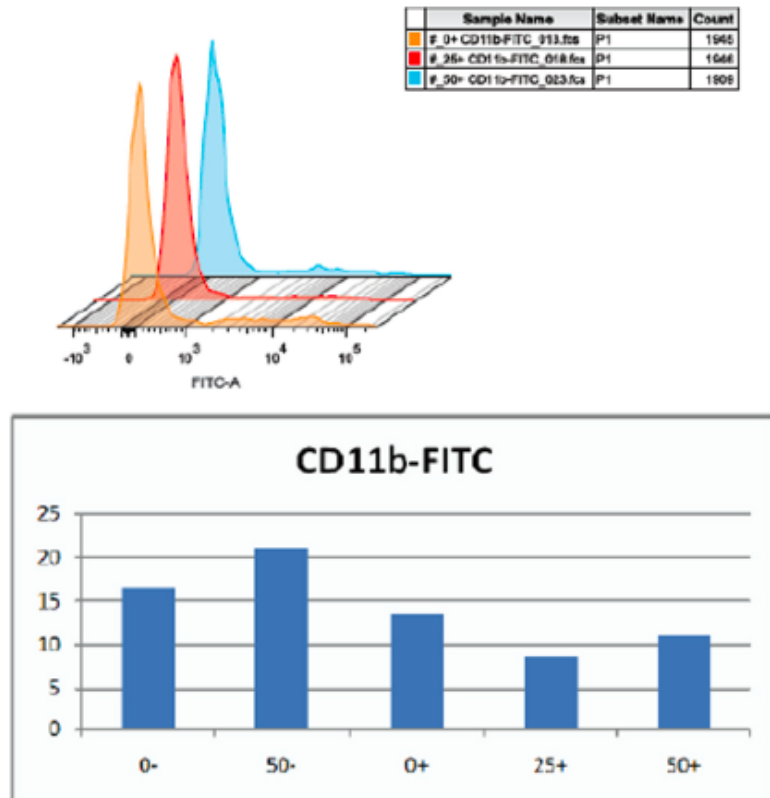


Figure 27

Flow cytometric analysis revealed that CD11b⁺ macrophages were depletion by diphtheria toxin (DT) in peripheral blood. *Csf1r-Cre/Esr1^{Tg};iDTR* mice were injected intraperitoneally tamoxifen 3mg daily for 2 days then DT (25 or 50 ng/g) was intraperitoneally single injected after tamoxifen. Ablation efficiency was confirmed by the percentage of CD11b⁺ macrophages from peripheral blood.

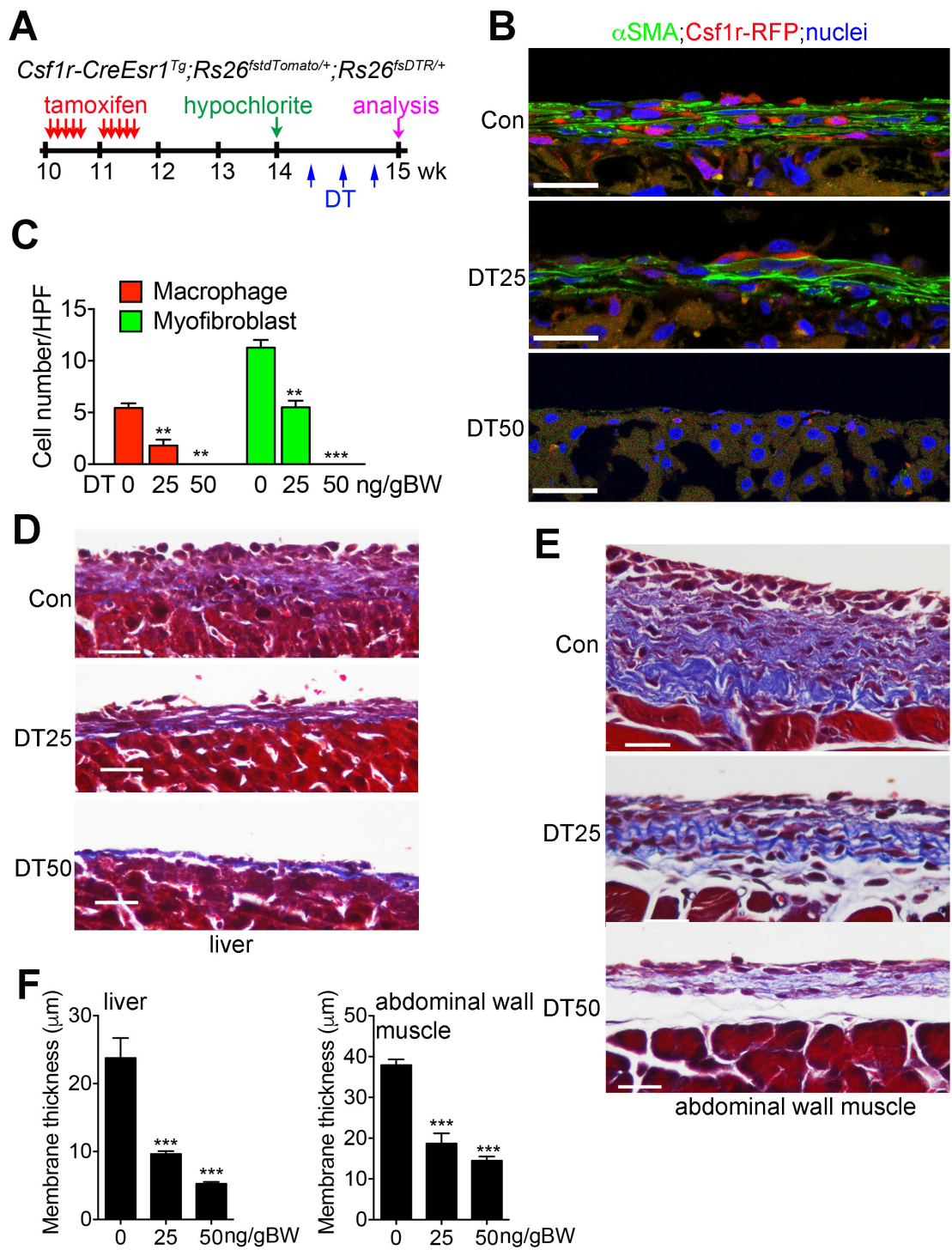



Figure 28

Ablation of macrophages could attenuate peritoneal fibrosis.



(A) Experimental schema for hypochlorite peritoneal injury and diphtheria toxin injection in *Csf1r-Cre/Esr1^{Tg}; ROSA26^{stdTomato}; iDTR* mice. Analysis is performed on the peritoneal covering of liver 7 days after hypochlorite injury and DT was injection intraperitoneally every other day for 3 times from day 2 after peritoneal injury. (B) Images show the cell number of α SMA+ myofibroblasts was reduced following RFP+ macrophages was ablation by diphtheria toxin. And the number of α SMA+ myofibroblasts, RFP+ macrophages, and the thickness of peritoneal fibrosis were all reduced by higher dose of DT. (C) The graph shows the cell number of macrophages was depletion in injured peritoneum by diphtheria toxin and the ablation efficiency was increased by higher dose of DT. The cell number of myofibroblasts was reduced following ablation of macrophages and by higher dose of DT. (n=6 per group) (D and E) Images show thickness of peritoneal covering of liver (D) and muscle wall (E) after hypochlorite injury were reduced following increased dose of DT in masson trichrome stain. (F) The graphs show thickness of peritoneal fibrosis of liver and muscle wall were reduced gradually when dose of diphtheria toxin were increased (n=6 per group). DAPI, 4',6-diamidino-2-phenylindole. Bar = 20 μ m. Original magnification, x630 (in B). Original magnification, x400 (in D and E).

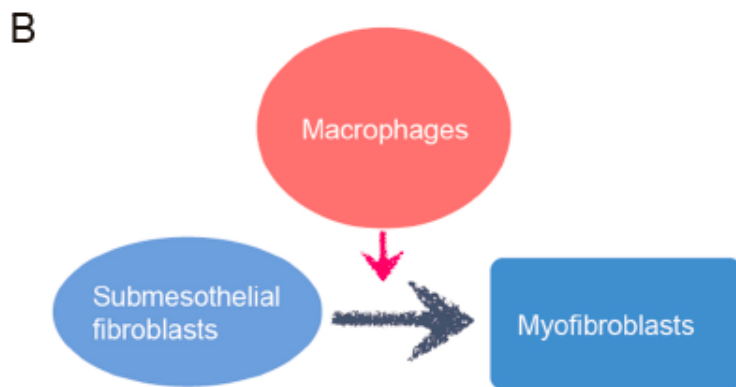
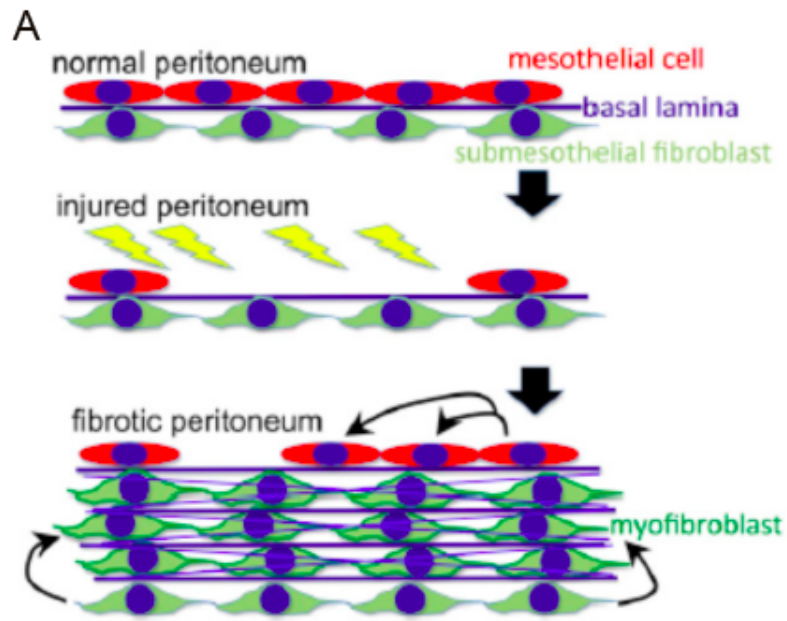


Figure 29

(A) The illustration indicates the major fates of MCs and SM fibroblasts after peritoneal injury. (B) Macrophages could cross talk with SM fibroblasts to activate SM fibroblasts transit to myofibroblasts during peritoneal fibrosis.



Chapter 6. References

1. Kdoqi. KDOQI Clinical Practice Guidelines and Clinical Practice Recommendations for Diabetes and Chronic Kidney Disease. *American journal of kidney diseases : the official journal of the National Kidney Foundation* 2007; **49**(2 Suppl 2): S12-154.
2. Grassmann A, Gioberge S, Moeller S, Brown G. ESRD patients in 2004: global overview of patient numbers, treatment modalities and associated trends. *Nephrology, dialysis, transplantation : official publication of the European Dialysis and Transplant Association - European Renal Association* 2005; **20**(12): 2587-93.
3. Shiao CC, Kao TW, Hung KY, et al. Seven-year follow-up of peritoneal dialysis patients in Taiwan. *Peritoneal dialysis international : journal of the International Society for Peritoneal Dialysis* 2009; **29**(4): 450-7.
4. Aroeira LS, Aguilera A, Sanchez-Tomero JA, et al. Epithelial to mesenchymal transition and peritoneal membrane failure in peritoneal dialysis patients: pathologic significance and potential therapeutic interventions. *Journal of the American Society of Nephrology : JASN* 2007; **18**(7): 2004-13.
5. Devuyst O, Margetts PJ, Topley N. The pathophysiology of the peritoneal membrane. *Journal of the American Society of Nephrology : JASN* 2010; **21**(7): 1077-85.
6. Krediet RT, Struijk DG. Peritoneal changes in patients on long-term peritoneal dialysis. *Nature reviews Nephrology* 2013; **9**(7): 419-29.
7. Rippe B. A three-pore model of peritoneal transport. *Peritoneal dialysis international : journal of the International Society for Peritoneal Dialysis* 1993; **13 Suppl 2**: S35-8.
8. Flessner MF. Osmotic barrier of the parietal peritoneum. *The American journal of physiology* 1994; **267**(5 Pt 2): F861-70.
9. Yang AH, Chen JY, Lin JK. Myofibroblastic conversion of mesothelial cells. *Kidney international* 2003; **63**(4): 1530-9.
10. Sarah E. Herrick SE. Mesothelial progenitor cells and their potential in tissue engineering. *The international journal of biochemistry & cell biology* 2004; **36**.
11. Yanez-Mo M, Lara-Pezzi E, Selgas R, et al. Peritoneal dialysis and epithelial-to-mesenchymal transition of mesothelial cells. *The New England*

journal of medicine 2003; **348**(5): 403-13.

12. Habib SM, Betjes MG, Fieren MW, et al. Management of encapsulating peritoneal sclerosis: a guideline on optimal and uniform treatment. *The Netherlands journal of medicine* 2011; **69**(11): 500-7.

13. Clatworthy MR, Williams P, Watson CJ, Jamieson NV. The calcified abdominal cocoon. *Lancet* 2008; **371**(9622): 1452.

14. Augustine T, Brown PW, Davies SD, Summers AM, Wilkie ME. Encapsulating peritoneal sclerosis: clinical significance and implications. *Nephron Clinical practice* 2009; **111**(2): c149-54; discussion c54.

15. Hoff CM. Experimental animal models of encapsulating peritoneal sclerosis. *Peritoneal dialysis international : journal of the International Society for Peritoneal Dialysis* 2005; **25 Suppl 4**: S57-66.

16. Nevado J, Peiro C, Vallejo S, et al. Amadori adducts activate nuclear factor-kappaB-related proinflammatory genes in cultured human peritoneal mesothelial cells. *British journal of pharmacology* 2005; **146**(2): 268-79.

17. Combet S, Miyata T, Moulin P, Pouthier D, Goffin E, Devuyt O. Vascular proliferation and enhanced expression of endothelial nitric oxide synthase in human peritoneum exposed to long-term peritoneal dialysis. *Journal of the American Society of Nephrology : JASN* 2000; **11**(4): 717-28.

18. Kihm LP, Wibisono D, Muller-Krebs S, et al. RAGE expression in the human peritoneal membrane. *Nephrology, dialysis, transplantation : official publication of the European Dialysis and Transplant Association - European Renal Association* 2008; **23**(10): 3302-6.

19. Honda K, Oda H. Pathology of encapsulating peritoneal sclerosis. *Peritoneal dialysis international : journal of the International Society for Peritoneal Dialysis* 2005; **25 Suppl 4**: S19-29.

20. Cho HJ, Baek KE, Saika S, Jeong MJ, Yoo J. Snail is required for transforming growth factor-beta-induced epithelial-mesenchymal transition by activating PI3 kinase/Akt signal pathway. *Biochemical and biophysical research communications* 2007; **353**(2): 337-43.

21. Bolos V, Peinado H, Perez-Moreno MA, Fraga MF, Esteller M, Cano A. The transcription factor Slug represses E-cadherin expression and induces epithelial to mesenchymal transitions: a comparison with Snail and E47 repressors. *Journal of cell science* 2003; **116**(Pt 3): 499-511.

22. Yang MH, Wu KJ. TWIST activation by hypoxia inducible factor-1 (HIF-1):

implications in metastasis and development. *Cell cycle* 2008; **7**(14): 2090-6.

23. Peinado H, Olmeda D, Cano A. Snail, Zeb and bHLH factors in tumour progression: an alliance against the epithelial phenotype? *Nature reviews Cancer* 2007; **7**(6): 415-28.

24. Margetts PJ, Bonniaud P, Liu L, et al. Transient overexpression of TGF- β 1 induces epithelial mesenchymal transition in the rodent peritoneum. *Journal of the American Society of Nephrology : JASN* 2005; **16**(2): 425-36.

25. Okada H, Inoue T, Kanno Y, et al. Selective depletion of fibroblasts preserves morphology and the functional integrity of peritoneum in transgenic mice with peritoneal fibrosing syndrome. *Kidney international* 2003; **64**(5): 1722-32.

26. Lin SL, Kisseleva T, Brenner DA, Duffield JS. Pericytes and perivascular fibroblasts are the primary source of collagen-producing cells in obstructive fibrosis of the kidney. *The American journal of pathology* 2008; **173**(6): 1617-27.

27. Kisseleva T, Cong M, Paik Y, et al. Myofibroblasts revert to an inactive phenotype during regression of liver fibrosis. *Proceedings of the National Academy of Sciences of the United States of America* 2012; **109**(24): 9448-53.


28. Hoyles RK, Derrett-Smith EC, Khan K, et al. An essential role for resident fibroblasts in experimental lung fibrosis is defined by lineage-specific deletion of high-affinity type II transforming growth factor beta receptor. *American journal of respiratory and critical care medicine* 2011; **183**(2): 249-61.

29. Sakai N, Chun J, Duffield JS, Wada T, Luster AD, Tager AM. LPA1-induced cytoskeleton reorganization drives fibrosis through CTGF-dependent fibroblast proliferation. *FASEB journal : official publication of the Federation of American Societies for Experimental Biology* 2013; **27**(5): 1830-46.

30. Sekiguchi Y, Hamada C, Ro Y, et al. Differentiation of bone marrow-derived cells into regenerated mesothelial cells in peritoneal remodeling using a peritoneal fibrosis mouse model. *Journal of artificial organs : the official journal of the Japanese Society for Artificial Organs* 2012; **15**(3): 272-82.

31. Kokubo S, Sakai N, Furuichi K, et al. Activation of p38 mitogen-activated protein kinase promotes peritoneal fibrosis by regulating fibrocytes. *Peritoneal dialysis international : journal of the International Society for Peritoneal Dialysis* 2012; **32**(1): 10-9.

32. Glik A, Douvdevani A. T lymphocytes: the "cellular" arm of acquired immunity in the peritoneum. *Peritoneal dialysis international : journal of the International Society for Peritoneal Dialysis* 2006; **26**(4): 438-48.

- 
33. Mosmann TR, Coffman RL. TH1 and TH2 cells: different patterns of lymphokine secretion lead to different functional properties. *Annual review of immunology* 1989; **7**: 145-73.
34. Littman DR, Rudensky AY. Th17 and regulatory T cells in mediating and restraining inflammation. *Cell* 2010; **140**(6): 845-58.
35. Waite JC, Skokos D. Th17 response and inflammatory autoimmune diseases. *International journal of inflammation* 2012; **2012**: 819467.
36. Liappas G, Gonzalez-Mateo GT, Majano P, et al. T Helper 17/Regulatory T Cell Balance and Experimental Models of Peritoneal Dialysis-Induced Damage. *BioMed research international* 2015; **2015**: 416480.
37. Rodrigues-Diez R, Aroeira LS, Orejudo M, et al. IL-17A is a novel player in dialysis-induced peritoneal damage. *Kidney international* 2014; **86**(2): 303-15.
38. Sandoval P, Loureiro J, Gonzalez-Mateo G, et al. PPAR-gamma agonist rosiglitazone protects peritoneal membrane from dialysis fluid-induced damage. *Laboratory investigation; a journal of technical methods and pathology* 2010; **90**(10): 1517-32.
39. Ahmad S, North BV, Qureshi A, et al. CCL18 in peritoneal dialysis patients and encapsulating peritoneal sclerosis. *European journal of clinical investigation* 2010; **40**(12): 1067-73.
40. Loureiro J, Aguilera A, Selgas R, et al. Blocking TGF-beta1 protects the peritoneal membrane from dialysate-induced damage. *Journal of the American Society of Nephrology : JASN* 2011; **22**(9): 1682-95.
41. Yao Q, Qian JQ, Lin XH, Lindholm B. Inhibition of the effect of high glucose on the expression of Smad in human peritoneal mesothelial cells. *The International journal of artificial organs* 2004; **27**(10): 828-34.
42. Yao Q, Pawlaczyk K, Ayala ER, et al. The role of the TGF/Smad signaling pathway in peritoneal fibrosis induced by peritoneal dialysis solutions. *Nephron Experimental nephrology* 2008; **109**(2): e71-8.
43. Guo H, Leung JC, Lam MF, et al. Smad7 transgene attenuates peritoneal fibrosis in uremic rats treated with peritoneal dialysis. *Journal of the American Society of Nephrology : JASN* 2007; **18**(10): 2689-703.
44. Patel P, Sekiguchi Y, Oh KH, Patterson SE, Kolb MR, Margetts PJ. Smad3-dependent and -independent pathways are involved in peritoneal membrane injury. *Kidney international* 2010; **77**(4): 319-28.
45. Banh A, Deschamps PA, Gaudie J, Overbeek PA, Sivak JG, West-Mays JA.

Lens-specific expression of TGF-beta induces anterior subcapsular cataract formation in the absence of Smad3. *Investigative ophthalmology & visual science* 2006; **47**(8): 3450-60.

46. Ada S, Ersan S, Sifil A, et al. Effect of bevacizumab, a vascular endothelial growth factor inhibitor, on a rat model of peritoneal sclerosis. *International urology and nephrology* 2015; **47**(12): 2047-51.

47. Fielding CA, Jones GW, McLoughlin RM, et al. Interleukin-6 signaling drives fibrosis in unresolved inflammation. *Immunity* 2014; **40**(1): 40-50.

48. Schmahl J, Raymond CS, Soriano P. PDGF signaling specificity is mediated through multiple immediate early genes. *Nature genetics* 2007; **39**(1): 52-60.

49. Patel P, West-Mays J, Kolb M, Rodrigues JC, Hoff CM, Margetts PJ. Platelet derived growth factor B and epithelial mesenchymal transition of peritoneal mesothelial cells. *Matrix biology : journal of the International Society for Matrix Biology* 2010; **29**(2): 97-106.

50. Chen YT, Chang FC, Wu CF, et al. Platelet-derived growth factor receptor signaling activates pericyte-myofibroblast transition in obstructive and post-ischemic kidney fibrosis. *Kidney international* 2011; **80**(11): 1170-81.

51. Hurst SM, Wilkinson TS, McLoughlin RM, et al. Il-6 and its soluble receptor orchestrate a temporal switch in the pattern of leukocyte recruitment seen during acute inflammation. *Immunity* 2001; **14**(6): 705-14.

52. Sime PJ, Xing Z, Graham FL, Csaky KG, Gauldie J. Adenovector-mediated gene transfer of active transforming growth factor-beta1 induces prolonged severe fibrosis in rat lung. *The Journal of clinical investigation* 1997; **100**(4): 768-76.

53. Huang JW, Yen CJ, Wu HY, et al. Tamoxifen downregulates connective tissue growth factor to ameliorate peritoneal fibrosis. *Blood purification* 2011; **31**(4): 252-8.

54. Nakamoto H, Imai H, Ishida Y, et al. New animal models for encapsulating peritoneal sclerosis--role of acidic solution. *Peritoneal dialysis international : journal of the International Society for Peritoneal Dialysis* 2001; **21 Suppl 3**: S349-53.

55. Mortier S, Faict D, Schalkwijk CG, Lameire NH, De Vriese AS. Long-term exposure to new peritoneal dialysis solutions: Effects on the peritoneal membrane. *Kidney international* 2004; **66**(3): 1257-65.

56. Mortier S, Faict D, Lameire NH, De Vriese AS. Benefits of switching from a conventional to a low-GDP bicarbonate/lactate-buffered dialysis solution in a rat

model. *Kidney international* 2005; **67**(4): 1559-65.

57. Velioglu A, Tugtepe H, Ascioglu E, et al. Role of tyrosine kinase inhibition with imatinib in an encapsulating peritoneal sclerosis rat model. *Renal failure* 2013; **35**(4): 531-7.

58. Zheng B, Zhang Z, Black CM, de Crombrughe B, Denton CP. Ligand-dependent genetic recombination in fibroblasts : a potentially powerful technique for investigating gene function in fibrosis. *The American journal of pathology* 2002; **160**(5): 1609-17.

59. Zhou B, Ma Q, Rajagopal S, et al. Epicardial progenitors contribute to the cardiomyocyte lineage in the developing heart. *Nature* 2008; **454**(7200): 109-13.

60. Andersson KB, Winer LH, Mork HK, Molkentin JD, Jaisser F. Tamoxifen administration routes and dosage for inducible Cre-mediated gene disruption in mouse hearts. *Transgenic research* 2010; **19**(4): 715-25.

61. Cailhier JF, Partolina M, Vuthoori S, et al. Conditional macrophage ablation demonstrates that resident macrophages initiate acute peritoneal inflammation. *Journal of immunology* 2005; **174**(4): 2336-42.

62. Wu JM, Hsueh YC, Ch'ang HJ, et al. Circulating cells contribute to cardiomyocyte regeneration after injury. *Circulation research* 2015; **116**(4): 633-41.

63. Lin SL, Castano AP, Nowlin BT, Lupper ML, Jr., Duffield JS. Bone marrow Ly6Chigh monocytes are selectively recruited to injured kidney and differentiate into functionally distinct populations. *Journal of immunology* 2009; **183**(10): 6733-43.

64. Humphreys BD, Lin SL, Kobayashi A, et al. Fate tracing reveals the pericyte and not epithelial origin of myofibroblasts in kidney fibrosis. *The American journal of pathology* 2010; **176**(1): 85-97.

65. Peters SO, Bauermeister K, Simon JP, Branke B, Wagner T. Quantitative polymerase chain reaction-based assay with fluorogenic Y-chromosome specific probes to measure bone marrow chimerism in mice. *Journal of immunological methods* 2002; **260**(1-2): 109-16.

66. Naglich JG, Metherall JE, Russell DW, Eidels L. Expression cloning of a diphtheria toxin receptor: identity with a heparin-binding EGF-like growth factor precursor. *Cell* 1992; **69**(6): 1051-61.

67. Koesters R, Kaissling B, Lehir M, et al. Tubular overexpression of transforming growth factor-beta1 induces autophagy and fibrosis but not

mesenchymal transition of renal epithelial cells. *The American journal of pathology* 2010; **177**(2): 632-43.

68. Asada N, Takase M, Nakamura J, et al. Dysfunction of fibroblasts of extrarenal origin underlies renal fibrosis and renal anemia in mice. *The Journal of clinical investigation* 2011; **121**(10): 3981-90.

69. Goritz C, Dias DO, Tomilin N, Barbacid M, Shupliakov O, Frisen J. A pericyte origin of spinal cord scar tissue. *Science* 2011; **333**(6039): 238-42.

70. Rock JR, Barkauskas CE, Cronic MJ, et al. Multiple stromal populations contribute to pulmonary fibrosis without evidence for epithelial to mesenchymal transition. *Proceedings of the National Academy of Sciences of the United States of America* 2011; **108**(52): E1475-83.

71. Dulauroy S, Di Carlo SE, Langa F, Eberl G, Peduto L. Lineage tracing and genetic ablation of ADAM12(+) perivascular cells identify a major source of profibrotic cells during acute tissue injury. *Nature medicine* 2012; **18**(8): 1262-70.

72. Bajo MA, Perez-Lozano ML, Albar-Vizcaino P, et al. Low-GDP peritoneal dialysis fluid ('balance') has less impact in vitro and ex vivo on epithelial-to-mesenchymal transition (EMT) of mesothelial cells than a standard fluid. *Nephrology, dialysis, transplantation : official publication of the European Dialysis and Transplant Association - European Renal Association* 2011; **26**(1): 282-91.

73. Hung C, Linn G, Chow YH, et al. Role of lung pericytes and resident fibroblasts in the pathogenesis of pulmonary fibrosis. *American journal of respiratory and critical care medicine* 2013; **188**(7): 820-30.

74. Li Y, Wang J, Asahina K. Mesothelial cells give rise to hepatic stellate cells and myofibroblasts via mesothelial-mesenchymal transition in liver injury. *Proceedings of the National Academy of Sciences of the United States of America* 2013; **110**(6): 2324-9.

75. Lichtnekert J, Kawakami T, Parks WC, Duffield JS. Changes in macrophage phenotype as the immune response evolves. *Current opinion in pharmacology* 2013; **13**(4): 555-64.

76. Murray PJ, Wynn TA. Protective and pathogenic functions of macrophage subsets. *Nature reviews Immunology* 2011; **11**(11): 723-37.

77. Barron L, Wynn TA. Fibrosis is regulated by Th2 and Th17 responses and by dynamic interactions between fibroblasts and macrophages. *American journal of*

physiology Gastrointestinal and liver physiology 2011; **300**(5): G723-8.

78. Roberts AB, Sporn MB, Assoian RK, et al. Transforming growth factor type beta: rapid induction of fibrosis and angiogenesis in vivo and stimulation of collagen formation in vitro. *Proceedings of the National Academy of Sciences of the United States of America* 1986; **83**(12): 4167-71.

79. Sunderkotter C, Steinbrink K, Goebeler M, Bhardwaj R, Sorg C. Macrophages and angiogenesis. *Journal of leukocyte biology* 1994; **55**(3): 410-22.

80. Shimokado K, Raines EW, Madtes DK, Barrett TB, Benditt EP, Ross R. A significant part of macrophage-derived growth factor consists of at least two forms of PDGF. *Cell* 1985; **43**(1): 277-86.

81. Bellon T, Martinez V, Lucendo B, et al. Alternative activation of macrophages in human peritoneum: implications for peritoneal fibrosis. *Nephrology, dialysis, transplantation : official publication of the European Dialysis and Transplant Association - European Renal Association* 2011; **26**(9): 2995-3005.